# Photoembossing for Biomedical Applications

A THESIS SUBMITTED TO THE UNIVERSITY OF LONDON

FOR THE DEGREE OF DOCTOR OF PHILOSOPHY

2014

By

**Nanayaa Freda Hughes-Brittain**

School of Engineering and Material Science

Queen Mary University of London

Mile End Road, London. E1 4NS

# Declaration

I declare that the work presented in this thesis has been performed entirely by myself during the course of my Ph.D. studies at Queen Mary University of London and has not been submitted for a degree at this or any other university.

# Acknowledgement

I would like to thank the Engineering and Physical Sciences Research council (EPSRC) for funding my Ph.D. thesis for 3 years. I would also like to thank my supervisors Ton Peijs and Cees Bastiaansen for their support and motivation throughout my Ph.D.

Ton, thank you for giving me the opportunity to do a Ph.D. and for being the calm head during the hectic times. You always had a solution! I have learnt so much from you since my Master's degree at Queen Mary and I will be calling myself a polymer expert after being taught by you.

Cees, there is nobody like you. I really enjoyed our discussions throughout my thesis and I am sure we will be having a discussion about this acknowledgement page shortly. Thank you for introducing me to relevant people in the field and helping me get a job at Xeltis in Eindhoven.

I would also like to thank John Connelly and Julien Gautrot for their training and supervision during the cell culturing portion of my Ph.D. I wish you both the very best in your careers at Queen Mary and hope we can collaborate or work together in the not too distant future.

I would also like to acknowledge my colleagues Olivier Picot and Lin Qiu for their friendly support and contributions to my thesis.

Olivier, thank you for being the go-to person when I could not fix the spin-coater, DSC, TGA or the UV box. We had some great discussions and collaborations together and I am looking forward to working together soon.

Lin, I learnt a lot from you when I was training you on photoembossing and I am sure you will do an excellent job with the rest of your thesis.

I would also like to thank Nanoforce Technology and their staff, especially Chris Reynolds, for allowing me to train on and use their equipment at the beginning of my Ph.D.

Chris, thanks for being a guiding hand at the beginning of my Ph.D. and introducing me to the technicians and laboratory managers in SEMS and the other relevant departments at Queen Mary.

Finally, I would like to thank my family and friends for being patient and understanding throughout the demanding Ph.D. years, especially during my final year. My parents Alan and Philomina Brittain, you have always been my rock and I could not have done this without your moral and financial support. YOU HAVE SACRIFICED SO MUCH FOR ME AND I AM DEDICATING THIS THESIS TO YOU, MUM AND DAD.

My loving husband Ian Bates, you have been wonderful! You moved to grotty east London for me so I could be near the University. You have been the provider and the caretaker of our home without complaint, especially during this final year. Thank you very much for your patience and understanding. Fun times ahead!

EWURADE ME DA WA SE!!!

# List of publications

Mian Dai , Olivier Thomas Picot , Nanayaa Freda Hughes-Brittain , Ton Peijs and Cees W. M. Bastiaansen, “Formation of relief structures on fibres by photo-embossing,” *Journal of Material Chemistry*, vol.21, pp.15527-15531, 2011.

N. F. Hughes-Brittain, O. T. Picot, M. Dai, T. Peijs, and C. W. M. Bastiaansen, "Effect of polymer binder on surface texturing by photoembossing," *Applied Surface Science,* vol. 258, pp. 8609-8612, 2012.

Nanayaa Freda Hughes-Brittain, Olivier T. Picot, Lin Qiu, Carlos Sanchez, Ton Peijs and Kees Bastiaansen, “photoembossing for surface texturing of films and fibres for biomedical applications,” *MRS online proceedings library*. vol. 1418, 2012

Olivier T. Picot Rafael Alcalá, Carlos Sánchez, Mian Dai, Nanayaa F. Hughes-Brittain, Dirk J. Broer, Ton Peijs1, Cees W. M. Bastiaansen, “.Manufacturing of surface relief structures in moving substrates using photoembossing and pulsed-interference holography,” *Macromolecular Materials and Engineering.* vol. 298, pp. 33-37, 2013

Nanayaa F. Hughes-Brittain , Lin Qiu1, Olivier T. Picot, Wen Wang , Ton Peijs and Cees. W.M. Bastiaansen, “photoembossing of surface relief structures texturing of in polymer films for biomedical applications,” *Journal of Biomedical and Materials Research B*. (Accepted)

# Abstract

Surface topography is known to be important in biomedical applications such as scaffolds for tissue regeneration and has been shown to affect wettability and cell behaviour. Traditionally, topographical effects such as surface texturing have been generated using methods such as photolithography, soft lithography, thermal embossing, and laser/electron beam techniques. This thesis introduces a relatively new technique known as photoembossing to create surface texturing for biomedical applications. Photoembossing is used to produce surface texturing on polymer surfaces by patterned ultraviolet (UV) exposure of a photopolymer blend without an etching step or an expensive mould. After a short general introduction and a literature review, the first experimental chapters describe surface patterning of poly(methyl methacrylate) (PMMA) photopolymer substrates by photoembossing. PMMA is blended with an acrylate monomer and photoinitiator by dissolution in a volatile solvent and processed into films by wire bar coating, and fibres are produced by electrospinning. Surface texture is achieved on both films and fibres by photoembossing. Endothelial cell culture shows that the substrates are biocompatible and cells readily adhere to the surface.

In tissue regeneration applications, scaffold degradation is often important to allow tissue in-growth. Thus, in subsequent studies polylactide-co-glycolide (PLGA) is used as a polymer binder. PLGA blended with a triacrylate monomer showed partial degradation after 10 weeks, with a cross-linked acrylate network remaining. Endothelial cell

adhesion was even better on the PLGA photopolymer substrates compared to PMMA. Furthermore, surface texture improved cell adhesion and proliferation on the PLGA photopolymer. To obtain completely degradable substrates, thiol monomer was used in addition to the acrylate to produce ester bonds after the thiol-ene reaction, which is cleavable by hydrolysis. Accelerated degradation in sodium hydroxide (NaOH) showed complete degradation of this photopolymer system. The degradation rate of the photopolymer could be tuned by the molecular weight of the acrylate monomer, with low molecular weight monomers degrading more slowly than high molecular weight species. Furthermore, the height of the surface relief structures could be enhanced by using low-molecular-weight acrylate monomers. Endothelial cell culture revealed biocompatibility of the blend and cells were able to adhere after 24 hours of seeding.

This thesis demonstrates that photoembossing is a viable technique in producing surface texture for tissue engineering applications. This surface texture can be achieved on both biocompatible and biodegradable photopolymer films and fibres.

# Table of contents

## Chapter 6



## Chapter 7



## Chapter 8

# List of Tables and Figures

## Chapter 1

No tables and figures

## Chapter 2

## Chapter 3



## Chapter 4

## Chapter 5

## Chapter 6

## Chapter 7

## Chapter 8

No tables and figures

# Chapter 1

# Introduction

## 1.1 **Motivation**

Surface topography has been studied widely for biomedical applications and has been shown to affect wettability and cell behaviour. The term “topography” includes both roughness and texture [1]. The influence of the surface topography on the behaviour of the cells was discovered by Harrison during the first part of the twentieth century when he observed that the directional movement of cells was influenced by linear spider web threads. Later on in the 1970’s, Rovensky et al. [2] and Maroudas [3] confirmed the effect of topography on cell behaviour. Since then, the hypothesis that microstructures

on the surfaces of implants can improve the response of cells on these surfaces has been widely accepted.

Early methods of creating microtextured surfaces include photolithography, soft lithography, thermal embossing, and laser/electron beam techniques. In photolithography, a photoresist is placed on the substrate and exposed to UV light via a contact mask grating. This is followed by an etching step to create the desired textures. The etching process consists of using polymer and resist solvent, or the use reactive ions directed by an electrical field onto the substrate. A further stage is needed to remove the resist using a strong solvent. Hot embossing and casting uses a pre-fabricated mould to create surface grooves. In hot embossing, the polymeric material is pressed into a hot mould, whereas in casting, a solution of polymer and solvent is dried on the mould. Lasers can also be used to remove material from a polymer surface to create textured topography. However, this method is relatively slow and it is therefore not used very often.

A recent technique known as photoembossing has also been used to create surface texturing for optical diffraction gratings. Photoembossing is a simple technique to create relief structures in photopolymers using a patterned contact mask exposure and a thermal development step. Typically, a photopolymer consists of a polymeric binder such as poly(benzyl methacrylate) (PBMA), a multifunctional monomer in a 50/50 weight ratio, and a photoinitiator.

## 1.2 **Aim**

Photoembossing has been studied for application in optical diffracting grating. This thesis evaluates the feasibility of employing the photoembossing technique in the biomedical field of cell and tissue culture. For this, biocompatible photopolymer blends are needed to promote cell adhesion and proliferation. Endothelial cells were used for most studies (excepting Chapter 5), as complete endothelial cell coverage on substrates is very important to vascular regeneration to prevent thrombosis. Therefore, if endothelial cells were able to adhere on these substrates, these materials could be deemed biocompatible. Also, in tissue engineering, scaffold degradation could be required to promote full regeneration of tissue. Therefore, another aim was to produce photoembossed scaffolds that were textured and biodegradable, using commercially available materials to make them more accessible to researchers and industry.

## 1.3 **Thesis outline**

*Chapter 2: Literature review*

The literature review focuses on cell adhesion on surfaces and their response to topography. We also review the different techniques commonly used in producing surface texture on polymer substrates. Scaffold fabrication of polymers is also discussed here, with more emphasis on electrospinning, which has become more prominent in the past decade in the field of tissue engineering. The final section of this chapter details the photoembossing technique and the effect of processing and compositional parameters on texture morphology.

*Chapter 3: Surface texturing of PMMA photopolymers*

PMMA polymer has been used in bone implants as cements to bind the implant to surrounding tissues, with cell adhesion on PMMA being crucial to the success of the implant. This chapter discusses mainly the surface patterning of PMMA photopolymer surfaces by photoembossing.

*Chapter 4: Biocompatibility of cells on PMMA photopolymers*

Photoembossing of PMMA photopolymer binders with different monomers is evaluated on films. The effect of monomer type on surface relief height and morphology is evaluated. Endothelial cell adhesion and proliferation is also studied here on the different acrylate monomers, and the effect of acrylate conversion after UV curing on biocompatibility is discussed.

*Chapter 5: Surface texturing of electrospun PMMA-triacrylate fibres*

Biocompatibility tests in Chapter 4 show that PMMA-triacrylate fibres had superior cell compatibility. Electrospinning of the photopolymer blend resulted in homogenous fibres that are photoembossed using a patterned holographic exposure by interference of two coherent beams. Keratinocyte cell adhesion is evaluated here. The change in cell type here is due to the unavailability of kertatinocytes. Nevertheless, the objective of cell compatibility on the surface of the fibres is evaluated.

*Chapter 6: Biocompatibility and degradation of PLGA-triacrylate photopolymer*

Photoembossing parameters are optimised here for this blend. Endothelial cell adhesion and proliferation is also studied on smooth and textured PLGA photopolymer films. Pure PLGA is used as a positive control. Degradation of the photopolymer is also evaluated, and the effect of surface texture on degradation is discussed.

*Chapter 7: Photoembossed degradable PLGA-acrylate-thiol blend:*

In Chapter 6, the PLGA blends are only partially degradable, i.e. only the PLGA binder degrades, leaving behind the acrylate network. Here, thiol monomer is added to the photopolymer containing PLGA and PEG-diacrylate, creating hydrolysable ester bonds formed from the thiol-ene reaction between the acrylate and thiol. Photoembossing is optimised on these substrates, and degradation and cell adhesion is also studied.

# Chapter 2

## Literature review

Biocompatible materials are used in biomedical applications for medical devices, drug delivery carriers, and tissue engineering (TE) scaffolds. Whereas medical implant devices do not need to be degradable *in vivo*, the latter two applications may require biomaterials that are degradable over time. The scaffold, by definition, is a temporary supporting structure for growing cells and tissues. It is also called a synthetic extracellular matrix (ECM) and plays a critical role in supporting and inhabiting cells. These cells then undergo proliferation, migration, and differentiation in three dimensions, which eventually leads to the formation of a specific tissue with appropriate

functions. The structural and behavioural characteristics of the tissue scaffold are critical to ensure normal cellular activities and functional engineered tissues. An ideal scaffold for tissue engineering should possess all of the qualities of native ECM and should function in the same way as that of ECM under physiological conditions. However, there is no clear guidance regarding which characteristic defines the so-called ideal scaffold. The native ECM in the body is a complex and dynamic environment filled with features on the nanoscale, including pores, molecules and fibres that exhibit tissue-specific structure and properties. These structures and architecture vary from tissue to tissue and therefore the characteristics of a scaffold vary according to the tissue types where the scaffold is to be applied. For example, a scaffold for engineering bone tissues requires osteoconductive features, but this is not required for engineering nerve tissues. Although mimicking the complexity of the native ECM is challenging, recent investigations suggest that a scaffold for tissue engineering should have some of the basic characteristics essential for tissue development [1-4]. Generally, the ECM consists of gycosaminoglycans (GAGs) and fibrous p. The fibrous proteins. The fibrous proteins are collagen, laminin and elastin.

Any scaffold, irrespective of application, should be biocompatible; that is, it should not provoke any rejection, inflammation, and immune responses. It should provide a template for the cells to attach and to guide their growth. It should have a porous architecture for the maximum loading of cells, cell-surface (scaffold) interaction, tissue in growth, and transportation of nutrients and oxygen. It is worth pointing out that most tissue engineering applications require scaffolds that are biodegradable. It is desirable

that the degradation rate of the scaffolds matches the rate of tissue regeneration but, in general, it should not be faster, because that faster rate may lead to a decrease in tissue functionality. It should also be mechanically strong enough to withstand *in vivo* biological forces, and it should support the cells to synthesize specific proteins and other biochemical and biological processes required for healthy tissue growth. Furthermore, the scaffold should be able to withstand sterilisation procedures to avoid toxic contaminations without compromising any structural and other related properties. Finally, the production process of scaffolds with all of the above unique characteristics must be accomplished in a reproducible, economical, and scalable manner. The realistic success of the tissue scaffold is not only dependent on the above measures, but is also dependent on the identity of various types of scaffolding material systems with which the host cells/tissues interact physiologically.

The five main types of blood vessels are arteries, arterioles, capillaries, venules and veins. Angiogenesis, which is the growth of new blood vessels, is an important process in embryonic and foetal development, development of new lining after menstruation, wound healing, and development of blood vessels around obstructed arteries in the coronary circulation.

Arteries carry blood away from the heart to other organs of the body. The wall of the arteries has three tunics (layers): tunica interna, tunica media and tunica externa. The tunica interna is the innermost layer and is made of an endothelium, a basement membrane, and a layer of elastic tissue called the internal elastic lamina. The endothelium is made up of a continuous layer of endothelial cells and is the only surface

that comes into contact with blood in a normally functioning tissue. The tunica media, usually the thickest layer, consists of elastin fibres and smooth muscle fibres that are arranged concentrically around the lumen. The tunica media also has elastic lamina (external). This part of the vascular wall is very compliant due to the high amount of elastin fibres, and it can stretch or expand without tearing in response to small increases in pressure. The outer layer, tunic externa, is composed of elastin and collagen fibres. An arteriole is a small artery with diameters ranging from 10-100 µm and processes three tunics. However, the regions very close to the capillaries consist of almost nothing more than a layer of endothelium surrounded by a few scattered smooth muscle fibres. Capillaries are microscopic vessels that connect the arterioles to the venules. They are about 4-10 µm in diameter and only have a single layer of endothelial cells and a basement membrane. The venules connect the capillaries to the veins and are about 10-100 µm thick. The venules closer to the capillaries only have tunica interna and media, while the ones near the veins contain all three tunics. The tunics in the veins are essentially the same three coats, but the relative thicknesses are different. The tunica externa is the thickest layer and consists of collagen and elastin fibres. Veins lack internal and external laminae found in arteries. However, they are distensible enough to accommodate variations in volume and pressure. The lumen of the vein is bigger than that of the artery. Vein diameters range from 0.1 mm to dimensions greater than 1 mm.

Cardiovascular disease is the leading cause of death in the United States, and each year over 570,000 coronary artery bypass graft procedures are performed. Typically, autologous saphenous veins and internal mammary arteries are grafted to bypass

occluded arteries [5, 6]. Peripheral vascular defects are also a large market, in which autogenous saphenous veins, acellular human umbilical veins, and synthetic grafts are used. Tissue engineered vascular implants are an alternative source for vascular grafts, particularly for patients who lack sufficient conduit. Atherosclerosis is the major disease of blood vessels, and affects the larger and medium sized arteries that contain an intima [7]. The atherosclerotic lesion consists of a raised focal plaque within the intima, consisting of a lipid core, surrounded by extracellular matrix and smooth muscle cells and covered by a fibrous cap. As it increases in size through intimal hyperplasia, it restricts blood flow and eventually blocks vessels. In cardiac and peripheral bypass surgery, these are usually replaced by autologous veins, or sometimes with autologous arteries. However, many patients do not have appropriate blood vessels for use as replacements, either due to diseased blood vessels or because the blood vessels were used in a previous surgery. In these cases, the patients are restricted to modest treatment modalities, with the results often leading to myocardial infarction or limb amputation. Unfortunately, although synthetic vascular grafts such as expanded polytetrafluroethylene (ePTFE) or Dacron have been used successfully in treating the pathology of large arteries > 6 mm internal diameter, these have generally not proven successful in replacing the smaller-diameter (< 6 mm internal diameter) vessels. There is, therefore, a massive clinical need for an alternative supply of vessels to replace diseased arteries. Tissue engineering offers the potential of providing vessels that can be used to replace diseased and damaged native blood vessels. Tissue engineering has already had success in generating materials for repair of chronic wounds and burns. The challenges faced by the approach of tissue engineering for replacing blood vessels are

substantial. They include providing a conduit that will have sufficient strength not to burst with changes in blood pressure, a vessel wall that is elastic and can withstand cyclic loading, matching compliance of the graft with the adjacent host vessel, and a lining of the lumen that is antithrombotic. Many tissue engineering approaches can rely on remodelling of the tissue *in vivo* to approach functionality with time; however, the tissue-engineered vascular graft must function immediately on implantation. It is predicted that tissue engineering offers the opportunity to use cell and tissue growth, biomaterial selection and scaffold fabrication, and cell type and phenotypic regulation, to manufacture blood vessels that can function long term *in vivo* [8].

Thrombosis occurs when blood comes into contact with surfaces without an endothelial layer, resulting in clotting of the blood in the vessels. One way of preventing thrombosis is to have a confluent adherent endothelial layer prior to implantation [9]. Deutch et al. showed a 68% patency in a 9-year clinical study using endothelialised 6 mm PTFE graft coated with fibrin [10]. In this method, the cell source and surface adhesion of cells is very important. Cell sources used for endothelialisation include fatty tissue (from liposuction), umbilical cord blood, and blood vessels themselves [8]. Cells that can activate protein C, express heparin sulphate proteoglycans, and produce nitric oxide, prostacyclin and tissue plasminogen activator could greatly reduce graft thrombosis [5]. Tissue-engineered (TE) vascular grafts are divided into three types: cell only, accellular matrix and cells with biocompatible scaffolds. L'Heureux et al. developed a vascular graft with scaffolds. They cultured smooth muscle cells and fibroblasts to form sheets of tissues that were rolled around a mandrel to form a tubular conduit, which was then

seeded with endothelial cells to form a 3-layer vascular graft. 50% patency was achieved 1 week after implantation in a canine model. Decellularisation of allogenic or xenogenic ECM has also been studied for TE vascular graft. The cells and all proteins are removed from the ECM, leaving behind a fibrous collagen and elastin structure that is placed directly into the defective area. Cells from the neighbouring healthy tissues are expected to invade this scaffold and produce new tissue [11]. Biocompatible scaffolds (degradable or non-degradable) should serve as a structural framework and promote cellular growth and matrix synthesis. The use of these scaffolds has been studied widely due to their ability to form tissue *in vitro* relatively rapidly, with the appropriate shape and dimensions [8]. Fibrous and porous biomaterials have been used for TE vascular implants. Nicklason et al. [12] seeded poly(glycolic acid) scaffolds with smooth muscle cells (SMC) in a pulsating bioreactor (to mimic a biological environment). After 8 weeks of implantation, the synthetic scaffold was completely replaced with a smooth muscle layer. This was then seeded with endothelial cells to form two tunics of the blood vessel. The cultured tissue was implanted in pigs and seemed to be patent after 4 weeks [12].

Improvements in the restenosis rate notwithstanding, metal stents have other important limitations, including thrombogenicity, permanence (sliding), and limited potential for local drug delivery. Metal stent surfaces are moderately thrombogenic and therefore require antiplatelet or anticoagulant therapy. Surgical revision of a stented vessel is also a practical impossibility, due to the difficulty of freeing the metal in the neointima. Coated metal stents have been introduced recently to provide controlled drug release, with very good short-term results [13-16]. Current practice is to use a

bioresorbable phosphoryl choline polymer, or other polymer coating [17, 18]. However, due to the thinness of the polymer layer, only a small amount of drugs can be loaded and eluted [19]. Several reports of resorbable and non-resorbable polymeric stents have been investigated [20-22] [23]. The rationale for the non-degradable stent is improved biocompatibility over the metal stent and convenient drug loading. Bioresorbable stents are being investigated to support the arterial wall only during vessel healing, with gradual transfer of the mechanical load to the tissue as the stent mass and strength decreases over time. In the longer-term, delivery of drug and/or gene therapy to the vessel is planned, with no need for a second surgery to remove the device [23, 24].

## 2.1. Cell culture on biomaterials

Scaffold materials can be of synthetic or natural (biological) origin. Currently, a variety of materials is available for manufacturing tissue scaffolds; options include polymers, ceramics, and their composites. The choice of materials depends on the type of tissue to be reconstructed. For example, ceramics and polymer-ceramic composites are widely used for manufacturing scaffolds for hard tissue reconstructions, whilst polymers are used for soft tissue reconstructions due to their mechanical properties. Owing to their functional properties and design flexibility, polymers are considered to be a unique class of scaffold material and are in demand for a variety of tissue engineering applications, compared to other types of materials. Polymers used in scaffold engineering can be grouped into (i) naturally derived and (ii) synthetic polymers. Examples of naturally derived polymers are biodegradables such as collagen, gelatin and elastin. The synthetic

polymers can be either biodegradable or non-biodegradable. Poly(lactic acid) (PLA), poly(glycolic acid) (PGA), and poly(lactic-co-glycolic acid) (PLGA) are examples of biodegradable polymers; poly(ethylene) (PE), poly(ethylene terephthalate) (PET), and poly(tetrafluoro ethylene) (PTFE) are some examples of non-biodegradable polymers [25]. In most circumstances, biodegradable polymers, either from natural or from synthetic origin, are considered as a good choice for scaffold engineering rather than non-biodegradable polymers. However, degraded products from the biodegradable polymers must be nontoxic and should not elicit any foreign-body reaction, because they hinder the process of tissue growth. In this part of the review, biodegradable collagen and aliphatic polyesters will be the main focus. Collagen is the most abundant natural polymer found in tissues, and thus the review of its structure and functions will be appropriate for this section. Synthetic aliphatic polyesters including poly(lactic acid), poly(glycolic acid), and their copolymers have been studied widely for TE applications due to their biocompatibility and have been approved by most standardization boards.

### Natural biomaterials

Collagen is one of the most widely used naturally derived polymers for manufacturing tissue scaffolds. It is a primary structural protein of the native ECM. Although many types of collagen exist in a living organism, the most abundant forms of collagen in the native tissue are types I and III. Type I collagen has a fibril diameter of about 50 nm and it is the most abundant in skin. The collagen structure is composed of three polypeptides (α-chains) that are each coiled into a left-handed helical pattern, and these three chains

are then wrapped around each other into a right-handed helical pattern that is well-organized (quarter stagger) into insoluble fibrils of great structural strength [26]. The quarter stagger arrangement gives the collagen fibrils a textured appearance. The fibrils form bundles of collagen fibres with diameters up to 10 µm [27].

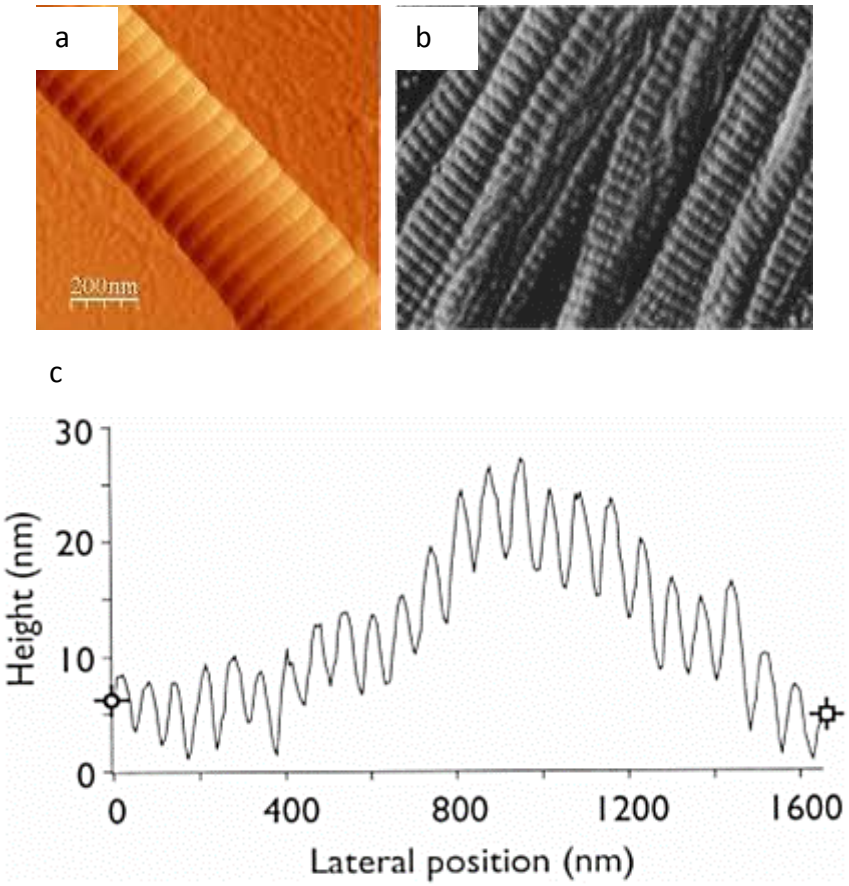


*Figure 2.1: Atomic force microscopy (a) and transmission electron microscopy (b) of a natural collagen fibril (c) shows the height of the textured collagen surface measured by AFM [28].*

Chemical and physical cues on these fibres provide binding sites for cellular receptors, which in turn send signals to cell interiors that regulate different cell behaviours, including differentiation and apoptosis. An important interaction site between a cell and

its matrix is known as a focal adhesion, mediated by a family of transmembrane proteins called integrins. Integrin $\alpha_2$ $\beta_1$ has been studied as the main receptor for collagen type I [29]. These collagen surfaces contain RGD motifs, which are recognised by integrins on the cells.

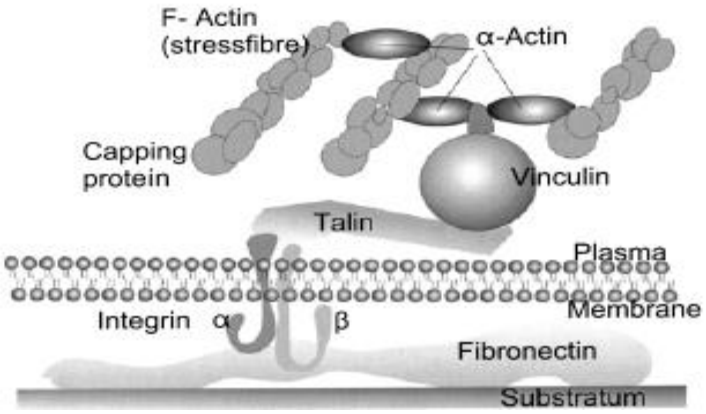


*Figure 2.2: Cell adhesion to a substrate showing different membrane protein [30].*

Furthermore, the effect of the D-banding on collagen fibres has been studied [31]. Friedrichs et al. [31] showed that cells aligned along the fibre axis on the nanopatterned collagen did not show any alignment on smooth surfaces [31]. This phenomenon was attributed to the superior strength of the d-banded collagen fibrils shown in Fig. 2.1 and Fig. 2.3. Deformation of fibres occurs perpendicular to the fibre axis, and thus cells align and move along the direction of the collagen fibres.

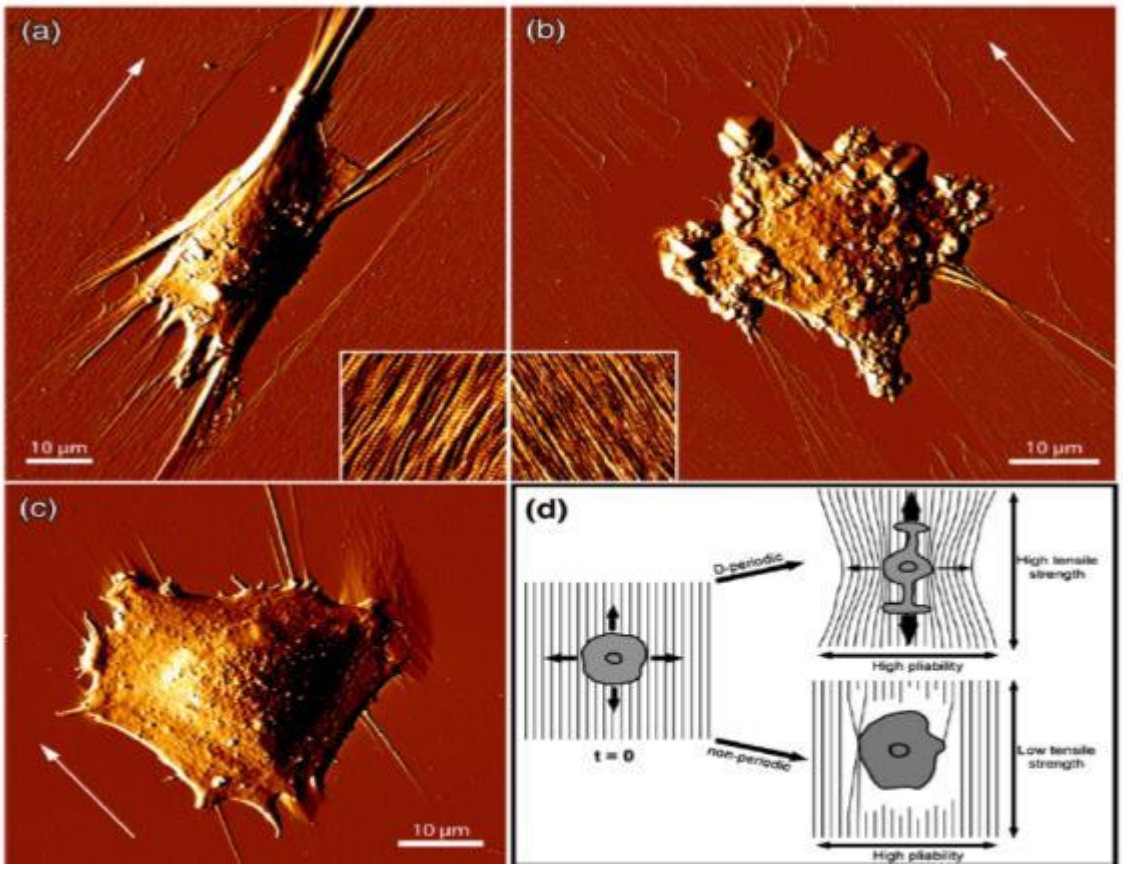


*Figure 2.3: Matrix rigidity anisotropy is required for cell polarization. SAOS-A2 cells were seeded on (a) D-periodic, (b) non-periodic or (c) (d) model illustrating how differences in matrix rigidity between D-periodic and non-periodic collagen matrices affect cell polarization [31].*

They also observed that cells without $\alpha_2\,\beta_1$ adhered on D-banded fibrils but did not align; thus, they suggested that the integrin $\alpha_2\ \beta_1$ is required for cell alignment but not necessarily adhesion for d-periodic collagen [31]. Tasi et al. [32] studies the influence of topography of nanofibrils of three-dimensional collagen gel beads on the phenotype, proliferation, and maturation of osteoblasts. In this study, alkaline phosphatase activity on the D-band periodicity collagen increased when compared to the non-D-band periodicity collagen on day 7. Moreover, type I collagen is expressed in the early stages of differentiation for bone formation and matrix production [32]. They also found that

the D-pattern of collagen did not only enhance the mineralization process of osteoblasts, but also induced the cells to display their normal phenotype [33].

Collagen as a scaffold material has a variety of functional properties favourable for cellular growth. It is a biocompatible, biodegradable, and nontoxic polymer. However, collagen extracted from the natural tissues is capable of eliciting certain immunogenic response upon implantation; therefore, direct use of this type of collagen is limited. Currently, a purified form of collagen, known as reconstituted collagen, is produced by biochemical processing, which has a lesser immunogenic response that could be used for tissue engineering applications. Collagen implants degrade through cascade of attacks by lysosomal enzymes. The *in vivo* resorption rate can be regulated by control of the density of the implant and the extent of inter-molecular cross-linking. Collagen with low density possesses higher interstitial space and, generally, larger pores for cell infiltration, leading to a higher rate of implant degradation [25]. Intermolecular cross-linking reduces the degradation rate by making the collagen molecules less susceptible to enzymatic attack. Cross-linking can be accomplished by various physical (e.g., UV radiation and dehydrothermal treatment) or chemical (e.g., glutaraldehyde, formaldehyde, and carbodiimides) treatments [34]. Although naturally derived materials have the potential advantage of biological recognition, they cannot be manufactured on a large scale because they are obtained from animals or human. Properties may differ from batch to batch, and obtaining large quantities is often limited due to regulation on animal rights and protection. Furthermore, collagen produced by algae is expensive and time-consuming to produce. Thus, synthetic biomaterials have

been studied widely for large-scale production with control over mechanical properties, degradation rate and microstructures [35].

### Synthetic biodegradable materials

Aliphatic polyesters of naturally occurring α-hydroxy acids, including PGA, PLA, and PLGA, are widely used in tissue engineering. These polymers have gained FDA approval for human use in a variety of applications, including sutures [35-37]. The ester bonds in these polymers are hydrolytically susceptible, and can degrade by non-enzymatic hydrolysis. The degradation products of PGA, PLA, and PLGA are nontoxic, natural metabolites and are eventually eliminated from the body in the form of carbon dioxide and water [1].

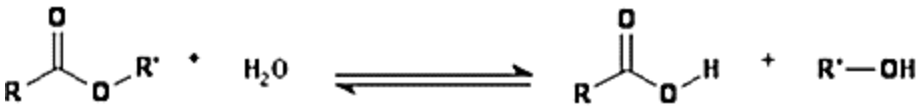


*Figure 2.4: Schematic hydrolysis of an ester group.*

The chemical structures of PLA and PGA are similar, except that the PLA has a methyl pendant group, and this fact contributes to differences in their degradation kinetics. As a result, the degradation rate of their copolymer PLGA depends on the exact ratio of PLA and PGA present in the polymer [38]. PGA is the simplest linear aliphatic polyester and was used to develop the first totally synthetic absorbable suture that has been marketed

as DEXON® since the 1960s by Davis and Geck [5, 6]. PGA is highly crystalline (45-55%) with a high melting point (220-225 $^{o}$C) and a glass transition temperature of 35-40 $^{o}$C [39]. Because of its high degree of crystallization, it is not soluble in most organic solvents; the exceptions are highly-fluorinated organic solvents such as hexafluoroisopropanol [36]. PGA can be broken down in two ways: by hydrolysis and by nonspecific esterases and carboxypeptidases [40]. The glycolic acid monomer is either excreted in the urine or enters the tricarboxylic acid cycle.

PLA has two enantiomeric forms: (i) the left handed (L-lactide) and (ii) the right-handed (D, L-lactide). These two enantiomers have different degradation rates. The L-lactide is widely used for tissue engineering applications, owing to its superior biocompatibility and prolonged biodegradation compared with D, L-lactide. It is a semi-crystalline polymer with a crystallinity of around 37%. The melting temperature is between 173-178 $^{o}$C, the glass transition between 60-65 $^{o}$C, and it possesses good strength and modulus. The D, L-lactide, in contrast, has a low strength and modulus, and undergoes rapid biodegradation in physiological environments [25]. The degradation rate of these polymers can be tailored from several weeks to several years by alteration of their crystallinity, initial molecular weight, ratio of enantiomeric forms (PLA), and the copolymer ratio of lactic to glycolic acid [36, 37]. PLA undergoes hydrolytic scission to its monomeric form, lactic acid, which is eliminated from the body by incorporation into the tricarboxylic acid cycle. The principal elimination path for lactic acid is respiration, and it is primarily excreted by the lungs as $CO_2$ [41].

Since these polymers are thermoplastics, they can easily be formed into a three-dimensional scaffold with a desired microstructure, shape architecture, and dimension by various techniques including spinning [25], moulding, extrusion [1], solvent casting [42], phase-separation techniques [43], and gas-foaming techniques [44].

Other biodegradable synthetic polymers that have been utilised as biomaterials include poly(anhydrides) and poly(ortho-esters) [45].

## 2.2. *Fabrication of polymers for biomedical applications*

Polymers are generally fabricated into 2D or 3D architecture by solution or melt processing. In solution processing, polymers are dissolved or dispersed in appropriate solvents. The solvent is then evaporated to obtain the final product. In melt processing, the polymer is heated above its glass transition or melting temperatures and pushed through a die or into a mould to form the device. Solution fabrication for film is usually done by coating, using wire-bar or doctor-blade coating, spin coating or dip coating.

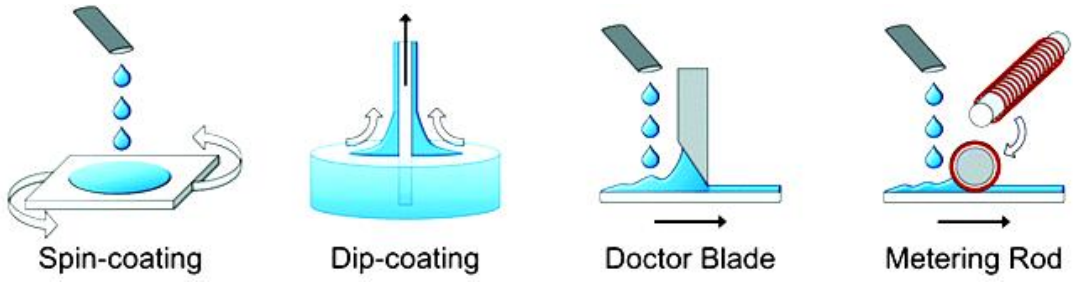


*Figure 2.5: Simple techniques of solution fabrication of thin films showing doctor blade, wire-bar, spin and dip coating [46].*

Spin-coating is widely used for smaller, laboratory-scale research due to its simplicity and high reproducibility. During this process, the substrate is secured to the spin-coater by vacuum, and the solution is applied to the surface. The substrate is rapidly accelerated, which drives solution flow radially outward. A uniform, thin film is left after spinning and solvent evaporation. Dip-coating results in coverage on both sides of the substrate. The substrate is immersed in a solution bath and withdrawn in a controlled manner to coat both sides of the substrate. Other scalable methods for coating a single side include doctor blade coating and wire bar coating, in which a solution is distributed, smoothed, and thinned across the surface of the substrate with a blade or rod, respectively. During doctor blading (knife-over-roll coating), the film thickness is controlled by a gap between the blade and the substrate. Instead of a blade, a wire-wound metering rod can also be used. The thickness here is determined by the diameter and thickness of the wire [46].

***3D solution processing***

Engineering 3D polymers with morphologies similar to tissue ECM is a challenging process and is essential for the success of regenerative medicine and medical implants. The ECM is defined as the non-cellular part of the tissue. The main components of the ECM include glycoproteins (collagen), proteoglycans and hyaluronic acid. However, other molecules can be present, depending on the tissue type; these molecules include hydroxyapatite, fibrin, fibronectin, laminins and serums [47]. Collagen in the ECM is generally fibrous, with a fibre diameter between 50 nm and several microns. The arrangement and orientation of these fibres are tissue-specific, and together with other

matrix components, these properties influence cell behaviour [25]. The use of man-made fibrous scaffolds has been used to mimic the ECM, as it serves as a synthetic ECM and thus should support the cells they accommodate. Cells on these scaffolds should proliferate, migrate and differentiate in this 3D structure, leading to the formation of functional tissues. Fibrous scaffolds can be made of natural polymers or synthetic materials. These have to be biocompatible; that is, they should not invoke or cascade infections, rejection, inflammation and/or immune responses. The scaffold should be porous enough to promote cell seeding, nutrient and oxygen transport, cell-cell interaction, and tissue ingrowth. Sometimes it is also necessary for these materials to be biodegradable to allow full tissue regeneration. The rate of degradation should be similar to the rate of tissue regeneration. It is important that the degradation rate is not faster than the tissue growth. The implant should be strong enough to support external loads and *in vivo* biological forces. Furthermore, these implants have to withstand sterilisation procedures to avoid toxic infections and contaminations. Industrially, these scaffolds should be economical, reproducible and scalable. Various methods of producing 3D scaffolds with all or some of these properties have been investigated. These include solid free forming, phase separation and particulate leaching, and electrospinning. In particular, electrospinning has become a more common method for fibre formation in tissue engineering due to the good control over alignment, porosity and fibre diameter.

### Solid free forming

Complex TE scaffolds are generated by depositing materials in a controlled, layer-by-layer process by using a hierarchical image-based or CAD systems. All solid free forming (SFF) systems use a triangular facet, representative of a unit structure, and build a 3D structure on a movable platform [48]. Available SFF techniques are classified into three major groups. The first group is laser-based machines that photopolymerise monomers or sinter powders. The second group involves direct printing of materials; for example, printing a chemical binder onto a material powder or directly printing wax. The third type is nozzle-based systems in which the material is processed thermally or chemically as it passes through the nozzle. Fig. 2.6 shows basic setups for these systems.

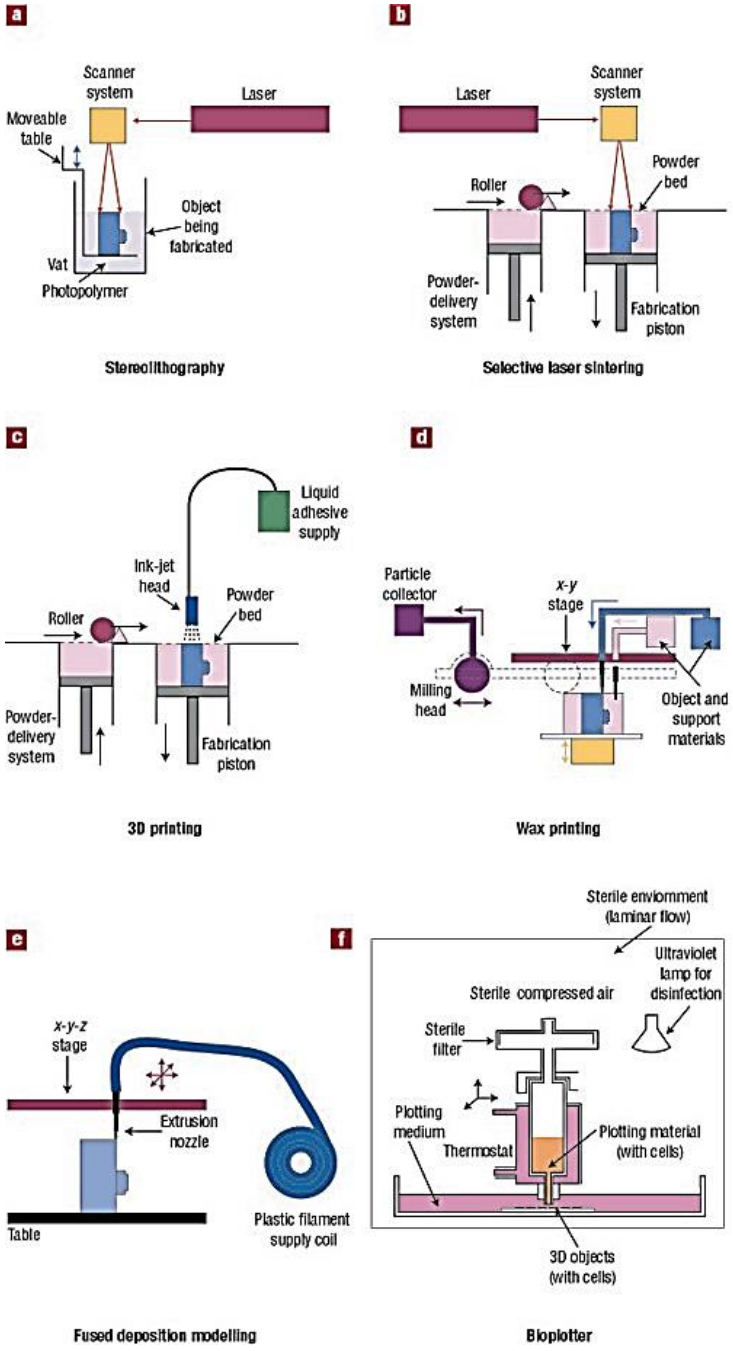


*Figure 2.6: Schematics of SFF systems categorized by processing technique. (a,b) Laser-based processing systems include the stereolithography system, which photopolyermerizes a liquid (a) and the SLS systems, which sinter powdered material (b). In each system, material is swept over a build platform that is lowered for each layer. (c,d) Printing-based systems, including 3D printing (c) and a wax printing machine (d). 3DP prints a chemical binder onto a powder bed. The wax-based system prints two types of wax material in sequence. (e,f) Nozzle-based systems. The fused deposition modeller prints a thin filament of material that is heated through a nozzle (e). The Bioplotter prints*

*material that is processed either thermally or chemically in a sterile environment (f). The Worldwide Guide to Rapid Prototyping (C) Copyright Castle Island Co. All rights reserved.*

These methods have been used to produce porous honeycomb and fibrous structures for tissue regeneration studies, especially in bone and cartilage. Although complex structures can be formed with SFF, this method can be time-consuming [49].

*Phase separation*

Phase separated scaffolds are produced by 5 main steps: raw material dissolution, gelation, solvent extraction, freezing, and drying. The polymer is dissolved in a solvent such as molten phenol, naphthalene [50], or dioxane [51] at a low temperature. Liquid-liquid or solid-liquid phase separation is induced by lowering the solution temperature. Subsequent removal of the solidified solvent-rich phase by sublimation leaves a porous polymer scaffold. One prominent advantage of this technique is the ability to incorporate bioactive molecules into the matrices without decreasing the activity of the molecule due to harsh chemical or thermal environments. A slight change in the parameters, such as types of polymer, polymer concentration, solvent/nonsolvent ratio, and most importantly, thermal quenching strategies, significantly affects the resultant porous scaffold morphology [52]. Chen and Ma produced fibrous PLLA scaffolds with good control over porosity, pore-interconnectivity, pore size, interfibre distance, and fibre diameter. Their aim was to mimic the fibrous architecture of type I collagen and to promote cell seeding throughout the interstices of the scaffold [53]. Yang et al. evaluated the potential of this type of scaffold as a TE implant for culturing

stem cell cells *in vitro*. The fibre diameters ranged from 50 to 300 nm, controlled by the polymer concentration. They observed cell differentiation and neurite growth on these scaffolds [54]. Although the porosity and mechanical properties of these scaffolds could be tuned, the fibres here cannot be aligned, and the steps used to obtain the fibrous structure could be time-consuming.

### *Electrospinning*

Electrospinning has been employed for creating nano- and microfibres used for tissue regeneration and various biomedical applications. Electrospinning can be described by these three stages:

- Initiation of jet and elongation along a straight path
- Growth of bending instabilities and further elongation to allow loops and spiral paths
- Solidification of jets into fibres

The principle of electrospinning is based on forces acting on a droplet of a solution at the tip of a needle. The droplet at the needle tip has a surface tension that causes the droplet to be more rounded to minimise surface area. When an electrical voltage is applied to the tip of the needle, there is an opposite force that acts on the droplet and elongates it. Electrostatic forces are then generated by electrostatic repulsion between the surface charges and Coulombic forces exerted by the applied electric field [55]. As the electric potential is increased, the tip of the droplet elongates until a hyperbolic cone is formed. This cone is known as the Taylor cone (named after the man who initially

discovered it). At even higher electric fields, the electrostatic forces overcome the surface tension, causing further elongation of the droplet to form a jet.

After jet elongation, a region of instability occurs, which is caused by radial charge repulsion. It was first thought that, in this region, the jet stream divided into smaller jets of similar diameter and charge per unit length, known as splaying [56]. However, in 2004, Li and Xia [55, 57] attributed splaying as a poor resolution of bending and whipping fibres. They indicated that under higher magnification and better resolution, the 'splaying' region is actually bent and whipped fibres. The bending and whipping of the fibres is caused by the jet trying to reduce its surface area as well as charge repulsion between the electric field and the charges on the jet surface. Furthermore, at this stage, there is further acceleration and elongation of the fibres, which results in formation of finer fibres [55, 57].

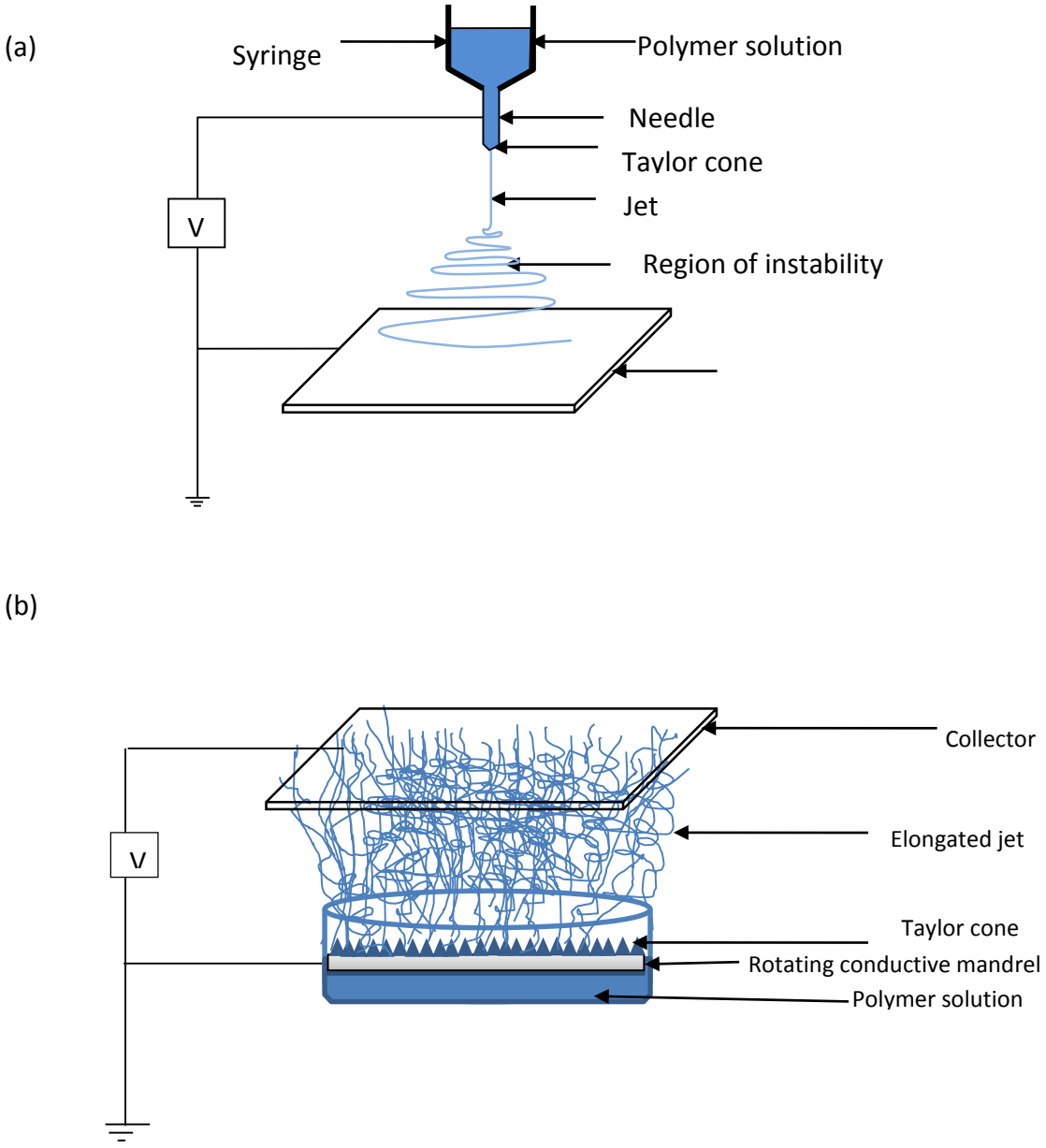


*Figure 2. 7: Schematic of two types of electrospinning setup. (a) represents a simple single nozzle set-up and (b) is the Nanospider© technology with multiple Taylor cones formed a rotating mandrel in the polymer solution.*

Ideally, the electrospinning process should produce long fibres with uniform cross-sectional areas. Beading and wetness of fibres are two main problems associated with electrospinning of fibres. Factors that control electrospinning and fibre morphology can be divided into three main categories: solution properties, operational conditions, and ambient conditions. Solution properties that affect the formation of fibres include viscosity, surface tension, conductivity and dielectric effect of the solvent.

The viscosity of a solution is affected by the molecular weight of the polymers and its concentration in solution. High molecular weight polymers consist of long chains that are entangled. The intrinsic viscosity of polymer in solution is related to the molecular weight by the equation below:

$$[\eta] = K M^{a} \quad (1)$$

where $K$ is a constant that depends on polymer and solvent properties and $a$ is a constant of approximately 3.4.

When a jet is formed, the presence of entanglements in the solution allows continuous stretch of the solution. At low molecular weight, there are fewer entanglements and thus the formation of short fibres or droplets occurs. The specific viscosity, which is dependent on concentration, is given by the equation:

$$\eta_{sp} = C [\eta] = K C M^{a} \quad (2)$$

This indicates that an increase in polymer concentration will cause an increase in viscosity, which enhances the formation of fibres. The type of solvent has also been shown to affect the viscosity of solution. This effect has been factored into the $K$ present

in the intrinsic viscosity equation. Alfrey et al. [58] showed that intrinsic viscosity is high in a ‘good’ solvent and low in a ‘bad’ solvent. It is important to note that an increase in specific viscosity will also increase the diameter of the fibres formed. Furthermore, at very high viscosity, it is almost impossible to draw the solution into the syringe, and the polymer solution dries very quickly at the tip of the spinneret. This will cause the formation of an unstable and discontinuous jet [59]. Although viscosity is the physical effect of increasing molecular weight or concentration, the formation of continuous fibres is controlled by having a viscoelastic solution. Therefore, chain length and entanglements are very vital, and these characteristics have significant impact on whether the jet will break into droplets or beaded fibre morphology. Thus, monomeric solutions do not form continuous fibres, regardless of concentration or viscosity [60, 61].

Another solution property that affects electrospinning is the surface tension. This is mainly characterised by the type of the solvent. As mentioned in the above section, for a jet to form, the charges on the solution surface have to be high enough to overcome the surface tension. Thus, a solvent with a high surface tension will facilitate the formation of beads to reduce its surface area. Surface tension of the solution is controlled by the surface tension of the solvent molecules. At high solvent concentrations, more solvent molecules are in contact with each other and form a spherical congregate due to surface tension. At low solvent concentration, the solvent molecules distribute evenly over the polymer chains with less solvent-solvent interaction.

An increase in conductivity of the system increases the charge density on the surface of the solution and this is also dictated by solvent type. However, the addition of ions to the solution can increase the conductivity of the system, and hence decrease the voltage needed to form a jet. The dielectric constant of the solvent also has a significant effect on the electrospinning process. Research by Son et al. [62] and Lee et al. [63] discovered that a high dielectric constant of solvent reduces the probability of forming beads and thick fibres. The dielectric constant of a solvent is related to the polarisability of the solvent.

The voltage for electrospinning has to be high enough for the solution to accumulate charges on the solution surface. This is important so that the electrostatic forces overcome the surface tension. The optimal voltage depends on factors such as feeding rate and surface tension. When voltage is too high for a given solution and feeding rate, a small Taylor cone is formed [59]. High voltages also result in more stretching at the elongation region, forming finer fibres [64]. At even higher voltages, the cone recedes into the needle and discontinuous fibres or beads are formed [65]. Another report showed that an even further increase in voltage resulted in joining of beads which formed thicker fibres [66].

High voltages can also affect the orientation of the molecules in the polymer fibre. The electrostatic field can generate order in the polymer fibre, inducing crystallinity. However, above a certain voltage, crystallinity reduces, and this has been attributed to short flight time. Orientation of molecules takes time, and thus a short flight time means that fibres will be deposited before the jet has time to align [67]. The jet path is also

determined by the external electric field between the source and collector. The collector is normally made of a conductor like aluminium foil. The collector is also grounded to maintain a stable electric field. This electric field can be used to manipulate the orientation and direction of fibre when collected [68]. For example, fibres align in between two charged electrode-collector separated by a gap. The electrodes generally have a slight bias opposite to that of the nozzle.

DC voltage has been used mainly for electrospinning; however, few researchers have also utilised AC voltage. The charging of solution is generally very rapid, and therefore jet initiation occurs before the voltage alternates. However, different segments of the fibres will have positive and negative charges on them. This helps to reduce repulsive forces between the jets and reduces bending instability. Also, there is a low tendency of charge accumulation when AC is used, and therefore thicker fibre mats can be collected in a localised region [69].

At a constant voltage, the feeding rates also affect fibre formation and morphology. Increase in feeding rate causes an increase in fibre diameter, as well as an increase in beading size. Beading occurs at a high feeding rate due to a decrease in charge versus polymer ratio and the greater volume of solution that is drawn from the needle tip [59]. At large fibre diameters, the fibres may not have enough time to dry, and fusion can occur due to the presence of residual solvent [70]. Also, at very low feeding rates, the stream becomes discontinuous and results in the formation of short fibres. Therefore, for a change in feeding rate, there must be a corresponding change in voltage applied.

Temperature and humidity are the main environmental factors that affect morphology of electrospun fibres. Temperature affects the viscosity of the solution and evaporation of the solvent. Increase in temperature reduces the viscosity of the solution and thus the associated effects mentioned above. High temperature also aids in the evaporation of solvent in flight, and thus prevents splashing of polymer upon reaching the collector. However, it is important to always work below the glass transition of the polymer; otherwise, splashing still occurs due to polymer flow. Furthermore, when incorporating biological molecules into fibres, it is important to choose an appropriate temperature so as to not destroy these molecules [71].

Increase in ambient humidity typically forms porous fibres [72, 73]. These groups studied the effect of humidity on polysulfone in tetrahydrofuran solvent. It was observed that relative humidity above 50% resulted in the formation of fibres with pores on the surface. The size of these pores increased with further increase in humidity, while above a certain level of humidity the size and depth of the pores begin to saturate [74]. Humidity also affects the rate of evaporation of solvent; high humidity lowers the rate of evaporation. This results in in more whipping and stretching of the jet. This is due to higher mobility of polymer chains with higher residual solvents. Low rate evaporation also causes the production of wet fibres, resulting in splashing and coalescing of fibres. Very low humidity can cause clogging of the needle tip due to the high evaporation rate of solvent [75]. High humidity also causes discharging in the electrospinning jet [76].

Pressure and type of atmosphere have not been studied widely; nevertheless, some researchers have shown the effect of these parameters on electrospinning. At low

pressures below atmospheric pressure, the solution flows out easily through the needle and hence a less stable cone and jet results. Low pressure also causes discharge of the electrical charges. When the gas content of the atmosphere is changed, different fibre morphologies are formed. Baumgarten [75] showed that gas with low breakdown voltage does not promote electrospinning. Gases like Freon-12 with high breakdown voltage as compared to air form fibres with larger diameter.

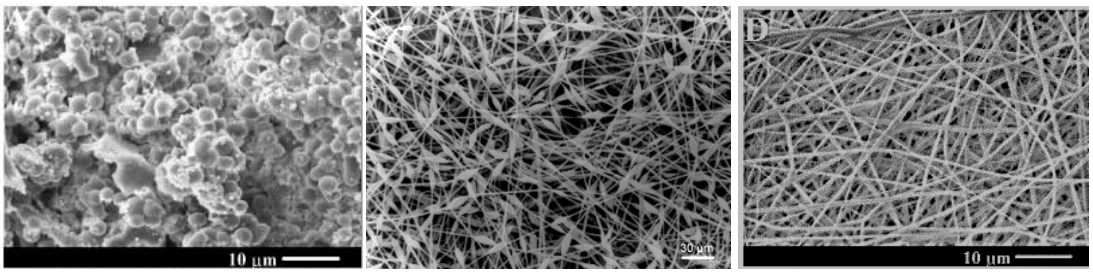


*Figure 2.8: Electrospun polymers with beads (a), beads-on-string (b) and continuous fibre morphology (c) [59, 77].*

Melt processing of microfibers, shown in Fig. 2.9, has been explored widely in manufacturing sutures. Polymer pellets are fed through a hopper into a spinning vessel. In the spinning vessel, the pellets melt as a result of the heating elements, and the melted mass passes through a melting grid and is collected on the pool. The melt is then pumped through the spinneret. The melt solidifies as it passes through a cooling chamber in which cold air current is swept across the filaments.

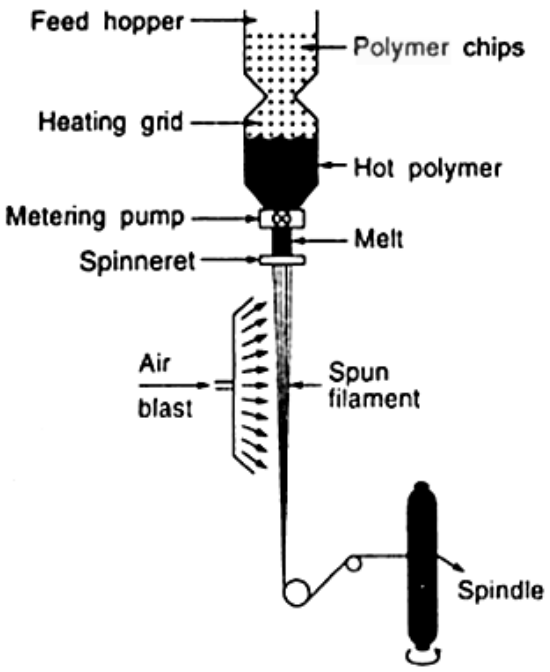


*Figure 2.9: Melt fibre spinning [78].*

## 2.3. *Cell response to textured films*

Surfaces of synthetic polymers have been modified by chemical or physical functionalization to improve biocompatibility. Chemical modification can be achieved via plasma or wet chemical treatment, grafting and layer by layer deposition [79], shown in Fig. 2.10. Appropriate selection of the plasma source enables the introduction of various functional groups on the target surface to improve biocompatibility or to allow subsequent covalent immobilization of various bioactive molecules. For example, typical plasma treatments with oxygen, ammonia, or air can generate carboxyl groups or amine groups on the surface [80-83]. A variety of extracellular matrix protein components such

as gelatin, collagen, laminin, and fibronectin can be immobilized onto the plasma-treated surface to enhance cellular adhesion and proliferation [84, 85].

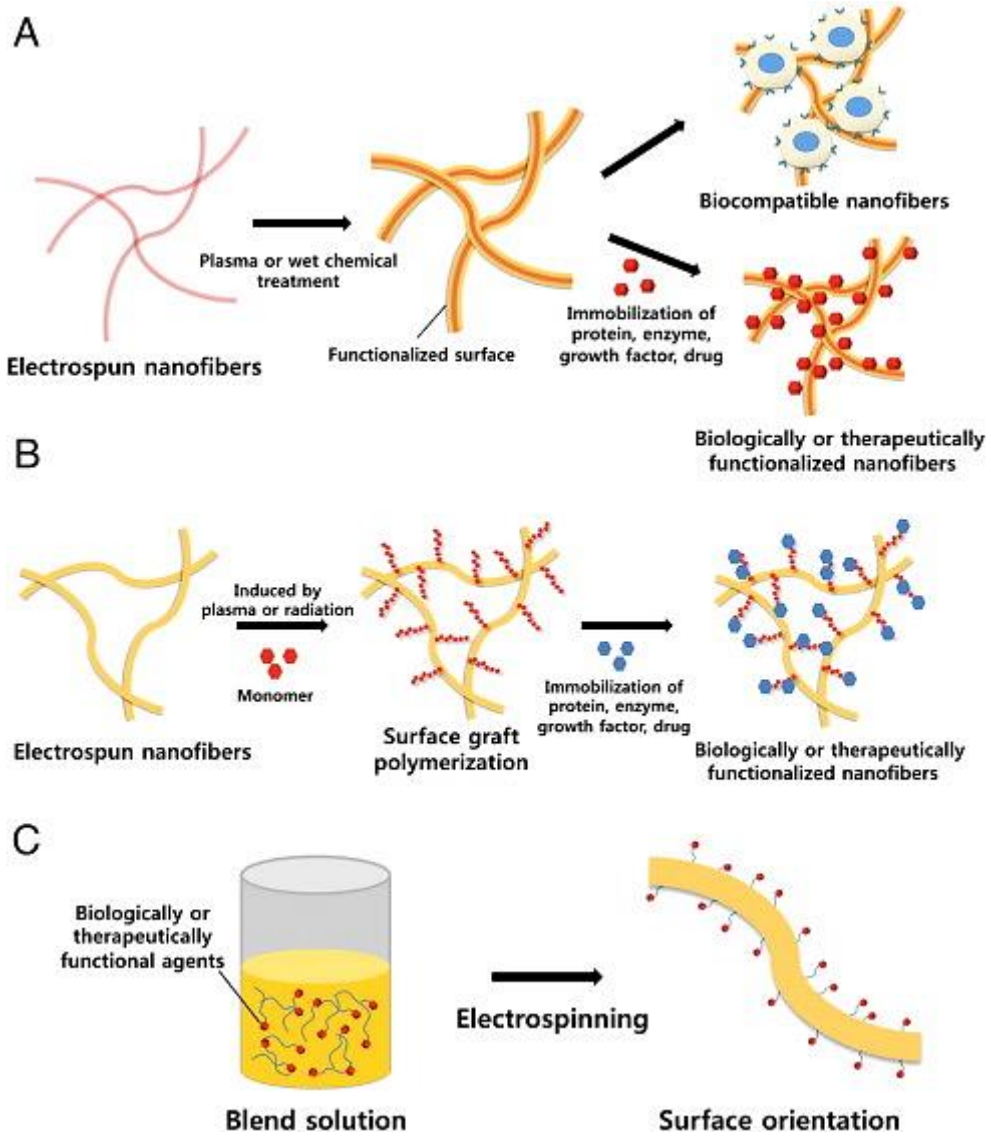


*Figure 2.10: Surface modification of electrospun fibres. (A) Plasma treatment or wet chemical method. (B) Surface graft polymerization. (C) Co-electrospinning [79].*

Cell attachment and proliferation also strongly depends on the physical properties of the scaffold surface. Materials with surface topography can be divided into roughness

and texture. Roughness is associated with non-standardised discontinuities, whereas texture is controlled standardised patterning [86]. Effect of surface topography on cell behaviour was first studied by Harrison in 1912. He observed that the direction of cell movement was affected by linear spiderweb threads [87]. The term 'contact guidance' was coined by Weiss in 1945 when he performed experiments on different types of substrates. He observed changes in cell behaviour with different substrates [88]. Work on topographical control of cells was resumed in the 1970s by Maroundas [89] and Rovensky et al. [90]. Since then, extensive work has been performed on textured surfaces for medical implants. The hypothesis was that microtexture on implants can benefit tissue regeneration due to their structural resemblance to natural ECM networks [91, 92]. Cell response to textured surfaces depends on cell type, shape of groove or protrusions, and dimensions. Anchorage-dependent cells like osteoblasts and vascular cells respond to textured surfaces by changing their adhesion, migration and alignment on the surface [93-95].

Downing et al. [96] developed a textured substrate analogous to the topographical interface found between the epidermis and dermis: the basal lamina. Collagen membranes have grooves of 50–200 μm in depth and width between 50-400 μm. These are dimensions that are similar to the invaginations found in basal lamina at the dermal - epidermal junction of native skin. They seeded keratinocytes on the surfaces of basal lamina analogs, and histological analyses were performed after 7 days of tissue culture. The keratinocytes formed a differentiated and stratified epidermis that conformed to the features of the microtextured membranes. Morphometric analyses of

immunostained skin equivalents suggest that keratinocyte stratification and differentiation increases as channel depth increases and channel width decreases.

Steinberg et al. [97] used PDMS pillars designed in arrays with a pillar head diameter of 5 µm, a height of 15 µm, and different pillar interspaces, namely 14, 11, and 8 µm, shown in Fig. 2.11. Decreasing distances of 11 and 8 µm revealed cytoplasmic extension of the early differentiation marker K1 on PDMS pillars. The most cytoplasmic K1 protein distribution was noted on the smallest pillar scale, and this correlated with higher ratios of K1 mRNA gene transcription [97].

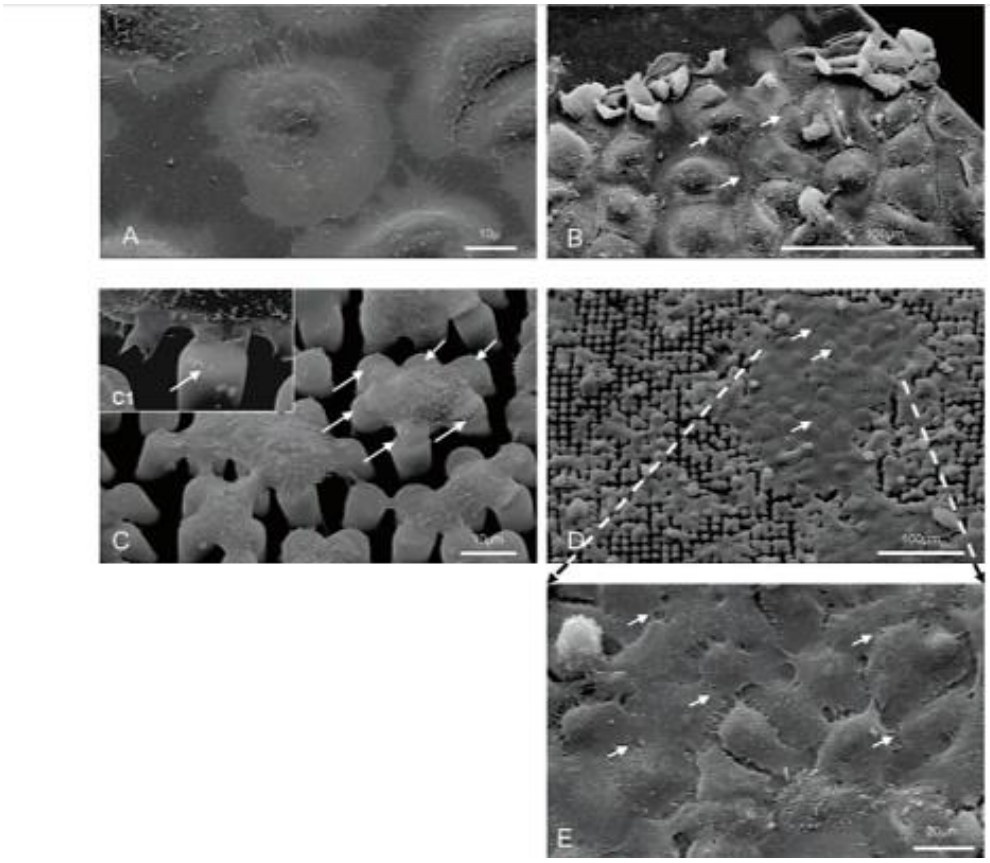


*Figure 2.11: SEM pictures of IHGKs on glass or micropillar surfaces. (A) Single IHGKs on a glass slide exhibiting proper adhesion and cell-to-cell interconnections. (B) A nearly confluent IHGK layer on FN-coated glass surface. The cell-to-cell interconnections are marked by arrows; bar corresponds to 100 µm. (C) IHGKs on a FN-coated micropillar array, with pillar head interspaces of 8 µm, and a single keratinocyte covering seven pillars (see arrows). The inlay (C1) shows a high-magnitude section of IHGK adhesion structures on a pillar head (see arrows); bar corresponds to 10 µm. (D) FN-coated micropillar array with a pillar head distance of 8 µm. The section shows IHKGs forming an island with cell-to-cell interconnections (see arrows); bar corresponds to 100 µm. For better visibility, Figure 11E provides picture section high-resolution magnification of cell-to-cell interconnections; bar corresponds to 20 µm [97].*

Dunn and Brown [98] demonstrated the relationship between groove depth and fibroblast cell morphology. They showed that cell alignment and elongation are determined by groove depth. The cells cultured in groove depth between 0.2 and 1.9

μm had an effect on fibroblast and epithelial cell elongation and migration. Green et al. [99] showed high growth rate of faces with pillars rather than wells.

Groove width, rather than depth, has been identified as the important parameter that affects cell adhesion [91, 100]. Meyle et al. [91] suggested that focal adhesions are preferably positioned on top of the ridges rather than in the grooves and are dependent on the width of the groove or ridge.

*Table 2.1: Overview of cell culture on textured surface*

| Cell Type | Surface property | Results | References |
|---|---|---|---|
| Human gingival fibroblasts | Square grooves 1 µm width and 1 µm depth on PDMS | Vinculin-positive attachment sites observed; cells aligned to grooves in PDMS, which had been made hydrophilic by glow discharge treatment; focal adhesion contacts also aligned to grooves | [101] |
| Human skin fibroblast | 2,5,10 µm widths and 0.5 µm depth on PDMS | Cell proliferation was higher on the 2 and 5 µm widths | [102] |
| Rat dermal fibroblasts | Square grooves 2,5,10 µm width and 0.5 µm depth<br><br>2,5,10 µm grooves with 0.5 µm depth | 2, 5 µm grooves induced stronger orientation than 10 µm grooves<br><br>Microfilaments and vinculin aggregates oriented along 2 µm grooves after 1, 3, 5, and 7 days, but was less oriented on 5 and 10 µm grooves; vinculin located primarily on surface ridges | [103]<br>[104] |
| Human dermal fibroblast and human umbilical artery smooth muscle cells | Different types of parallel groove shapes on collagen fibrillar hydrogel. V shape and truncated V with 2 µm groove depth. A holographic grating (sinusoidal) with 1 µm depth. | Alignment was enhanced on the all-grooved surface. The v and truncated v shaped grooves showed better cell alignment | [105] |

| | | | |
|---|---|---|---|
| Human abdomen fibroblasts | Square wells and nodes with 2,5 and 10 µm in diameter with a height of 0.5 µm on PDMS substrates | Cells on the 2 and 5 µm nodes had a higher cell proliferation compared to the well counterparts. The 10µm substrates had similar effects as smooth surfaces | [99] |
| Foreskin human keratinocytes | Groove textured collagen with width 50-400 µm and depth between 50 and 200 µm | Keratinocyte stratification and differentiation increased with decrease in width and increase in depth. The best substrate was the one with the highest aspect ratio, 50 µm wide and 200 µm deep. | [96] |
| human gingival keratinocytes | Pillars with 5 µm pillars with 8,11 and 14 µm inter-pillar distances | Cell-cell interactions were tighter with the low inter-pillar distances. Differentiation markers and genes were significantly higher in the 8 µm distances; 4 folds higher than that of the 14 µm | [106] |
| Bovine corneal epithelial cells | 1,2,5, and 10 µm width with 1 and 5 µm depth | Cell alignment observed on all textured substrates. Highest alignment on the 2,5 µm wide substrates.<br>Migration was slower on the 5 µm deep samples. Area and distance of migration was low. | [107] |
| Bovine aortic endothelial cells | 200 nm,500 nm, 1 µm and 5 µm depth with 8 µm pitch | Increase in depth corresponded to increase in aligned cell percentage. Alignment in the 1 µm deep samples was observed until confluence. No significant change in proliferation was observed. | [108] |

Physical changes to the surface of electrospun fibres have been created through pore formation or creating a bead-on-string morphology, achieved by high surface energy. Solid phase separation can cause the formation of porous fibres without the need of extracting one component. This is achieved by using appropriate solvents and favourable ambient conditions. Solvents with high volatility cause the formation of pores on electrospun fibres. During solvent evaporation, the solution becomes thermodynamically unstable, and phase separation leads to a polymer-rich and a polymer-lean phase. The polymer-rich region solidifies more quickly after phase separation and forms the matrix, whereas the polymer-lean phase forms the pores. Another mechanism to be considered in the formation of porous electrospun fibres is that recently described by Srinivasarao et al. [109]. Porous fibre surfaces occur as a result of evaporative cooling due to rapid solvent evaporation, thereby significantly cooling the surface of the electrospinning jet as it travels from the syringe to the target. As the surface cools, moisture in the air condenses and grows in the form of droplets. The droplets remain as individual entities acting as hard spheres due to convection currents on the surface of the jet. As the jet dries, leaving dried fibres, the water droplets leave an imprint on the surface of the fibres in the form of pores as shown in Fig. 2.12 [72]. Both high humidity and low solvent vapour pressure have been found to promote this effect of pore formation [72, 73, 110].

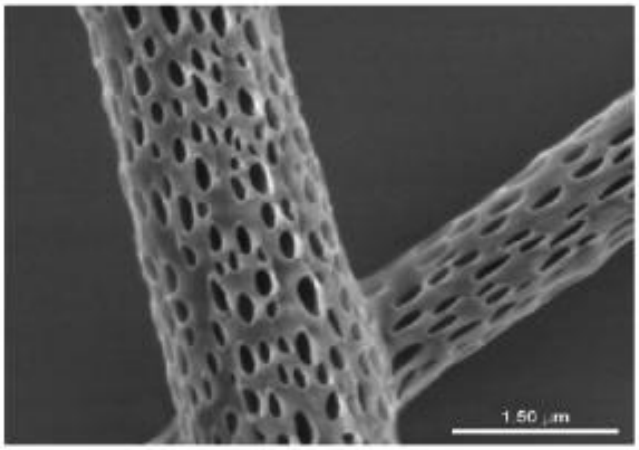


*Figure 2.12: Pores formed in an electrospun fibre [73].*

Moroni et al. [111] studied the effect of porosity on morphology and proliferation of human mesenchymal embryonic stem cells. They observed that nanopores in a 10 µm fibre enhanced cell spreading and proliferation of the cells compared to smooth nanofibres. Self-crimping fibres with wavy morphology have also been created using a thermal treatment to simulate the natural morphology of ECM fibres. These fibres enhanced fibroblast proliferation and matrix synthesis [111]. Xia and Li [76] also demonstrated that porous fibres can be formed by coaxial spinning of two immiscible polymers in a common solvent. The miscibility of the solvent with both polymers can cause one component to be embedded in the other during solvent evaporation. The embedded component can be extracted to form porous fibres. So far, surface texturing of electrospun fibres has not been achieved due to limitations of traditional surface texturing techniques.

## 2.4. Surface texturing techniques

### *Common surface texturing techniques*

Photolithography texturing is achieved by pattern exposure of a photoresist to UV light through a photo-mask. The polymer is coated with a primer and then a photoresist that is exposed to the UV via a photomask with the desired pattern. This is followed by an etching step at the exposed region (negative) or the non-exposed regions (positive). Etching is done by chemicals (wet) or by ion beams or ions derived from plasma (dry); higher resolutions are achieved with dry etching. The resolution of the photolithographic process determines the width of the channels. In most photolithography, UV light is used, and thus texturing with a photomask with spacing less than half the wavelength of UV (250 nm) results in blurred and fused features. Some work has been performed to achieve resolutions on the order of 70 nm [112, 113]. This has been accomplished by changing the radiation source from UV to X-rays or extreme UV light [113]. However, for polymers, these high-energy radiations can lead to damage or degradation of the material. Thus, instead of using photomasks, interferometric patterning of silicon wafers has been used to achieve nanoscopic textures on large surface areas. This is known as holographic or interference lithography [114]. In this method, two coherent beams are overlaid to generate constructive and destructive interference, giving dark and bright exposures.

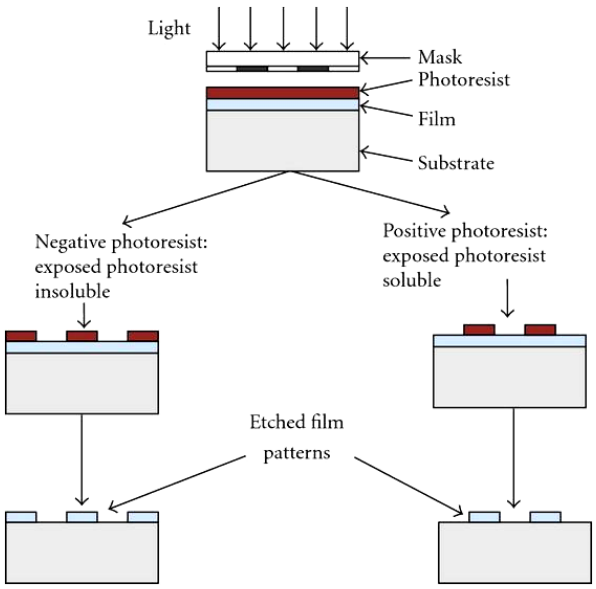


*Figure 2.13: Basic photolithography setup [115].*

Other methods that have been used to produce surface-textured polymers include soft lithography and thermal embossing. In soft lithography, a pre-polymer or a polymer solution is casted in a mould or on a stamp surface. This is followed by the solidification through polymerisation or solvent removal. Examples of soft lithography include replica moulding (REM), microtransfer moulding, micromoulding in capillaries (MIMIC), and solvent-assisted micromoulding (SAMIM) [116]. Fig. 2.14 shows schematics of these techniques.

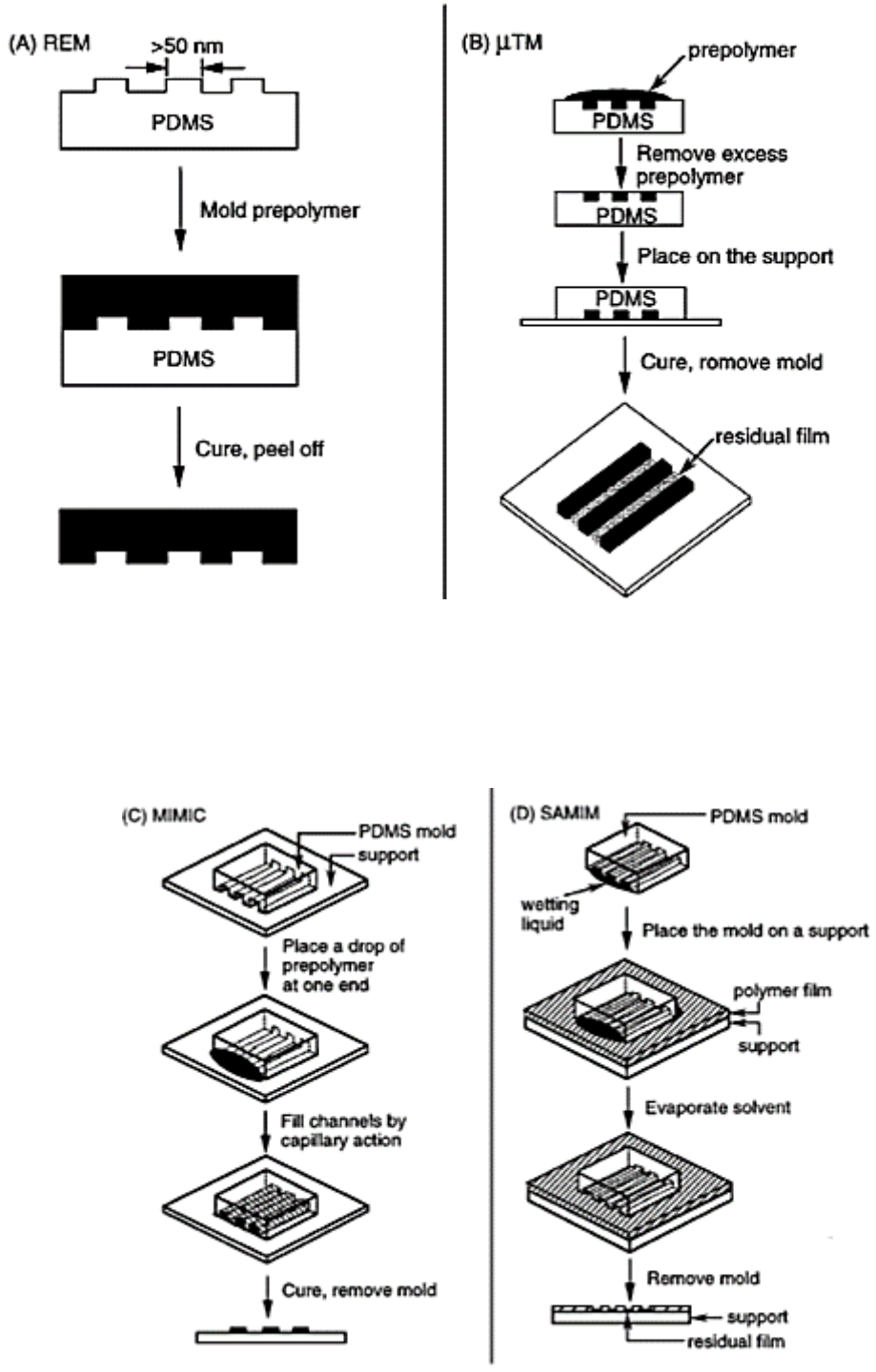


*Figure 2.14: Schematic of replica moulding and micro transfer moulding [116].*

Thermal embossing uses a rigid mould to form microstructures by imprinting the mould on the surface of a thermally-softened polymer. The softened polymer can also be injected into a mould cavity; this is known as injection moulding. In injection moulding, a thermoplastic material, usually in granulate or powder form, is placed into a cylinder that is kept at a constant temperature by electric heating elements. The material is transformed into its molten state by heat transfer from the cylinder wall. Since polymers are poor heat conductors, the heating is performed over a long period of time, and thus care must be taken not to degrade the polymer. When the material is sufficiently heated, it is plunged through a narrow nozzle under high pressure into a mould cavity. In the cooled mould, the polymer cools down under pressure and is ejected after solidification. This method can also be used on rubbers and thermosets. Here, the mould is heated rather than cooled to promote vulcanisation or curing. This technique has been used to make CDs based on imprinting on polycarbonate with a nickel master mould for commercial application [117]. Recently, these two techniques have been used to form textures with lateral dimensions < 50 nm in microelectronic circuitry [118].

a)

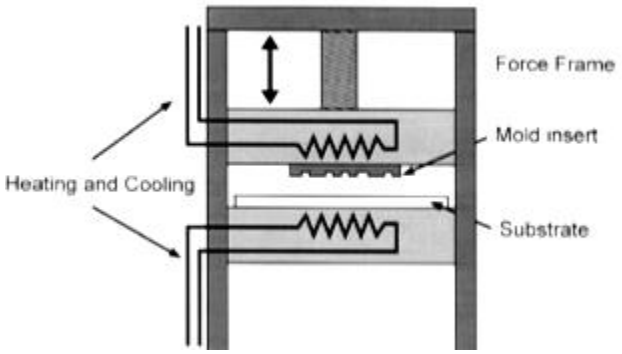


b)

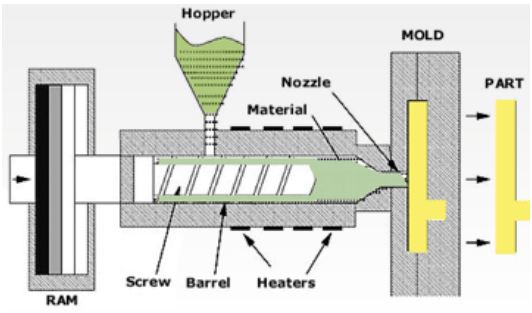


*Figure 2.15: An example of a thermal embossing(a) and injection moulding (b) setup [119].*

### Photoembossing

Photoembossing has become an important technique to form relief structures due to the following advantages over general lithographic techniques: 1) it does not need an etching or solvent removal step, 2) it does not require expensive complex moulds, 3) it is faster than other techniques. Photoembossing uses a photopolymer with a blend of multifunctional monomer, polymeric binder and a photoinitiator [120]. This process of creating relief structures entails four steps shown in Fig. 2.16.

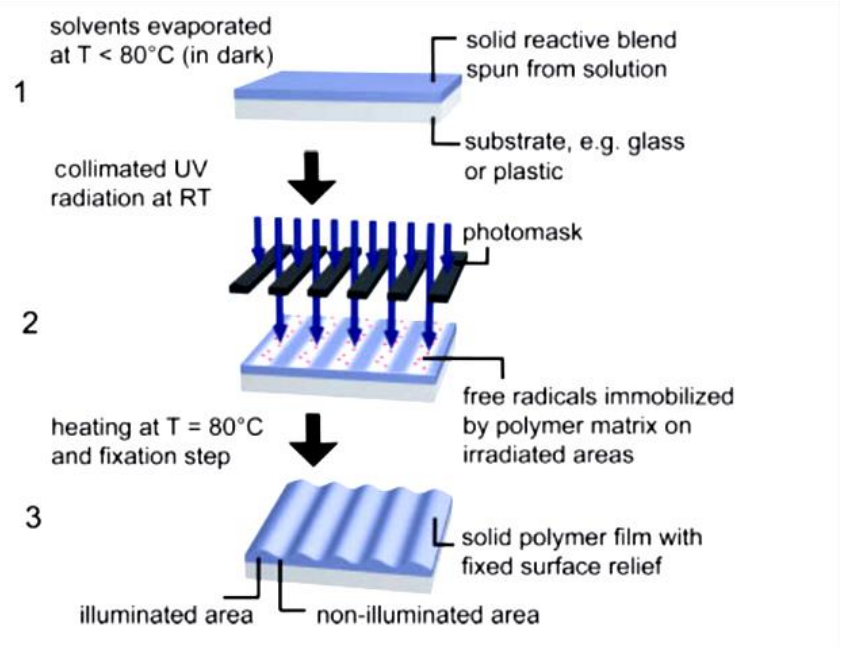


*Figure 2.16: The steps of photoembossing [120].*

Initially, a photopolymer blend containing a monomer, polymer binder, and a photoinitiator is dissolved in an appropriate solvent. The solution is then processed into a film and the residual solvent is evaporated. The sample is exposed to patterned UV radiation via a contact photo mask. This radiation activates the initiator, which catalyses the formation of radicals in exposed areas. During a thermal processing step, polymerisation of monomer in the illuminated areas generates a chemical potential and concentration gradient between the exposed regions and non-exposed regions, which results in the diffusion of monomer from non-exposed to exposed regions. The resulting increase and decrease in mass in exposed and non-exposed areas creates the surface relief structures [121]. After the diffusion stage, the structure is exposed to UV again without the mask at elevated temperature to fully cure all the monomers [120, 122-

125]. Instead of a contact photo-mask, an interference pattern of two coherent beams generated with a pulse or continuous laser can also be used for the patterned exposure [126].

The main drawback of photoembossing is the formation of relief structures with low aspect ratio in comparison with lithographic techniques. Changes in photopolymer composition and processing parameters have been studied to optimise relief heights [120, 124]. UV dosage and processing temperature are the two main processing parameters that affect the photoembossing process.

***Processing parameters***

Irradiation of the photopolymer film generates radicals that are immobile at room temperature, similar to the monomer. This is due to the glassy nature of the photopolymer blend. Heating enhances diffusion, and polymerisation occurs at the irradiated areas. The chemical potential and composition gradient triggers the diffusion process. In addition, local shrinkage in the exposed regions creates free volume in these area and promotes diffusion [120]. At low dosages, a very small amount of the photoinitiator is activated, resulting in a low conversion of monomer and thus low relief structures. The relief structures formed here are sinusoidal. At the optimum dosage, an optimum height is achieved, above which, the height begins to decrease, the shape changes, and two peaks begin to appear at the edges of the illuminated area as shown in Fig. 2.17.

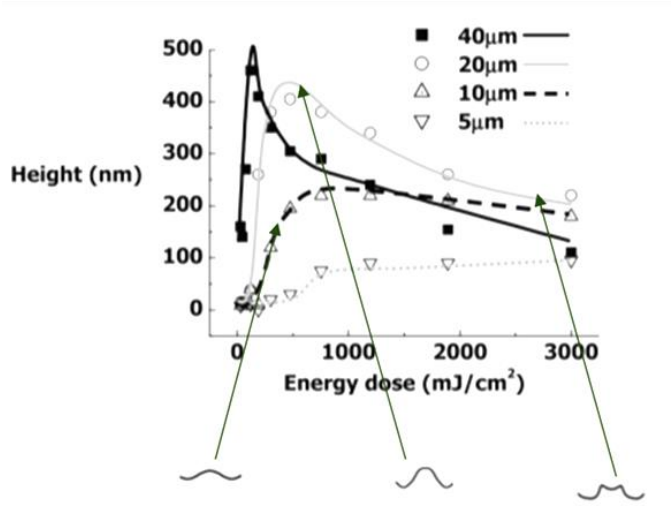


*Figure 2.17: Effect of UV dosage on resultant relief structures [120].*

The diffusing monomers do not reach the central part of the exposed areas, as diffusion is hindered by the high crosslinking density. Thus, the monomers react mainly at the 2 edges of the exposed areas, resulting in double peaks. Sanchez et al. [120] explained that in this case, the balance between the diffusion and polymerization kinetics is in favour of polymerisation. The same shape trend is observed as the period decreases. It was also noted that the optimum height is observed at higher energy doses for these smaller periods. Since the lateral dimensions are smaller, the appearance of the side shoulders requires higher degrees of crosslinking to hinder monomer diffusion to the central part of the exposed area and to produce accumulation of material in the lateral side of the exposed area. This demonstrates that the typical diffusion length of monomer is within the range of the periodicity of the structures and can be accurately

controlled by the degree of curing. Note also that lower relief heights (at optimum dose) are obtained for smaller pitches. The energetic cost derived from the generation of new surface area [10] could explain this, since a decrease of the pitch at the same height would lead to the generation of more surface, which is expensive in terms of energy [120, 127].

Sanchez et al. [101] also studied the effect of the developing temperature on the height and shape of a photopolymer film. An optimum temperature was also observed in their system. An increase in temperature enhances diffusivity of the monomer and thus favours migration to the illuminated regions. However, at very high temperatures, above the optimal, there is a decrease in height and this was attributed to unwanted diffusion paths of monomers. At these high temperatures, the monomers migrate to both illuminated and non-illuminated regions due to high mobility, and this reduces the driving force for diffusion [120]. This effect was more pronounced in the films with small pitches. Their topographic analysis also showed that double peaks observed at the edges and caused by high UV dosages, disappeared with higher processing temperatures. This resulted in a more rounded shape due to an increase in monomer mobility [120].

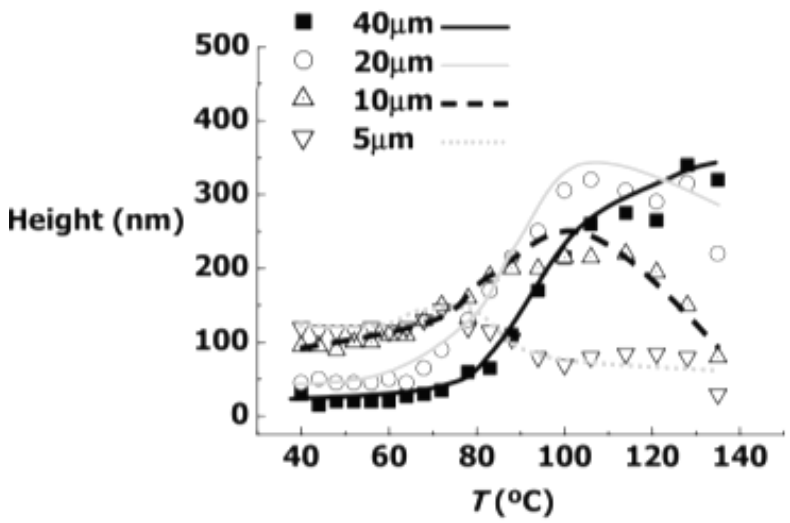


*Figure 2.18: Effect of processing temperature on relief heights. Each curve represents a different pitch size [120].*

***Photopolymer composition***

The role of the monomer in photoembossing is very important because this is the reactive and diffusing species. It is therefore logical to say that increasing the monomer content will result in high aspect ratios. However, Sanchez et al. observed that photopolymers with a very high monomer content resulted in the formation of tacky and turbid samples caused by partial phase separation, undesirable for the photoembossing process [120]. At low monomer content, less material is available for the diffusion-polymerisation process, and the samples become less-plasticised, hence reducing the mobility of the monomer [120, 128, 129]. To date, the selection of monomer types in photoembossing has been rather arbitrary; in the latter part of this thesis, the effect of monomer and polymer type is evaluated. Sanchez et al. also observed that increasing the thickness of the sample resulted in higher aspect ratios,

especially for large pitches. This was because more monomer is able to participate in the diffusion process. However, there was no obvious effect of thickness on low pitches. This showed that, in general, the thickness of the photopolymer does not contribute to the relief formation to the same extent. The lower layers of the photopolymer have a minor influence on relief generation when the lateral dimensions are similar to or larger than the thickness of the film [120].

Another important component in the photopolymer system is the photoinitiator. The concentration of the initiator dictates the volume of radicals generated. At constant UV dosage, it has been shown that the optimum initiator concentration is reached at low content for large pitches. Sanchez et al. showed that for a 40 µm pitch, the optimum initiator concentration was 1 wt.%. At concentrations above this, the height decreases again and two peaks begin to appear. For smaller pitches, the relief height increases photoinitiator content, although this trend is less marked for smaller pitches. These results are qualitatively identical to those found for the energy dose pitch library. In both cases, there were libraries with a gradient in radical concentration; optimum radical concentration gives rise to a nearly sinusoidal profile with optimum height. Above this optimum concentration, the high crosslink density hinders the diffusion of monomer to the central part of the exposed areas, resulting in lower heights and the appearance of double peaks at the exposed area [120].

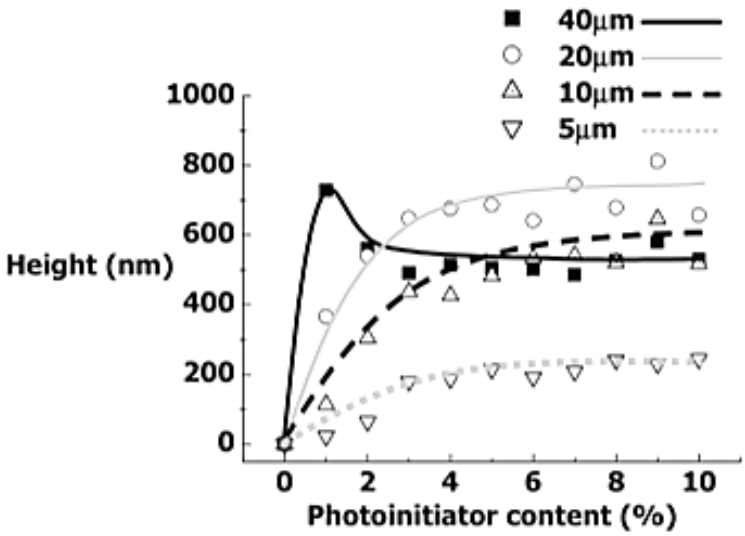


*Figure 2.19: Effect of photoinitiator concentration on height of photoembossed relief structure [120].*

Researchers have also found that the addition of chemicals that control the polymerisation kinetics can increase the height of relief structures [129][111][130]. Hermans et al. [129] showed that the retarder/inhibitor t-butyl hydroquinone (TBHQ) increases the aspect ratio by a factor of 7 in the absence of oxygen. The presence of this inhibitor/retarder reduces the rate of polymerisation, allowing more diffusing species to reach the illuminated regions. Furthermore, TBHQ forms a metastable compound with the initiator radical and temporarily reduces the number of free radicals. These reactive species are reactivated again during the heating step, when the structures are being formed, and thus increase the number of free radicals. The increased number of radicals enhances the consumption of monomer and upon heating increases the driving force for diffusion. Thus, TBHQ becomes a latent initiator that controls the kinetics of the

polymerisation, while at the same time preserving all of the activation sites. TBHQ is only effective in inert atmosphere as ambient oxygen reacts with it [129].

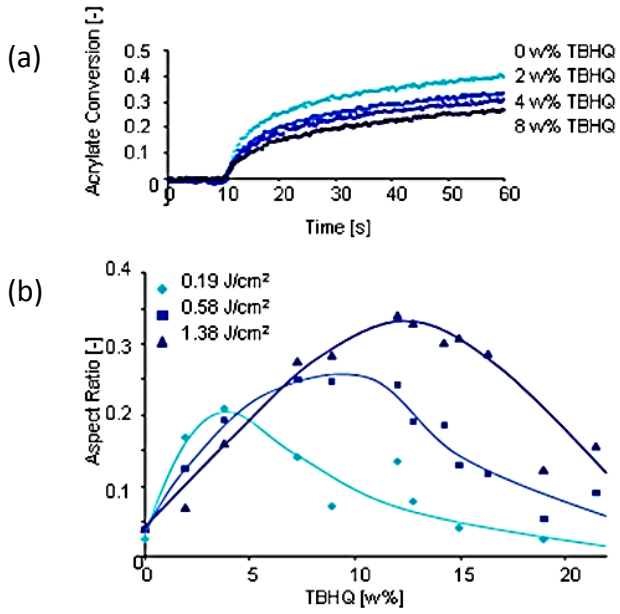


*Figure 2.20: Effect of TBHQ on acrylate conversion (a) and aspect ratio of photoembossed structures (b) [129].*

In Fig. 2.20a, increase in TBHQ content results in a decrease in the acrylate conversion rate. This decrease in conversation rate resulted in a higher aspect ratio of relief structures until an optimum TBHQ concentration was achieved. Above this concentration, TBHQ behaves more like an inhibitor rather than a retarder, and therefore reduces the driving force for diffusion [126].

Perelaer et al. [111] utilised reversible addition-fragmentation chain transfer agent (RAFT) to increase aspect ratios by the same mechanism as TBHQ. However, these molecules do not react in ambient air, and thus an inert atmosphere is not needed. They showed that the presence of RAFT increases the aspect ratio of the relief structure. The

optimum height attained with increasing RAFT concentration is coupled with increase in UV dose [130]. Fig. 2.21 shows the effect of the RAFT agent on the aspect ratio at different concentrations at ambient and inert atmosphere. No significant difference is observed between those processed in ambient or inert atmospheres [130].

(a)

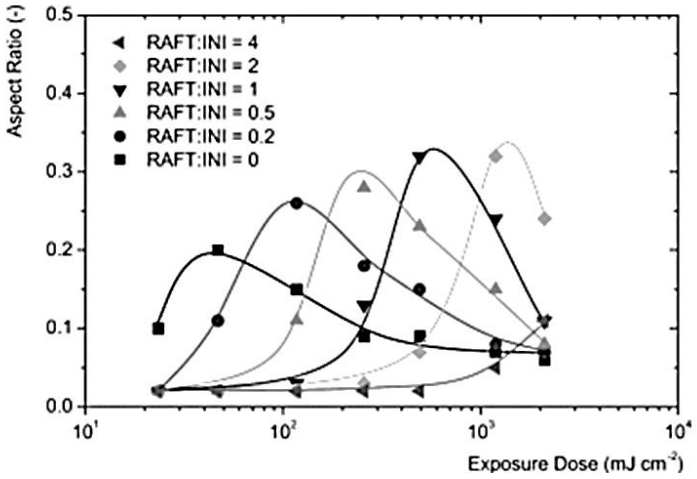


(b)

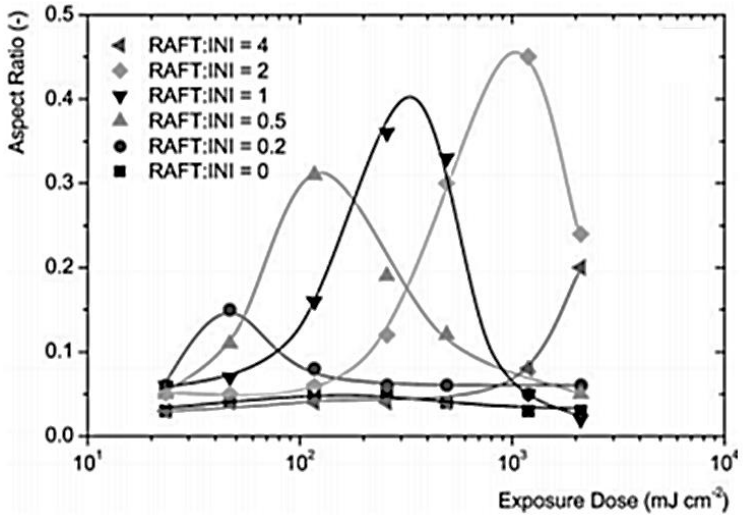


*Figure 2.21: Aspect ratio as function of exposure dose for different RAFT agent to initiator ratios under (a) ambient and (b) inert atmosphere. The data shown is for the 20 mm grating size.*

Paraffin oil has also been shown to improve relief heights by 30% when it is spread over the surface of film prior to diffusion in the thermal development step [124]. This was explained by considering that the development of the relief structures is based on a balance between diffusion and surface/interfacial tension (γ) [127, 131].

Hermans et al. [124] stated that when paraffin oil was applied to the photopolymer layer, the interfacial tension is estimated to be lowered from ±35 mN $m^{-1}$ in an ambient environment to ±17 mN $m^{-1}$. This suggested that upon reduction of the interfacial tension, the height of the relief structures is enhanced [124] .

To adapt photoembossing to biomedical applications, the photopolymer used should be biocompatible and promote cell adhesion. Thus, all components of the photopolymer (i.e. polymer, monomer, initiator and other additives) should not cause cell apoptosis. Furthermore, it could be necessary that these materials biodegrade over time to allow tissue infiltration and take over after a certain period of time. Although biodegradable polymer binders could be used for these applications, a crosslinked network could be left behind. To achieve full degradation, the monomers used should be degradable after crosslinking. Degradable photo-crosslinked networks are reviewed in the next section.

## 2.5. Degradable cross-linked networks

Extensive research into covalently crosslinked, degradable biomaterial networks has occurred over the past 25 years. Three main polymerisation mechanisms are used to form covalently crosslinked polymeric biomaterials, including chain-growth, step-

growth, and mixed mode chain and step growth mechanisms, shown in Fig. 2.22 [132]. During formation of a typical chain-growth network, active centres rapidly propagate through monomers containing multiple carbon–carbon double bonds to form high-molecular weight kinetic chains that are covalently crosslinked (Fig. 2.22a). The initiating species in these chain-growth systems, typically radicals, are generated by a variety of methods including thermal energy [133], redox reactions [134], and cleavage of a photoinitiator molecule when irradiated with UV or visible light [135, 136].

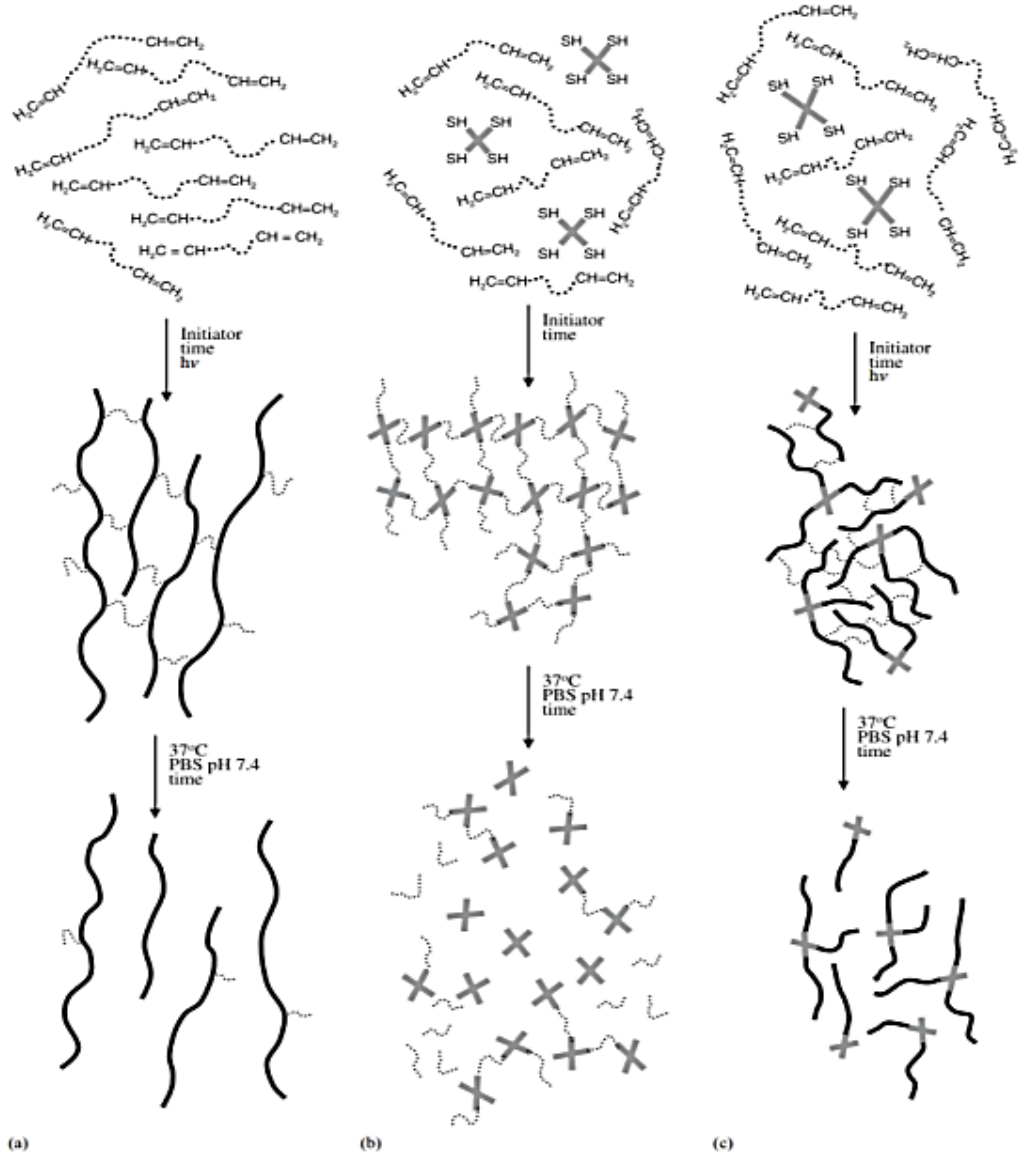


*Figure 2.22: Schematic of initial monomer molecules, crosslinked polymer networks and degradation products formed from (a) chain-growth polymerisation mechanism, (b) step-growth polymerisation mechanism, and (c) mixed mode mechanisms [132].*

Degradation is incorporated into covalently crosslinked networks through inclusion of hydrolytically cleavable anhydride or ester groups [137-139] or enzymatically cleavable peptide linkages [140-143] in the crosslink segments. For each type of degradable network, the degradation products are comprised of the original monomer core from

the starting materials, individual repeat units from the degradable segments, and the high-molecular-weight kinetic chains generated during polymerization. Modifications to the monomer core-chemistry in chain-growth networks directly impact the network's crosslinks and allow degradation behaviour, modulus, elasticity, and equilibrium swelling ratios to be tailored [144-146]. For example, highly crosslinked networks formed from low-molecular-weight, hydrophobic dimethacrylated polyanhydrides degrade through a surface erosion mechanism, while moderately crosslinked hydrogels formed from high-molecular-weight, hydrophilic dimethacrylated poly(lactic acid)-b-poly(ethylene glycol)-b-poly(lactic acid) (PEG-PLA) undergo bulk erosion [147-149]. Another example is the ability to tailor the mechanical strength and modulus of oligo(poly (ethylene glycol) fumarate) hydrogels through modifications of the PEG molecular weight [150], crosslinker mole fraction [151], and porogen content [152]. However, for these types of networks, only the crosslink segments degrade, leaving high-molecular-weight kinetic chains that must be excreted from the body [148].

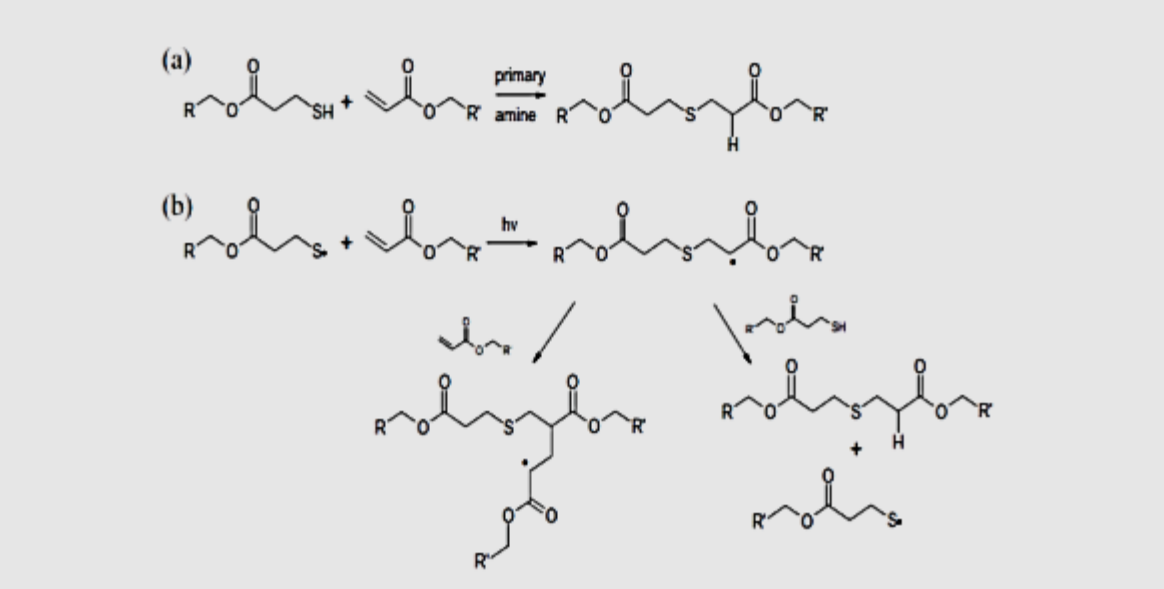


*Figure 2.23: Basic mechanisms for thiol-acrylate reactions using (a) a catalyst or (b) a photo-cure.*

Hubbell *et al.* [153, 154] developed degradable networks formed through Michael-addition-type reactions between thiol and acrylate, acrylamide, or vinyl sulfone groups. These networks form through a step-growth polymerization of the thiol and vinyl groups (Fig. 2.23 b). The step-growth nature of these Michael-addition reactions stems from a two-part propagation process in which a thiolate ion reacts with a vinyl group to form a carbon-based anion, which then reacts with another thiol group to regenerate another thiolate ion. The repetition of these events in a system of multifunctional monomers generates a covalently crosslinked network with better control of the crosslinking density and corresponding material properties than the photoinitiated chain polymerization of acrylates [154]. Additionally, the degradable segments are incorporated throughout the network, eliminating the high-molecular-weight degradation products containing the backbone kinetic chains formed during chain-

growth polymerization [132]. The Michael-addition reaction is catalyzed in a slightly basic environment, eliminating the need to add any initiators. Unfortunately, it is not possible to spatially and temporally control network formation in these materials, and the network gelation rates are considerably slower than those exhibited by the photoinitiated chain polymerization of a multifunctional class of degradable thiolacrylate biomaterials formed through a mixed-mode polymerization mechanism that is a combination of chain-growth and step-growth reactions (Fig. 2.24), where both reactions are radically mediated. Three reactions are involved in the propagation mechanism of thiol-acrylate polymerizations and are shown in Fig. 2.24 (Steps 1–3) [155]. Steps 1 and 2 are identical to the classical photoinitiated step growth thiol-ene polymerization, in which propagation and chain transfer occur sequentially [132, 156, 157]. An additional propagation step occurs in thiol-acrylate polymerisations, due to the ability of the acrylate groups to react with carbon-based radicals (Step 3). This additional reaction results in acrylate homopolymerisation, similar to the chain-growth polymerization mechanism of pure acrylates. The unique thiol-acrylate molecular structure evolves from the mixed-mode polymerization mechanism and is directly impacted by thiol : acrylate ratios, transitioning from being more chain-like to more step-like as the ratio of thiol to acrylate groups increases. In addition to their unusual mixed-mode polymerization mechanism, thiol-acrylates have a number of unique and attractive attributes. They can polymerize upon exposure to UV light, with or without added photoinitiator molecules, allowing samples with thicknesses well in excess of 10 cm to be formed. The use of light to initiate the reaction affords spatial and temporal control of the polymerisation.

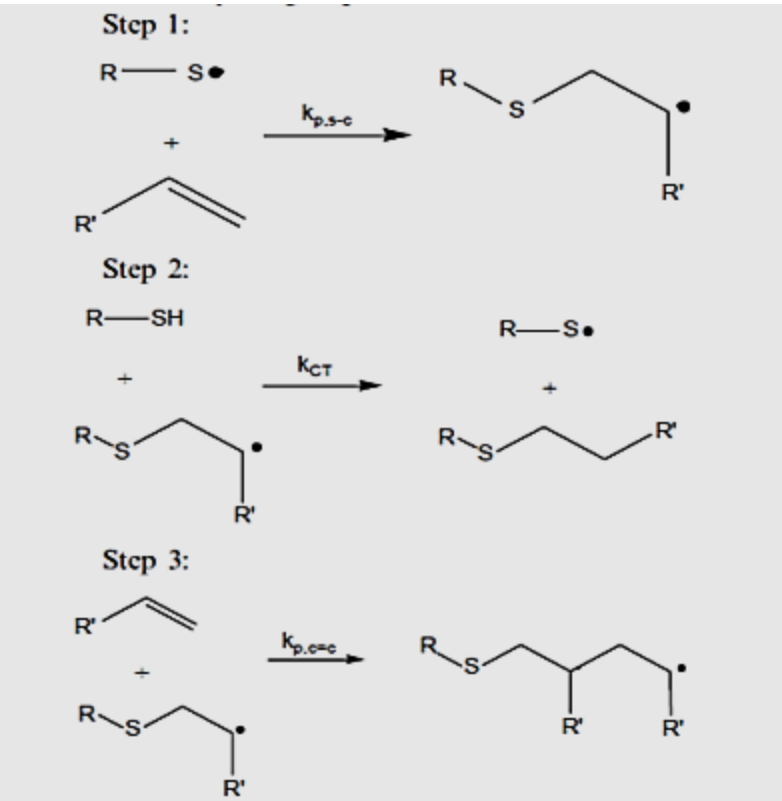


*Figure 2.24: Schematic for thiol-acrylate photopolymeristation.*

Hudalla et al. [158], described a simple approach to create hydrolytically labile PEG-acrylate networks. The approach involved reacting excess PEG-diacrylate chains with a dithiol, specifically dithiothreitol (DTT), to form water-soluble (-PEG-DTT-)n PEG polymer chains. Because of the stoichiometric imbalance in favour of the PEG-diacrylate, this step growth polymerization reaction resulted in chains that were acrylate-terminated and could therefore be photocrosslinked into a hydrogel network using UV. Here, the crosslinks themselves are not degradable but dithiol “bridges,” which are hydrolytically labile (Fig. 2.25). The hydrolytic lability of DTT bridges is due to the presence of a thioether bond proximal to the acrylate ester bond. Specifically, the presence of this

proximal thioether group establishes a more positive atomic charge on the carbonyl carbon of the ester, thereby enhancing ester hydrolysis [158]. Therefore, the extent of network degradation and erosion can be modulated in the networks by simply varying the ratio of DTT bridges to photo-induced crosslinks. They also showed that the degradation rate increases when higher molecular weight of PEG-diacrylate was used.

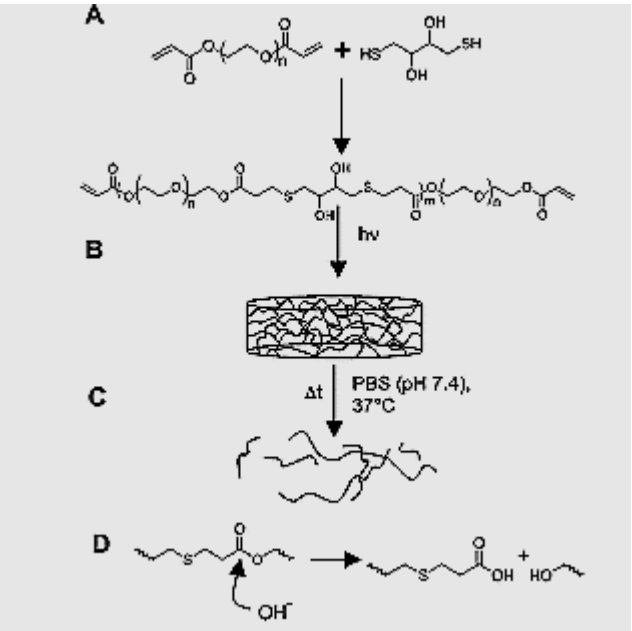


*Figure 2.25: Schematic representation of (A) Michael-type addition reaction between poly(ethylene glycol) diacrylate and dithiothreitol to introduce hydrolytically labile linkages into the polymer chain, (B) photocrosslinking of acrylate-terminated polymers to form hydrogels containing hydrolytically labile bridges, (C) incubation of hydrogels in buffer simulating a physiological environment, leading to hydrogel degradation over time, and (D)labile bond and degradation products [155].*

Summary

This literature review shows that surface texturing of polymer surfaces enhances cell adhesion and can be beneficial in the field of tissue engineering, in which cell adhesion is important for the proliferation and synthesis of tissue. Various techniques have been used to produce surface texture on films for biomedical applications, but so far no single technique has been developed to produce surface texture on fibres. Photoembossing appears to be a plausible technique to achieve surface relief structures on both films and fibres. This technique has only been used to produce diffractive surfaces for optical applications. In the following chapters, we will assess the feasibility of using photoembossing in tissue engineering by creating surface relief structures on biocompatible photopolymer films and fibres. Degradable photocrosslinked networks reviewed in the literature will also be patterned by photoembossing to obtain biocompatible and biodegradable textured photopolymer film and fibres.

## References

[1] L. E. Freed, G. Vunjak-Novakovic, R. J. Biron, D. B. Eagles, D. C. Lesnoy, S. K. Barlow, and R. Langer, "Biodegradable Polymer Scaffolds for Tissue Engineering," *Nat Biotech,* vol. 12, pp. 689-693, 1994.

[2] J. A. Hubbell, "Biomaterials in tissue engineering," *Bio/technology,* vol. 13, pp. 565-76, 1995.

[3] C. T. Laurencin, A. M. Ambrosio, M. D. Borden, and J. A. Cooper, Jr., "Tissue engineering: orthopedic applications," *Annual review of biomedical engineering,* vol. 1, pp. 19-46, 1999.

[4] R. Murugan and S. Ramakrishna, "Development of nanocomposites for bone grafting," *Composites Science and Technology,* vol. 65, pp. 2385-2406, 2005.

[5] S. L. Mitchell and L. E. Niklason, "Requirements for growing tissue-engineered vascular grafts," *Cardiovascular Pathology,* vol. 12, pp. 59-64, 2003.

[6] K. A. Eagle, R. A. Guyton, R. Davidoff, F. H. Edwards, G. A. Ewy, T. J. Gardner, J. C. Hart, H. C. Herrmann, L. D. Hillis, A. M. Hutter Jr, B. W. Lytle, R. A. Marlow, W. C. Nugent, T. A. Orszulak, E. M. Antman, S. C. Smith Jr, J. S. Alpert, J. L. Anderson, D. P. Faxon, V. Fuster, R. J. Gibbons, G. Gregoratos, J. L. Halperin, L. F. Hiratzka, S. A. Hunt, A. K. Jacobs, and J. P. Ornato, "ACC/AHA 2004 Guideline Update for Coronary Artery Bypass Graft Surgery: Summary Article: A Report of the American College of Cardiology/American Heart Association Task Force on Practice Guidelines (Committee to Update the 1999 Guidelines for Coronary Artery Bypass Graft Surgery)," *Journal of the American College of Cardiology,* vol. 44, pp. 1146-1154, 2004.

[7] D. G. Benditt, M. A. Goldstein, W. J. Reyes, and S. Milstein, "Supraventricular tachycardias: mechanisms and therapies," *Hosp Pract (Off Ed). 15,* vol. 23(8):161-183, 1988.

[8] A. Ratcliffe, "Tissue engineering of vascular grafts," *Matrix Biology,* vol. 19, pp. 353-357, 2000.

[9] S. P. Schmidt, T. J. Hunter, W. V. Sharp, G. S. Malindzak, and M. M. Evancho, "Endothelial cell-seeded four-millimeter Dacron vascular grafts: Effects of blood flow manipulation through the grafts," *Journal of Vascular Surgery,* vol. 1, pp. 434-441, 1984.

[10] M. Deutsch, J. Meinhart, T. Fischlein, P. Preiss, and P. Zilla, "Clinical autologous in vitro endothelialization of infrainguinal ePTFE grafts in 100 patients: A 9-year experience," *Surgery,* vol. 126, pp. 847-855, 1999.

[11] O. E. Teebken and A. Haverich, "Tissue Engineering of Small Diameter Vascular Grafts," *European Journal of Vascular and Endovascular Surgery,* vol. 23, pp. 475-485, 2002.

[12] L. E. Niklason, J. Gao, W. M. Abbott, K. K. Hirschi, S. Houser, R. Marini, and R. Langer, "Functional Arteries Grown in Vitro," *Science,* vol. 284, pp. 489-493, 1999.

[13] A. A. Bavry, D. J. Kumbhani, T. J. Helton, P. P. Borek, G. R. Mood, and D. L. Bhatt, "Late thrombosis of drug-eluting stents: a meta-analysis of randomized clinical trials," *The American journal of medicine,* vol. 119, pp. 1056-1061, 2006.

[14] P. G. M. P. Valgimigli M and et al., "Tirofiban and sirolimus-eluting stent vs abciximab and bare-metal stent for acute myocardial infarction: A randomized trial," *JAMA,* vol. 293, pp. 2109-2117, 2005.

[15] D. E. Drachman, E. R. Edelman, P. Seifert, A. R. Groothuis, D. A. Bornstein, K. R. Kamath, M. Palasis, D. Yang, S. H. Nott, and C. Rogers, "Neointimal thickening after stent delivery of paclitaxel: Change in composition and arrest of growth over six months," *Journal of the American College of Cardiology,* vol. 36, pp. 2325-2332, 2000.

[16] T. Suzuki, G. Kopia, S.-i. Hayashi, L. R. Bailey, G. Llanos, R. Wilensky, B. D. Klugherz, G. Papandreou, P. Narayan, M. B. Leon, A. C. Yeung, F. Tio, P. S. Tsao, R. Falotico, and A. J. Carter, "Stent-Based Delivery of Sirolimus Reduces Neointimal Formation in a Porcine Coronary Model," *Circulation,* vol. 104, pp. 1188-1193, 2001.

[17] P. K. Campbell, "Metal reinforced polymer stent," Google Patents, 1997.

[18] I. K. De Scheerder, K. L. Wilczek, E. V. Verbeken, J. Vandorpe, P. N. Lan, E. Schacht, J. Piessens, and H. De Geest, "Biocompatibility of biodegradable and nonbiodegradable polymer-coated stents implanted in porcine peripheral arteries," *Cardiovascular and interventional radiology,* vol. 18, pp. 227-232, 1995.

[19] R. C. Eberhart, S.-H. Su, K. T. Nguyen, M. Zilberman, L. Tang, K. D. Nelson, and P. Frenkel, "Review: Bioresorbable polymeric stents: current status and future promise," *Journal of Biomaterials Science, Polymer Edition,* vol. 14, pp. 299-312, 2003.

[20] G. W. Stone, S. G. Ellis, L. Cannon, J. T. Mann, J. D. Greenberg, D. Spriggs, C. D. O'Shaughnessy, S. DeMaio, P. Hall, and J. J. Popma, "Comparison of a polymer-based paclitaxel-eluting stent with a bare metal stent in patients with complex coronary artery disease," *JAMA: the journal of the American Medical Association,* vol. 294, pp. 1215-1223, 2005.

[21] H. M. Wache, D. J. Tartakowska, A. Hentrich, and M. H. Wagner, "Development of a polymer stent with shape memory effect as a drug delivery system," *Journal of Materials Science: Materials in Medicine,* vol. 14, pp. 109-112, 2003.

[22] W. J. van der Giessen, A. M. Lincoff, R. S. Schwartz, H. M. M. van Beusekom, P. W. Serruys, D. R. Holmes, S. G. Ellis, and E. J. Topol, "Marked Inflammatory Sequelae to Implantation of Biodegradable and Nonbiodegradable Polymers in Porcine Coronary Arteries," *Circulation,* vol. 94, pp. 1690-1697, 1996.

[23] J. Goldberg and R. Sinclair, "Biodegradable stent," Google Patents, 1992.

[24] H. Tamai, K. Igaki, E. Kyo, K. Kosuga, A. Kawashima, S. Matsui, H. Komori, T. Tsuji, S. Motohara, and H. Uehata, "Initial and 6-month results of biodegradable poly-l-lactic acid coronary stents in humans," *Circulation,* vol. 102, pp. 399-404, 2000.

[25] R. Murugan and S. Ramakrishna, "Design strategies of tissue engineering scaffolds with controlled fiber orientation," *Tissue Engineering,* vol. 13, pp. 1845-66, 2007.

[26] G. N. Ramachandran, "Stereochemistry of collagen*," *International Journal of Peptide and Protein Research,* vol. 31, pp. 1-16, 1988.

[27] M. Vanderrest and R. Garrone, "Collagen Family of Proteins," *Faseb Journal,* vol. 5, pp. 2814-2823, 1991.

[28] D. R. Baselt, J. P. Revel, and J. D. Baldeschwieler, "Subfibrillar Structure of Type-I Collagen Observed by Atomic-Force Microscopy," *Biophysical Journal,* vol. 65, pp. 2644-2655, 1993.

[29] J. Jokinen, E. Dadu, P. Nykvist, J. Kapyla, D. J. White, J. Ivaska, P. Vehvilainen, H. Reunanen, H. Larjava, L. Hakkinen, and J. Heino, "Integrin-mediated cell adhesion to type I collagen fibrils," *Journal of Biological Chemistry,* vol. 279, pp. 31956-31963, 2004.

[30] X. F. Walboomers, L. A. Ginsel, and J. A. Jansen, "Early spreading events of fibroblasts on microgrooved substrates," *Journal of Biomedical Materials Research,* vol. 51, pp. 529-534, 2000.

[31] J. Friedrichs, A. Taubenberger, C. M. Franz, and D. J. Muller, "Cellular remodelling of individual collagen fibrils visualized by time-lapse AFM," *Journal of Molecular Biology,* vol. 372, pp. 594-607, 2007.

[32] S.-W. Tsai, C.-C. Chen, P.-L. Chen, and F.-Y. Hsu, "Influence of topography of nanofibrils of three-dimensional collagen gel beads on the phenotype, proliferation, and maturation of osteoblasts," *Journal of Biomedical Materials Research Part A,* vol. 91A, pp. 985-993, 2009.

[33] S. W. Tsai, H. M. Liou, C. J. Lin, K. L. Kuo, S. Hung, R. C. Weng, and F. Y. Hsu, "MG63 Osteoblast-Like Cells Exhibit Different Behavior when Grown on Electrospun Collagen Matrix versus Electrospun Gelatin Matrix," *Plos One,* vol. 7, 2012.

[34] W. H. Hendren and E. F. Reda, "Bladder mucosa graft for construction of male urethra," *Journal of Pediatric Surgery,* vol. 21, pp. 189-92, 1986.

[35] B. S. Kim, C. E. Baez, and A. Atala, "Biomaterials for tissue engineering," *World Journal of Urology,* vol. 18, pp. 2-9, 2000.

[36] J. C. Middleton and A. J. Tipton, "Synthetic biodegradable polymers as orthopedic devices," *Biomaterials,* vol. 21, pp. 2335-2346, 2000.

[37] D. K. Gilding and A. M. Reed, "Biodegradable polymers for use in surgery--polyglycolic/poly(actic acid) homo- and copolymers: 1," *Polymer,* vol. 20, pp. 1459-1464, 1979.

[38] R. A. Miller, J. M. Brady, and D. E. Cutright, "Degradation rates of oral resorbable implants (polylactates and polyglycolates): Rate modification with changes in PLA/PGA copolymer ratios," *Journal of Biomedical Materials Research,* vol. 11, pp. 711-719, 1977.

[39] K. Burg and S. Shalaby, "Absorbable/Biodegradable Polymers," in *Absorbable and Biodegradable Polymers*: CRC Press, 2003.

[40] N. D. Miller and D. F. Williams, "The in vivo and in vitro degradation of poly(glycolic acid) suture material as a function of applied strain," *Biomaterials,* vol. 5, pp. 365-368, 1984.

[41] J. M. Schakenraad, M. J. Hardonk, J. Feijen, I. Molenaar, and P. Nieuwenhuis, "Enzymatic-Activity toward Poly(L-Lactic Acid) Implants," *Journal of Biomedical Materials Research,* vol. 24, pp. 529-545, 1990.

[42] A. G. Mikos, A. J. Thorsen, L. A. Czerwonka, Y. Bao, R. Langer, D. N. Winslow, and J. P. Vacanti, "Preparation and Characterization of Poly(L-Lactic Acid) Foams," *Polymer,* vol. 35, pp. 1068-1077, 1994.

[43] Y. S. Nam and T. G. Park, "Porous biodegradable polymeric scaffolds prepared by thermally induced phase separation," *Journal of Biomedical Materials Research,* vol. 47, pp. 8-17, 1999.

[44] L. D. Harris, B. S. Kim, and D. J. Mooney, "Open pore biodegradable matrices formed with gas foaming," *Journal of Biomedical Materials Research,* vol. 42, pp. 396-402, 1998.

[45] N. A. Peppas and R. Langer, "New challenges in biomaterials," *Science,* vol. 263, pp. 1715-20, 1994.

[46] R. M. Pasquarelli, D. S. Ginley, and R. O'Hayre, "Solution processing of transparent conductors: from flask to film," *Chemical Society Reviews,* vol. 40, pp. 5406-5441, 2011.

[47] T. K. Borg, "It's the matrix! ECM, proteases, and cancer," *Am J Pathol,* vol. 164, pp. 1141-2, 2004.

[48] S. J. Hollister, "Porous scaffold design for tissue engineering," *Nature Materials,* vol. 4, pp. 518-24, 2005.

[49] S. Yang, K.-F. Leong, Z. Du, and C.-K. Chua, "The design of scaffolds for use in tissue engineering. Part II. Rapid Prototyping Techniques," *Tissue Engineering,* vol. 8, pp. 1-11, 2002.

[50] H. Lo, S. Kadiyala, S. E. Guggino, and K. W. Leong, "Poly(L-lactic acid) foams with cell seeding and controlled-release capacity," *Journal of Biomedical Materials Research,* vol. 30, pp. 475-484, 1996.

[51] Y. S. Nam and T. G. Park, "Biodegradable polymeric microcellular foams by modified thermally induced phase separation method," *Biomaterials,* vol. 20, pp. 1783-1790, 1999.

[52] S. F. Yang, K. F. Leong, Z. H. Du, and C. K. Chua, "The design of scaffolds for use in tissue engineering. Part II. Rapid prototyping techniques," *Tissue Engineering,* vol. 8, pp. 1-11, 2002.

[53] V. J. Chen and P. X. Ma, "Nano-fibrous poly(-lactic acid) scaffolds with interconnected spherical macropores," *Biomaterials,* vol. 25, pp. 2065-2073, 2004.

[54] F. Yang, R. Murugan, S. Ramakrishna, X. Wang, Y. X. Ma, and S. Wang, "Fabrication of nano-structured porous PLLA scaffold intended for nerve tissue engineering," *Biomaterials,* vol. 25, pp. 1891-1900, 2004.

[55] D. Li, Y. L. Wang, and Y. N. Xia, "Electrospinning of polymeric and ceramic nanofibers as uniaxially aligned arrays," *Nano Letters,* vol. 3, pp. 1167-1171, 2003.

[56] D. H. Reneker and I. Chun, "Nanometre diameter fibres of polymer, produced by electrospinning," *Nanotechnology,* vol. 7, pp. 216-223, 1996.

[57] D. H. Reneker, A. L. Yarin, H. Fong, and S. Koombhongse, "Bending instability of electrically charged liquid jets of polymer solutions in electrospinning," *Journal of Applied Physics,* vol. 87, pp. 4531-4547, 2000.

[58] T. Alfrey, J. D. Justice, and S. J. Nelson, "The effect of solvent-type and temperature on the specific viscosities of polystyrene solutions," *Transactions of the Faraday Society,* vol. 42, pp. B050-B056, 1946.

[59] X. Zong, K. Kim, D. Fang, S. Ran, B. S. Hsiao, and B. Chu, "Structure and process relationship of electrospun bioabsorbable nanofiber membranes," *Polymer,* vol. 43, pp. 4403-4412, 2002.

[60] C. J. Buchko, L. C. Chen, Y. Shen, and D. C. Martin, "Processing and microstructural characterization of porous biocompatible protein polymer thin films," *Polymer,* vol. 40, pp. 7397-7407, 1999.

[61] S. L. Shenoy, W. D. Bates, H. L. Frisch, and G. E. Wnek, "Role of chain entanglements on fiber formation during electrospinning of polymer solutions: good solvent, non-specific polymer-polymer interaction limit," *Polymer,* vol. 46, pp. 3372-3384, 2005.

[62] W. K. Son, J. H. Youk, T. S. Lee, and W. H. Park, "The effects of solution properties and polyelectrolyte on electrospinning of ultrafine poly(ethylene oxide) fibers," *Polymer,* vol. 45, pp. 2959-2966, 2004.

[63] K. H. Lee, H. Y. Kim, M. S. Khil, Y. M. Ra, and D. R. Lee, "Characterization of nano-structured poly([epsilon]-caprolactone) nonwoven mats via electrospinning," *Polymer,* vol. 44, pp. 1287-1294, 2003.

[64] J. S. Lee, K. H. Choi, H. D. Ghim, S. S. Kim, D. H. Chun, H. Y. Kim, and W. S. Lyoo, "Role of molecular weight of atactic poly(vinyl alcohol) (PVA) in the structure and properties of PVA nanofabric prepared by electrospinning," *Journal of Applied Polymer Science,* vol. 93, pp. 1638-1646, 2004.

[65] J. M. Deitzel, J. D. Kleinmeyer, J. K. Hirvonen, and N. C. B. Tan, "Controlled deposition of electrospun poly(ethylene oxide) fibers," *Polymer,* vol. 42, pp. 8163-8170, 2001.

[66] R. V. N. Krishnappa, K. Desai, and C. M. Sung, "Morphological study of electrospun polycarbonates as a function of the solvent and processing voltage," *Journal of Materials Science,* vol. 38, pp. 2357-2365, 2003.

[67] S. L. Zhao, X. H. Wu, L. G. Wang, and Y. Huang, "Electrospinning of ethyl-cyanoethyl cellulose/tetrahydrofuran solutions," *Journal of Applied Polymer Science,* vol. 91, pp. 242-246, 2004.

[68] W. E. Teo and S. Ramakrishna, "A review on electrospinning design and nanofibre assemblies," *Nanotechnology,* vol. 17, pp. R89-R106, 2006.

[69] R. Kessick, J. Fenn, and G. Tepper, "The use of AC potentials in electrospraying and electrospinning processes," *Polymer,* vol. 45, pp. 2981-2984, 2004.

[70] X. Y. Yuan, Y. Y. Zhang, C. H. Dong, and J. Sheng, "Morphology of ultrafine polysulfone fibers prepared by electrospinning," *Polymer International,* vol. 53, pp. 1704-1710, 2004.

[71] S. Ramakrishna, *An introduction to electrospinning and nanofibers*: World Scientific Publishing Company, 2005.

[72] S. Megelski, J. S. Stephens, D. B. Chase, and J. F. Rabolt, "Micro- and nanostructured surface morphology on electrospun polymer fibers," *Macromolecules,* vol. 35, pp. 8456-8466, 2002.

[73] M. Bognitzki, W. Czado, T. Frese, A. Schaper, M. Hellwig, M. Steinhart, A. Greiner, and J. H. Wendorff, "Nanostructured fibers via electrospinning," *Advanced Materials,* vol. 13, pp. 70-79, 2001.

[74] C. L. Casper, J. S. Stephens, N. G. Tassi, D. B. Chase, and J. F. Rabolt, "Controlling surface morphology of electrospun polystyrene fibers: Effect of humidity and molecular weight in the electrospinning process," *Macromolecules,* vol. 37, pp. 573-578, 2004.

[75] Baumgart.Pk, "Electrostatic spinning of acrylic microfibers," *Journal of Colloid and Interface Science,* vol. 36, pp. 71-80, 1971.

[76] D. Li and Y. N. Xia, "Electrospinning of nanofibers: Reinventing the wheel?," *Advanced Materials,* vol. 16, pp. 1151-1170, 2004.

[77] A. Greiner and J. H. Wendorff, "Electrospinning: A fascinating method for the preparation of ultrathin fibers," *Angewandte Chemie International Edition,* vol. 46, pp. 5670-5703, 2007.

[78] B. K. Sharma, *Industrial Chemistry (including Chemical Engineering)*: GOEL Publishing House, 1997.

[79] H. S. Yoo, T. G. Kim, and T. G. Park, "Surface-functionalized electrospun nanofibers for tissue engineering and drug delivery," *Advanced Drug Delivery Reviews,* vol. 61, pp. 1033-1042, 2009.

[80] S. C. Baker, N. Atkin, P. A. Gunning, N. Granville, K. Wilson, D. Wilson, and J. Southgate, "Characterisation of electrospun polystyrene scaffolds for three-dimensional in vitro biological studies," *Biomaterials,* vol. 27, pp. 3136-3146, 2006.

[81] H. Park, K. Y. Lee, S. J. Lee, K. E. Park, and W. H. Park, "Plasma-treated poly(lactic-co-glycolic acid) nanofibers for tissue engineering," *Macromolecular Research,* vol. 15, pp. 238-243, 2007.

[82] Z. W. Ma, W. He, T. Yong, and S. Ramakrishna, "Grafting of gelatin on electrospun poly(caprolactone) nanofibers to improve endothelial cell spreading and proliferation and to control cell orientation," *Tissue Engineering,* vol. 11, pp. 1149-1158, 2005.

[83] Z. W. Ma, M. Kotaki, T. Yong, W. He, and S. Ramakrishna, "Surface engineering of electrospun polyethylene terephthalate (PET) nanofibers towards development of a new material for blood vessel engineering," *Biomaterials,* vol. 26, pp. 2527-2536, 2005.

[84] W. He, Z. W. Ma, T. Yong, W. E. Teo, and S. Ramakrishna, "Fabrication of collagen-coated biodegradable polymer nanofiber mesh and its potential for endothelial cells growth," *Biomaterials,* vol. 26, pp. 7606-7615, 2005.

[85] W. He, T. Yong, Z. W. Ma, R. Inai, W. E. Teo, and S. Ramakrishna, "Biodegradable polymer nanofiber mesh to maintain functions of endothelial cells," *Tissue Engineering,* vol. 12, pp. 2457-2466, 2006.

[86] A. F. Vonrecum and T. G. Vankooten, "The influence of micro-topography on cellular-response and the implications for silicone implants," *Journal of Biomaterials Science-Polymer Edition,* vol. 7, pp. 181-198, 1995.

[87] R. G. Harrison, "The cultivation of tissues in extraneous media as a method of morpho-genetic study," *The Anatomical Record,* vol. 6, pp. 181-193, 1912.

[88] P. Weiss, "Experiments on cell and axon orientation in vitro: The role of colloidal exudates in tissue organization," *Journal of Experimental Zoology,* vol. 100, pp. 353-386, 1945.

[89] N. G. Maroudas, "Anchorage dependence - correlation between amount of growth and diameter of bead, for single cells grown on individual glass beads," *Experimental Cell Research,* vol. 74, pp. 337-&, 1972.

[90] Y. A. Rovensky, I. L. Slavnaja, and J. M. Vasiliev, "Behaviour of fibroblast-like cells on grooved surfaces," *Experimental Cell Research,* vol. 65, pp. 193-201, 1971.

[91] J. Meyle, H. Wolburg, and A. F. von Recum, "Surface micromorphology and cellular interactions," *Journal of biomaterials applications,* vol. 7, pp. 362-74, Apr 1993.

[92] A. S. G. Curtis and P. Clark, "The effects of topographic and mechanical-properties of materials on cell behavior," *Critical Reviews in Biocompatibility,* vol. 5, pp. 343-362, 1990.

[93] Y. Wan, Y. Wang, Z. Liu, X. Qu, B. Han, J. Bei, and S. Wang, "Adhesion and proliferation of OCT-1 osteoblast-like cells on micro- and nano-scale topography structured poly(L-lactide)," *Biomaterials,* vol. 26, pp. 4453-9, 2005.

[94] X. F. Walboomers, H. J. E. Croes, L. A. Ginsel, and J. A. Jansen, "Contact guidance of rat fibroblasts on various implant materials," *Journal of Biomedical Materials Research,* vol. 47, pp. 204-212, 1999.

[95] J. Tan and W. M. Saltzman, "Biomaterials with hierarchically defined micro- and nanoscale structure," *Biomaterials,* vol. 25, pp. 3593-3601, 2004.

[96] B. R. Downing, K. Cornwell, M. Toner, and G. D. Pins, "The influence of microtextured basal lamina analog topography on keratinocyte function and epidermal organization," *J Biomed Mater Res A,* vol. 72, pp. 47-56, 2005.

[97] T. Steinberg, S. Schulz, J. P. Spatz, N. Grabe, E. Mussig, A. Kohl, G. Komposch, and P. Tomakidi, "Early keratinocyte differentiation on micropillar interfaces," *Nano Letters*, vol7(2), pp.287-94, 2007.

[98] G. A. Dunn and A. F. Brown, "Alignment of fibroblasts on grooved surfaces described by a simple geometric transformation," *Journal of Cell Science,* vol. 83, pp. 313-340, 1986.

[99] A. M. Green, J. A. Jansen, J. P. C. M. Vanderwaerden, and A. F. Vonrecum, "Fibroblast response to microtextured silicone surfaces - texture orientation into or out of the surface," *Journal of Biomedical Materials Research,* vol. 28, pp. 647-653, 1994.

[100] K. Matsuzaka, F. Walboomers, A. de Ruijter, and J. A. Jansen, "Effect of microgrooved poly-l-lactic (PLA) surfaces on proliferation, cytoskeletal organization, and mineralized matrix formation of rat bone marrow cells," *Clinical Oral Implants Research,* vol. 11, pp. 325-33, 2000.

[101] J. Meyle, K. Gultig, M. Brich, H. Hammerle, and W. Nisch, "Contact guidance of fibroblasts on biomaterial surfaces," *Journal of Materials Science-Materials in Medicine,* vol. 5, pp. 463-466, 1994.

[102] T. G. van Kooten, J. F. Whitesides, and A. F. von Recum, "Influence of silicone (PDMS) surface texture on human skin fibroblast proliferation as determined by cell cycle analysis," *Journal of Biomedical Materials Research,* vol. 43, pp. 1-14, 1998.

[103] E. T. Denbraber, J. E. Deruijter, H. T. J. Smits, L. A. Ginsel, A. F. Vonrecum, and J. A. Jansen, "Effect of parallel surface microgrooves and surface-energy on cell-growth," *Journal of Biomedical Materials Research,* vol. 29, pp. 511-518, 1995.

[104] E. T. den Braber, J. E. de Ruijter, L. A. Ginsel, A. F. von Recum, and J. A. Jansen, "Orientation of ECM protein deposition, fibroblast cytoskeleton, and attachment

complex components on silicone microgrooved surfaces," *Journal of Biomedical Materials Research,* vol. 40, pp. 291-300, 1998.

[105] R. B. Vernon, M. D. Gooden, S. L. Lara, and T. N. Wight, "Microgrooved fibrillar collagen membranes as scaffolds for cell support and alignment," *Biomaterials,* vol. 26, pp. 3131-3140, 2005.

[106] T. Steinberg, B. Dannewitz, P. Tomakidi, J. D. Hoheisel, E. Mussig, A. Kohl, and M. Nees, "Analysis of interleukin-1beta-modulated mRNA gene transcription in human gingival keratinocytes by epithelia-specific cDNA microarrays," *Journal of periodontal research,* vol. 41, pp. 426-46,2006.

[107] B. A. Dalton and J. G. Steele, "Migration mechanisms: corneal epithelial tissue and dissociated cells," *Exp Eye Res,* vol. 73, pp. 797-814, 2001.

[108] S. L. Goodman, P. A. Sims, and R. M. Albrecht, "Three-dimensional extracellular matrix textured biomaterials," *Biomaterials,* vol. 17, pp. 2087-2095, 1996.

[109] M. Srinivasarao, D. Collings, A. Philips, and S. Patel, "Three-dimensionally ordered array of air bubbles in a polymer film," *Science,* vol. 292(5514):79-83, 2001.

[110] L. Moroni, R. Licht, J. de Boer, J. R. de Wijn, and C. A. van Blitterswijk, "Fiber diameter and texture of electrospun PEOT/PBT scaffolds influence human mesenchymal stem cell proliferation and morphology, and the release of incorporated compounds," *Biomaterials,* vol. 27, pp. 4911-22, 2006.

[111] D. C. Surrao, J. W. Hayami, S. D. Waldman, and B. G. Amsden, "Self-crimping, biodegradable, electrospun polymer microfibers," *Biomacromolecules,* vol. 11, pp. 3624-9, 2010.

[112] G. M. Whitesides and J. Christopher Love, "The art of building small," *Scientific American,* vol. 285, pp. 38-47, 2001.

[113] R. Soufli, E. Spiller, M. A. Schmidt, J. C. Davidson, R. F. Grabner, E. M. Gullikson, B. B. Kaufmann, S. Mrowka, S. L. Baker, H. N. Chapman, R. M. Hudyma, J. S. Taylor, C. C. Walton, C. Montcalm, and J. A. Folta, "Multilayer optics for an extreme ultraviolet lithography tool with 70 nm resolution," *Emerging Lithographic Technologies V,* vol. 4343, pp. 51-59, 2001.

[114] D. Mijatovic, J. C. T. Eijkel, and A. van den Berg, "Technologies for nanofluidic systems: top-down vs. bottom-up - a review," *Lab on a Chip,* vol. 5, pp. 492-500, 2005.

[115] M. M. Bellah, S. M. Christensen, and S. M. Iqbal, "Nanostructures for medical diagnostics," *Journal of Nanomaterials,* vol. 2012.

[116] Y. N. Xia and G. M. Whitesides, "Soft lithography," *Annual Review of Materials Science,* vol. 28, pp. 153-184, 1998.

[117] J. Winslow, "Mastering and Replication of Optical Videodiscs," *Journal of the Optical Society of America,* vol. 66, pp. 379-379, 1976.

[118] S. Y. Chou, P. R. Krauss, and P. J. Renstrom, "Imprint of Sub-25 Nm Vias and Trenches in Polymers," *Applied Physics Letters,* vol. 67, pp. 3114-3116, 1995.

[119] H. Becker and U. Heim, "Polymer hot embossing with silicon master structures," *Sensors and Materials,* vol. 11, pp. 297-304, 1999.

[120] C. Sanchez, B. J. de Gans, D. Kozodaev, A. Alexeev, M. J. Escuti, C. van Heesch, T. Bel, U. S. Schubert, C. W. M. Bastiaansen, and D. J. Broer, "Photoembossing of periodic relief structures using polymerization-induced diffusion: A combinatorial study," *Advanced Materials,* vol. 17, pp. 2567-2571, 2005.

[121] C. Sánchez, B. J. de Gans, D. Kozodaev, A. Alexeev, M. J. Escuti, C. van Heesch, T. Bel, U. S. Schubert, C. W. M. Bastiaansen, and D. J. Broer, "Photoembossing of periodic relief structures using polymerization- induced diffusion: A Combinatorial Study," *Advanced Materials,* vol. 17, pp. 2567-2571, 2005.

[122] N. Adams, B. J. De Gans, D. Kozodaev, C. Sanchez, C. W. M. Bastiaansen, D. J. Broer, and U. S. Schubert, "High-throughput screening and optimization of photoembossed relief structures," *Journal of Combinatorial Chemistry,* vol. 8, pp. 184-191, 2006.

[123] K. Hermans, S. Z. Harnidi, A. B. Spoelstra, C. W. M. Bastiaansen, and D. J. Broer, "Rapid, direct fabrication of antireflection-coated microlens arrays by photoembossing," *Applied optics,* vol. 47, pp. 6512-6517, 2008.

[124] K. Hermans, M. van Delden, C. W. M. Bastiaansen, and D. J. Broer, "An in situ sealing method for liquid-filled micro-cavities based on photoembossing," *Journal of Micromechanics and Microengineering,* vol. 18, pp.1 -6, Sep 2008.

[125] J. Perelaer, K. Hermans, C. W. M. Bastiaansen, D. J. Broer, and U. S. Schubert, "Photo-embossed surface relief structures with an increased aspect ratio by addition of kinetic interfering compounds," *Journal of Photopolymer Science and Technology,* vol. 22, pp. 667-670, 2009.

[126] M. Dai, T. M. de Jong, C. Sanchez, O. T. Picot, D. J. Broer, T. Peijs, and C. W. M. Bastiaansen, "Surface structuring of bi-component fibres with photoembossing," *RSC Advances,* vol. 2, pp. 9964-9968, 2012.

[127] C. M. Leewis, A. M. de Jong, L. J. van IJzendoorn, and D. J. Broer, "Simulations with a dynamic reaction-diffusion model of the polymer grating preparation by patterned ultraviolet illumination," *Journal of Applied Physics,* vol. 95, pp. 8352-8356, 2004.

[128] B. J. de Gans, C. Sanchez, D. Kozodaev, D. Wouters, A. Alexeev, M. J. Escuti, C. W. M. Bastiaansen, D. J. Broer, and U. S. Schubert, "Optimizing photo-embossed gratings: A gradient library approach," *Journal of Combinatorial Chemistry,* vol. 8, pp. 228-236, 2006.

[129] K. Hermans, F. K. Wolf, J. Perelaer, R. A. J. Janssen, U. S. Schubert, C. W. M. Bastiaansen, and D. J. Broer, "High aspect ratio surface relief structures by photoembossing," *Applied Physics Letters,* vol. 91, pp. 3117 - 3121, 2007.

[130] J. Perelaer, K. Hermans, C. W. M. Bastiaansen, D. J. Broer, and U. S. Schubert, "Photo-embossed surface relief structures with an increased aspect ratios by addition of a reversible addition-fragmentation chain transfer agent," *Advanced Materials,* vol. 20, pp. 3117-3121, 2008.

[131] C. M. Leewis, A. M. de Jong, L. J. van IJzendoorn, and D. J. Broer, "Reaction-diffusion model for the preparation of polymer gratings by patterned ultraviolet illumination," *Journal of Applied Physics,* vol. 95, pp. 4125-4139,2004.

[132] A. E. Rydholm, C. N. Bowman, and K. S. Anseth, "Degradable thiol-acrylate photopolymers: polymerization and degradation behavior of an in situ forming biomaterial," *Biomaterials,* vol. 26, pp. 4495-4506, 2005.

[133] J. S. Temenoff, H. Park, E. Jabbari, D. E. Conway, T. L. Sheffield, C. G. Ambrose, and A. G. Mikos, "Thermally cross-linked oligo(poly(ethylene glycol) fumarate) hydrogels support osteogenic differentiation of encapsulated marrow stromal cells in vitro," *Biomacromolecules,* vol. 5, pp. 5-10, 2004.

[134] E. Behravesh, S. Jo, K. Zygourakis, and A. G. Mikos, "Synthesis of in situ cross-linkable macroporous biodegradable poly(propylene fumarate-co-ethylene glycol) hydrogels," *Biomacromolecules,* vol. 3, pp. 374-381, 2002.

[135] A. Gutowska, B. Jeong, and M. Jasionowski, "Injectable gels for tissue engineering," *Anatomical Record,* vol. 263, pp. 342-349, 2001.

[136] K. T. Nguyen and J. L. West, "Photopolymerizable hydrogels for tissue engineering applications," *Biomaterials,* vol. 23, pp. 4307-4314, 2002.

[137] J. Heller, B. K. Fritzinger, S. Y. Ng, and D. W. H. Penhale, "In vitro and in vivo release of levonorgestrel from poly(ortho esters). II. Crosslinked polymers," *Journal of Controlled Release,* vol. 1, pp. 233-238, 1985.

[138] A. S. Sawhney, C. P. Pathak, and J. A. Hubbell, "Bioerodible hydrogels based on photopolymerized poly(ethylene glycol)-co-poly(α-hydroxy acid) diacrylate macromers," *Macromolecules,* vol. 26, pp. 581-587, 1993.

[139] A. K. Burkoth and K. S. Anseth, "A review of photocrosslinked polyanhydrides: In situ forming degradable networks," *Biomaterials,* vol. 21, pp. 2395-2404, 2000.

[140] M. Kurisawa, M. Terano, and N. Yui, "Doublestimuli-responsive degradable hydrogels for drug delivery: Interpenetrating polymer networks composed of oligopeptide-terminated poly(ethylene glycol) and dextran," *Macromolecular Rapid Communications,* vol. 16, pp. 663-666, 1995.

[141] W. N. E. Van Dijk-Wolthuis, O. Franssen, H. Talsma, M. J. Van Steenbergen, J. J. Kettenes-van Den Bosch, and W. E. Hennink, "Synthesis, characterization, and polymerization of glycidyl methacrylate derivatized dextran," *Macromolecules,* vol. 28, pp. 6317-6322, 1995.

[142] M. P. Lutolf, G. P. Raeber, A. H. Zisch, N. Tirelli, and J. A. Hubbell, "Cell-responsive synthetic hydrogels," *Advanced Materials,* vol. 15, pp. 888-892, 2003.

[143] J. L. West and J. A. Hubbell, "Polymeric biomaterials with degradation sites for proteases involved in cell migration," *Macromolecules,* vol. 32, pp. 241-244, 1999.

[144] J. S. Temenoff and A. G. Mikos, "Injectable biodegradable materials for orthopedic tissue engineering," *Biomaterials,* vol. 21, pp. 2405-2412, 2000.

[145] A. T. Metters, K. S. Anseth, and C. N. Bowman, "Fundamental studies of a novel, biodegradable PEG-b-PLA hydrogel," *Polymer,* vol. 41, pp. 3993-4004, 2000.

[146] M. N. Mason, A. T. Metters, C. N. Bowman, and K. S. Anseth, "Predicting controlled-release behavior of degradable PLA-b-PEG-b-PLA hydrogels," *Macromolecules,* vol. 34, pp. 4630-4635, 2001.

[147] A. Göpferich, "Mechanisms of polymer degradation and erosion," *Biomaterials,* vol. 17, pp. 103-114, 1996.

[148] A. T. Metters, C. N. Bowman, and K. S. Anseth, "A statistical kinetic model for the bulk degradation of PLA-b-PEG-b-PLA hydrogel networks," *Journal of Physical Chemistry B,* vol. 104, pp. 7043-7049, 2000.

[149] K. S. Anseth and D. J. Quick, "Polymerizations of multifunctional anhydride monomers to form highly crosslinked degradable networks," *Macromolecular Rapid Communications,* vol. 22, pp. 564-572, 2001

.

[150] J. S. Temenoff, K. A. Athanasiou, R. G. Lebaron, and A. G. Mikos, "Effect of poly(ethylene glycol) molecular weight on tensile and swelling properties of oligo(poly(ethylene glycol) fumarate) hydrogels for cartilage tissue engineering," *Journal of Biomedical Materials Research,* vol. 59, pp. 429-437, 2002.

[151] A. K. Shung, E. Behravesh, S. Jo, and A. G. Mikos, "Crosslinking characteristics of and cell adhesion to an injectable poly(propylene fumarate-co-ethylene glycol) hydrogel using a water-soluble crosslinking system," *Tissue Engineering,* vol. 9, pp. 243-254, 2003.

[152] B. D. Porter, J. B. Oldham, S. L. He, M. E. Zobitz, R. G. Payne, K. N. An, B. L. Currier, A. G. Mikos, and M. J. Yaszemski, "Mechanical properties of a biodegradable bone regeneration scaffold," *Journal of Biomechanical Engineering,* vol. 122, pp. 286-288, 2000.

[153] M. P. Lutolf, N. Tirelli, S. Cerritelli, L. Cavalli, and J. A. Hubbell, "Systematic modulation of Michael-type reactivity of thiols through the use of charged amino acids," *Bioconjugate Chemistry,* vol. 12, pp. 1051-1056, 2001.

[154] M. P. Lutolf and J. A. Hubbell, "Synthesis and physicochemical characterization of end-linked poly(ethylene glycol)-co-peptide hydrogels formed by Michael-type addition," *Biomacromolecules,* vol. 4, pp. 713-722, 2003.

[155] M. P. Lutolf, J. L. Lauer-Fields, H. G. Schmoekel, A. T. Metters, F. E. Weber, G. B. Fields, and J. A. Hubbell, "Synthetic matrix metalloproteinase-sensitive hydrogels for the conduction of tissue regeneration: Engineering cell-invasion characteristics," *Proceedings of the National Academy of Sciences of the United States of America,* vol. 100, pp. 5413-5418, 2003.

[156] A. F. Jacobine, *Thiol-ene Photopolymerization,* pp. 219-268, 1993.

[157] T. Posner, "Unsaturated compounds. II. Addition of mercaptans to unsaturated hydrocarbons," *Ber. Dtsch. Chem. Ges.,* vol. 38, pp. 646-657, 1905.

[158] G. A. Hudalla, T. S. Eng, and W. L. Murphy, "An approach to modulate degradation and mesenchymal stem cell behavior in poly(ethylene glycol) networks," *Biomacromolecules,* vol. 9, pp. 842-849, 2008.

# Chapter 3

## Effect of polymer binder on photoembossing

Photoembossing is a simple and versatile technique to create relief structures in polymers using a patterned contact mask exposure and a thermal development step. Typically, the photo-resist consists of a polymeric binder such as poly(benzyl methacrylate) (PBMA) and a multifunctional monomer in a 50/50 weight ratio, and the mixture is a solid and non-tacky material at room temperature. Here, new mixtures for photoembossing are presented that contain higher monomer content and therefore show greater material flux during photopolymerization. These mixtures are solid at room temperature (RT) even at high monomer contents (60 wt.%), which is achieved by

using a polymer binder with a higher glass-transition temperature ($T_g$) such as poly(methyl methacrylate) (PMMA). Differential scanning calorimetry (DSC) experiments indicated that the interactions between monomer and PMMA are less strong compared with PBMA. The combined effect of increased monomer content and weakened interactions with PMMA led to a greater mobility of the monomer and an increase in height of the relief structures by 50%.

## 3.1. Materials and methods

Poly(benzyl methacrylate) (PBMA) and poly(methyl methacrylate) (PMMA) with molecular weight of respectively 70,000 $gmol^{-1}$ and 75,000 $gmol^{-1}$ were obtained from Scientific Polymer. The monomer used was dipentaerythritolpenta-/hexa-acrylate (DPPHA) from Sigma Aldrich. The photo-initiator (Irgacure 819) and the retarder/ inhibitor (*tert*-butyl hydroquinone, TBHQ) were obtained from Sigma Aldrich.

Mixtures containing the polymer, monomer, retarder and photo-initiator were dissolved in a volatile solvent (propylene glycol mono methyl ether acetate; PGMEA). In accordance with previous studies by Hermans et al. [1], the weight ratio between retarder and photo-initiator (5:7) was kept identical. Also, a relatively high photo-initiator to monomer ratio (1:10) was used [1]. The monomer concentrations in the polymeric binder were 0, 15, 30, 40, 50 and 60 wt.%.

Each type of photopolymer film that was prepared by spin-coating was placed in a DSC pan. First, each sample was heated from room temperature to 80 $^{o}$C at a rate of 10

$^{o}$C/min and held at this temperature for 10 min to remove any residual solvent. This was followed by cooling to -40 $^{o}$C at 10 $^{o}$C/min and the sample was kept at -40 $^{o}$C for 10 min. A second heating step was performed from -40 $^{o}$C to 120 $^{o}$C at 10 $^{o}$C/min, and this second heating step was used to determine the glass transition temperatures. The $T_g$ of the pure PBMA and PMMA was also evaluated by the same process, except that the second heating step was done from -40 $^{o}$C to 160 $^{o}$C at 10 $^{o}$C/min.

Photopolymer solutions were spin-coated on glass substrates to obtain films with a thickness of 40 ± 10 µm. The films were dried for 20 min in a convection oven at 80 $^{o}$C. The sample was then irradiated with UV-light (Omnicure S2000® from Lumen Dynamics) through a patterned contact photo-mask (with a pitch of 20 µm) for one min at different light intensities in a nitrogen atmosphere. The photo-mask was then removed and the film was heated for 20 min to elevated temperatures in a nitrogen atmosphere. The optimum temperature for this heating step was obtained by varying the temperatures between 60 $^{o}$C and 160 $^{o}$C for 20 min [2]. After this thermal treatment, the films were flood exposed to UV-light (without a photo-mask) and heated for 10 min in nitrogen at elevated temperature.

The relief structures were measured by semi-contact mode atomic force microscopy (AFM, NT-MDT).

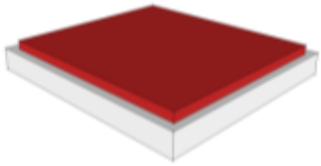

a. Film preparation (wire-bar coating)

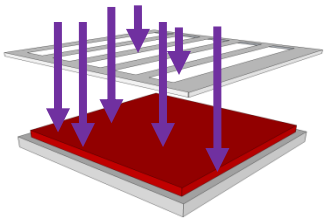

b. UV exposure through a patterned photo-mask. The mask has to be in contact with the film (it is not in contact here to clearly show the different components)

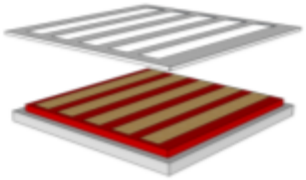

c. Removal of photo-mask followed by thermal treatment

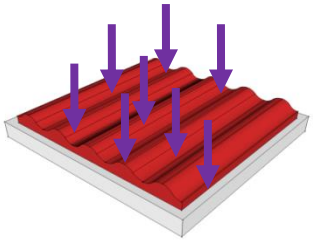

d.Flood exposure to UV light to cure residual monomer

*Figure 3.1: Photoembossing procedure.*

## 3.2. Results and discussion

Usually it is preferred to perform photoembossing using a contact mask exposure as shown in Fig. 3.1, and this requires a solid photo-resist with a glass transition temperature ($T_g$) above room temperature to avoid contamination of the mask and damage to the film. Fig. 3.2 shows the DSC traces for 0, 15, 30, 50 and 60 wt% mixtures of DPPHA in PMMA. With increasing monomer content, the *Tg* of the monomers broadens, and it is increasingly difficult to detect with the DSC as shown. Nevertheless, in all cases only a single phase transition is observed in the DSC results, which shows miscibility of both polymer binders and the DPPHA monomer, which is important for the photoembossing procedure [2]. Fig. 3.3 plots the glass transition temperature for both photopolymer systems as a function of monomer content. It is shown that the $T_g$ of the photopolymer mixtures initially decrease rapidly with increasing monomer content. The PMMA-DPPHA mixtures have higher $T_g$ compared with PBMA-DPPHA mixtures, which is expected because the $T_g$ of the polymeric binder is higher. However, the depression in $T_g$ is slightly steeper for the PMMA photopolymer compared to that of the PBMA photopolymer. Although the initial depression of $T_g$ is higher for the PMMA-DPPHA photopolymer, the $T_g$ of the mixtures remains high in comparison to PBMA-DPPHA mixtures, and non-tacky mixtures were obtained even at relatively high monomer contents. The depression in $T_g$ of a polymer-diluent system has been attributed to size of diluent and interaction between the polymer and diluent [3]. In our study, the diluent (monomer) is kept constant, and thus it can be assumed that the $T_g$ depression is controlled generally by the interaction between polymer and monomer. Stukalin et al.

computed that weak attractive interactions between diluent and polymer matrix result in steeper $T_g$ depressions [3]. This weak interaction could be a bonus with respect to diffusion of the monomers to the UV irradiated areas.

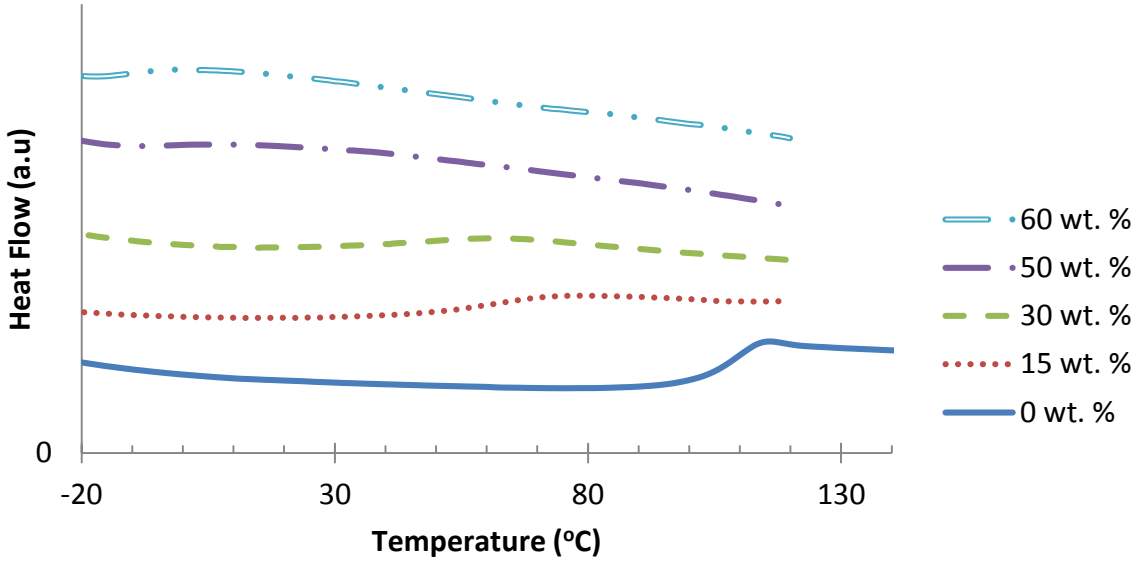


*Figure 3.2: DSC traces of PMMA-DPPHA films at different DPPHA concentration.*

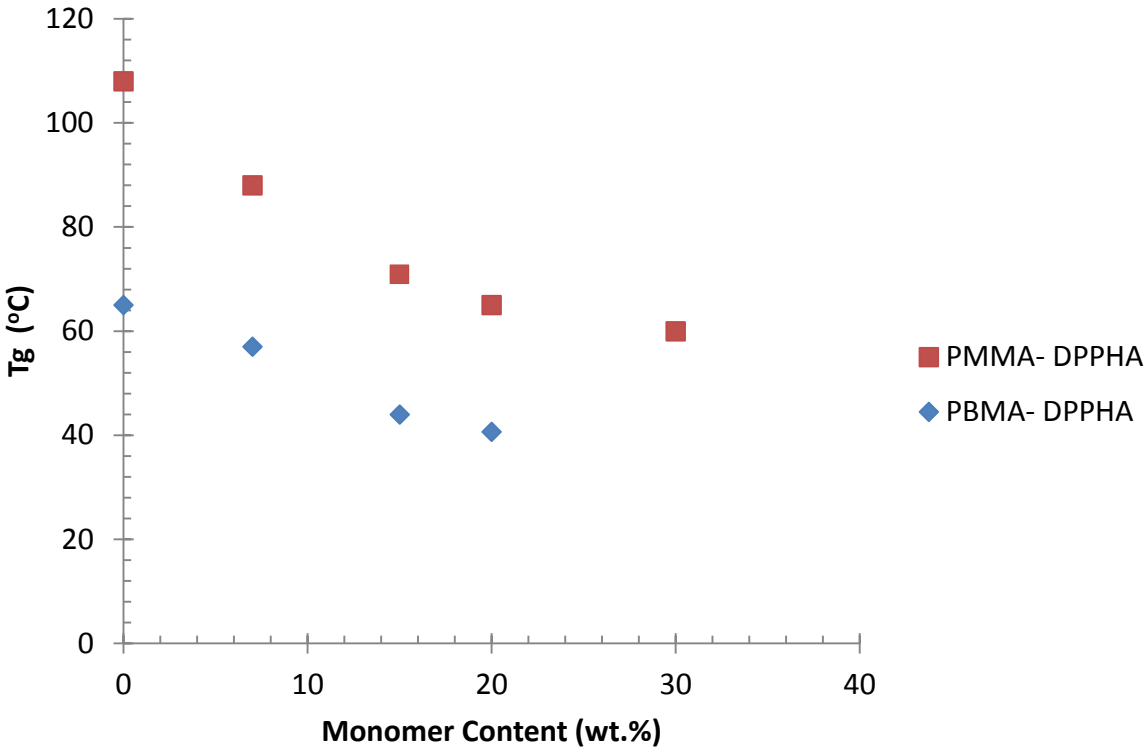


*Figure 3.3: Glass transition temperature of PMMA-DPPHA and PBMA-DPPHA photopolymer at different DPPHA monomer concentration measured by DSC.*

In the next paragraphs, the performance of these mixtures in photoembossing is discussed in terms of the height, shape and aspect ratio of the relief structures that are generated.

Photo-initiator and inhibitor/retarder were added to the mixtures and photoembossing was performed using a range of UV-light dosages (0.12 - 2.2 $J.cm^{-2}$) and temperatures (60 - 160 $^{o}C$) to obtain the optimum conditions. It was found that the optimum UV-light dosage (1.5 $J.cm^{-2}$) was relatively the same for all photopolymers. However, the optimum temperature for the generation of the relief structures in the PBMA-DPPHA

mixtures (110 $^{o}$C) investigated by Sanchez et al. was approximately 20 $^{o}$C lower than for PBMA-DPPHA mixtures (130 $^{o}$C), which is hardly surprising in view of the higher $T_g$ of the PMMA-based mixtures (Fig. 3.3). At identical monomer contents, the photopolymer mixtures containing the PMMA binder had a slightly higher height (about 20 %), especially at a monomer content of 30 and 50 wt% (Fig. 3.4). Increase in relief height in photoembossing is dependent on monomer diffusion to the irradiated region before they are cured. The diffusion process can therefore be influenced by mobility of monomers, interaction between polymer-monomer, and chain flexibility [3, 4]. The $T_g$ measurement provides information about the temperature at which the system mobility is activated. The PBMA-DPPHA system showed lower $T_g$ compared with the PMMA-DPPHA systems, and this is reflected in the lower optimum processing temperature for the PBMA-DPPHA photopolymer. However, the $T_g$ depression with increasing monomer concentration as observed in the DSC results, although only a qualitative finding, suggests that the interaction between PMMA and DPPHA is weaker than for PBMA and DPPHA. A low polymer-monomer interaction is desirable to allow easier diffusion of monomer to the irradiated areas (very low interaction may result in phase separation) [3], and may have caused the increase in relief height for the same monomer concentration of the PMMA-DPPHA system. However, the advantage of using a PMMA binder becomes even more apparent when higher monomer contents can be used. In the case of PBMA, very tacky samples are obtained at monomer contents above 50 wt%, and these mixtures cannot be processed easily, i.e. the mask adheres to the photo-resist and photo-resist residues tend to pollute the mask upon removal. In the

case of PMMA, the monomer content can be increased above 50 wt% without major tackiness issues, and this increases the height of the relief structures (i.e. the maximum height is increased from ~1.5 µm (PBMA-DPPHA) to ~2.2 µm (PMMA-DPPHA), which corresponds to an increase of approximately 50%).

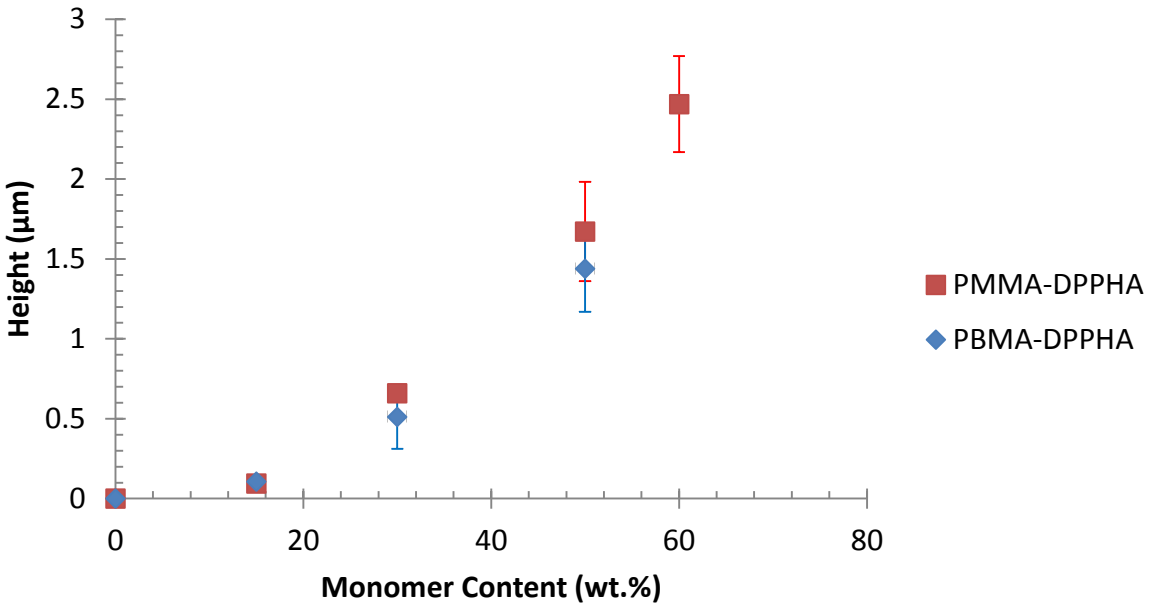


*Figure 3.4: Height of relief structures at different monomer concentration at 1.2 J/cm$^2$ at developing temperatures of 110 $^o$C for PBMA and 130 $^o$C for PMMA, measured by AFM.*

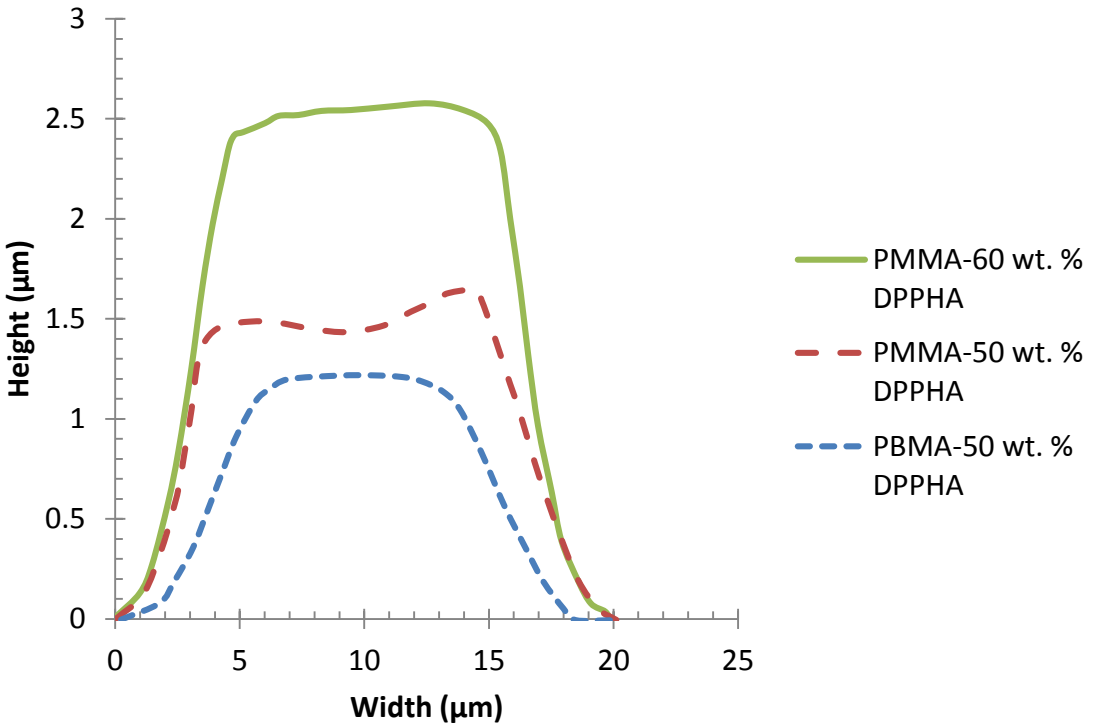


*Figure 3.5: Shape profile of photoembossed substrate measured by AFM.*

The shape of the relief structures obtained was measured and experimental data are shown in Fig. 3.4. Here, double peaks are observed for the PMMA-DPPHA sample containing 50 wt% of monomer, although the effect is not very pronounced. Nevertheless, a rather smooth profile of the relief structure was obtained for the PMMA-DPPHA sample with 60 wt% of monomer, which illustrates that a rather accurate reproduction of the mask is generated.

## 3.3. Conclusions

A high aspect ratio of surface relief structures is often vital in, among others, optical [5] and biomedical applications [6]. Here, it was shown that a PMMA polymer binder with a high $T_g$ allowed the use of higher monomer content diffusible species, which resulted in higher relief structures by photoembossing. The increased monomer content in combination with a weaker polymer-monomer interaction for the PMMA-DPPHA system led to a 50% increase in relief heights of the photoembossed structures.

PMMA as a polymer has been deemed biocompatible and is used in bone cements. Here we have shown that PMMA-DPPHA can be photoembossed to produce surface texture. In the next chapter, PMMA-photopolymer blends are evaluated for biocompatibility.

## References

[1] K. Hermans, F. K. Wolf, J. Perelaer, R. A. J. Janssen, U. S. Schubert, C. W. M. Bastiaansen, and D. J. Broer, "High aspect ratio surface relief structures by photoembossing," *Applied Physics Letters,* vol. 91, pp 1-6 2007.

[2] C. Sánchez, B. J. de Gans, D. Kozodaev, A. Alexeev, M. J. Escuti, C. van Heesch, T. Bel, U. S. Schubert, C. W. M. Bastiaansen, and D. J. Broer, "Photoembossing of periodic relief structures using polymerization-induced diffusion: a combinatorial study," *Advanced Materials,* vol. 17, pp. 2567-2571, 2005.

[3] E. B. Stukalin, J. F. Douglas, and K. F. Freed, "Plasticization and antiplasticization of polymer melts diluted by low molar mass species," *Journal of Chemical Physics,* vol. 132, 2010.

[4] W. S. Kim, Y. C. Jeong, J. K. Park, C. W. Shin, and Nam-Kim, "Diffraction efficiency behavior of photopolymer based on P(MMA-co-MAA) copolymer matrix," *Optical Materials,* vol. 29, pp. 1736-1740, 2007.

[5] K. Hermans, I. Tomatsu, M. Matecki, R. P. Sijbesma, C. W. M. Bastiaansen, and D. J. Broer, "Highly efficient surface relief formation via photoembossing of a supramolecular polymer," *Macromolecular Chemistry and Physics,* vol. 209, pp. 2094-2099, 2008.

[6] X. F. Walboomers and J. A. Jansen, "Cell and tissue behavior on micro-grooved surfaces," *Odontology,* vol. 89, pp. 0002-0011, 2001.

# Chapter 4

## Photoembossing of surface relief structures in polymer films for biomedical applications

Here, new mixtures for photoembossing are presented that are potentially biocompatible. Poly(methyl methacrylate) is used as a polymer binder, and two different acrylate monomers, trimethylolpropane ethoxylate triacrylate (TPETA) and dipentaerythritol penta-/hexa-acrylate (DPPHA), are tested, with the PMMA-TPETA system showing higher surface relief features. In this mixture, the inihibitor TBHQ (used in Chapter 3) was not used because it is toxic to cells. The photoembossing procedure was therefore performed in air, using oxygen as an inhibitor. Biocompatibility is evaluated by culturing human umbilical vein endothelial cells (HUVECs) on films of these photopolymer blends. PMMA with TPETA and PMMA-DPPHA films showed enhanced cell adhesion compared to PMMA. The cells also showed alignment on surface-textured films, with the highest degree of alignment on films with 20 μm pitch and 2 μm heights.

This study shows that photoembossing is a feasible method to produce surface textures on films that can be adopted in the field of tissue engineering to promote cell adhesion and alignment.

## 4.1. Materials and methods

Poly(methyl methacrylate) with a molecular weight of 120,000 g/mol, trimethylolpropane ethoxylate triacrylate (TPETA), dipentaerythritol penta-/hexa-acrylate (DPPHA), and 2-benzyl-2-(dimethylamino)-4'-morpholinobutyrophenone were used, all from Sigma-Aldrich. The solvent used here was propylene glycol monomethyl ether acetate (PGMEA) and was used as received from Sigma-Aldrich. Polystyrene culture well plates were used as received from Sigma Aldrich.

Two types of solutions were prepared: PMMA and DPPHA at a ratio of 50:50 wt%. Photoinitiator 2-benzyl-2-(dimethylamino)-4'-morpholinobutyrophenone was added at 10 wt% of DPPHA. All components were dissolved in 70 wt% of PGMEA. Similar solutions were prepared using TPETA as the monomer. These solutions were coated on glass slides using a wire bar coater to obtain a film thickness of 20 ± 6 µm. The coated glass slides were subsequently irradiated with UV light via a contact photo-mask followed by a thermal development step for 20 min in ambient air. The films were then fully exposed to UV light for 20 min to cure residual monomer in nitrogen. The curing was done at room temperature and at 130 $^{o}$C in nitrogen, and the total conversion was analysed using Fourier transform infrared- attenuated total reflection (FTIR-ATR). The UV dosages

during mask exposure and development temperature were varied to study the effect on relief height.

Relief structures were measured by atomic force microscopy (AFM, NT-MDT®) in semi-contact mode.

Human umbilical vein endothelial cells (HUVECs) (Life Technologies Ltd.) were cultured in T75 flasks (Sigma-Aldrich Co. LLC) using M199 (Life Technologies Ltd.) supplemented with 20% foetal bovine serum (FBS), 1 ng/mL β-endothelial cell growth factor, 3 µg/mL endothelial cell growth supplement from bovine neural tissue, 1.25 µg/mL thymidine, 10 µg/mL Heparin, 0.2 mMol/mL L-glutamine, 10 U/mL Penicillin, and 10 mg/mL Streptomycin (all supplements were purchased from Life Technologies Ltd.) at 37 °C in 95% air/5% $CO_2$. Cells were sub-cultured every week, and the medium was changed every 2 days. Cells at passages 3-7 were used in the experiments. It has been previously shown that cells between passages 3-7 behaved in a similar manner in response to surface topography [1]. HUVECs were seeded onto pure PMMA, PMMA-DPPHA and PMMA-TPETA films coated on 13 mm glass slides at a density of 20,000 cells/well in the non-treated polystyrene 24-well dishes (Thermo Fisher Scientific Inc.) in M199 with all the supplements and 20% FBS. PS well plate and glass slides were used for the reference experiment. All the polymer films were sterilized under ultra violet (UV) light for 30 min, followed by 2 times wash with 70% ethanol and 2 times wash with PBS (Sigma-Aldrich Co. LLC). Cells were then trypsinised and stained with Typan Blue® to count live and dead cells after 72 hrs. Fluorescent staining of cells was also performed with 4 µM of ethidium homodimer-2 (EthD-2) and 2 µM Calcein AM for live and dead cells, respectively. Cell

orientation was investigated using a scanning electron microscope (SEM). The cells were fixed with 3% paraformaldehyde in PBS and incubated at room temperature for 8 min. This was followed by dehydrating the cells using ethanol/ deionised water solution with 10, 50, 60, 70, 80, 90 and 100 v/v%. The samples were dried for 24 hrs in a biosafety cabinet. Samples were sputter coated with gold and observed in a SEM (FEI Inspect-F®) using a voltage of 10 kV. Cell orientation was analysed using *Image J®* Java software.

## 4.2. Results and discussion

***Photoembossing***

The migration of monomer to irradiated areas and the overall height of the surface structures is determined by the polymerisation-induced monomer concentration gradient, diffusivity differences, crosslinking properties, interaction between components, and surface free energy [2]. For both photopolymer systems, a photo-mask with a pitch of 10 µm was used to study the effect of UV dosage and developing temperature shown in Fig. 4.1a and Fig. 4.1b, respectively.

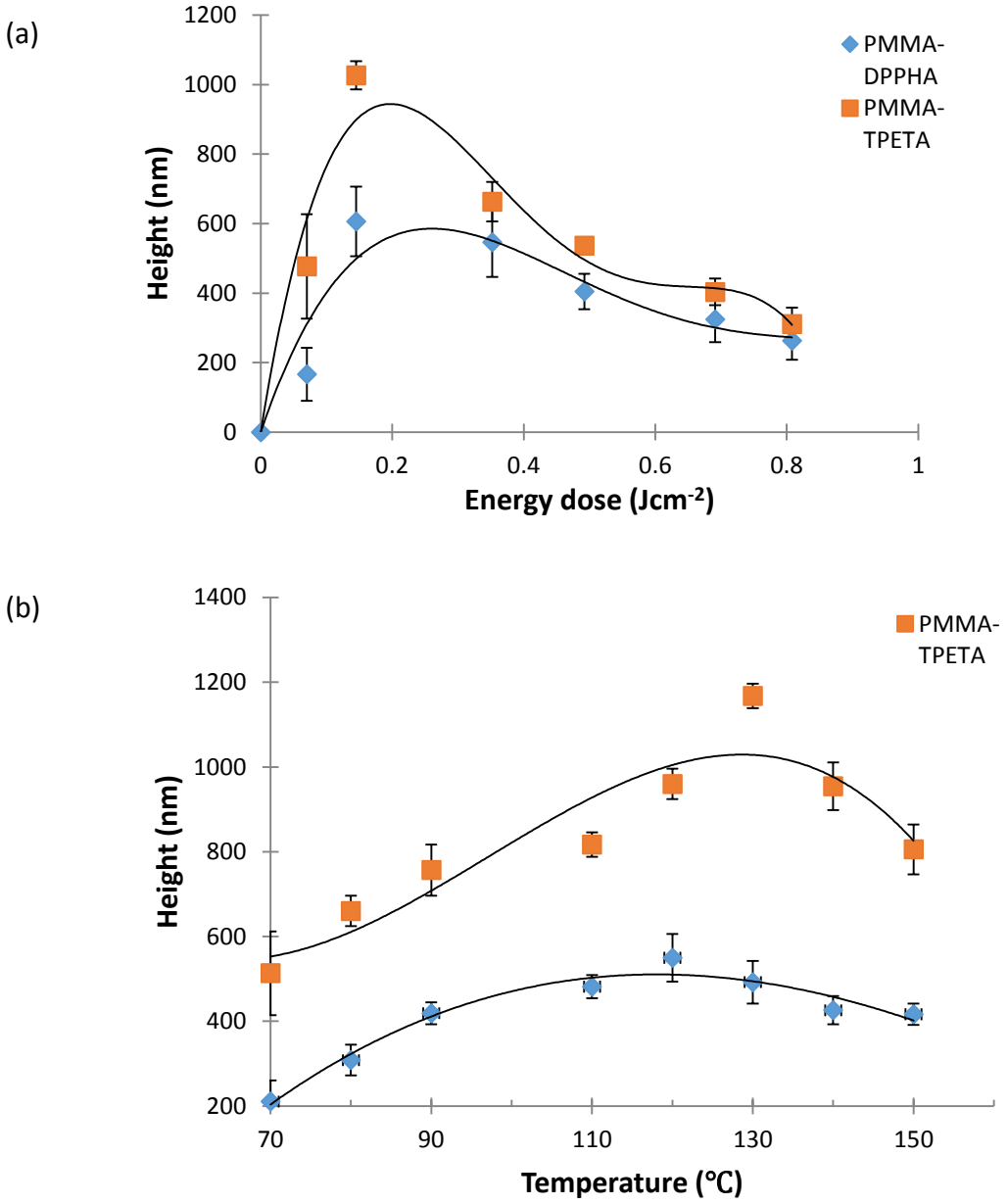


*Figure 4.1: Effect of (a) UV dosage and (b) temperature on relief height of photoembossed films. Lines are used to join data points as a guide for the eyes and not as a trendline.*

The height of the relief structure increases to an optimum UV dosage of approximately 0.145 J/cm$^2$. Sanchez et al. [2] described the effect of UV dosage on photoembossed films. At low intensities, only small amounts of photoinitiator are activated, and thus a smaller amount of monomer is converted. This reduces the concentration and chemical gradient in the film, and thus lower structures are formed. At dosages above the optimum, a very large amount of photo-initiator is activated, resulting in very high polymerisation rates and an increase in conversion. This reduces the mobility of the monomer through the polymer network. Therefore, monomers do not reach the central part of the irradiated regions, but react on the edges forming double peaks [2]

Developing temperature was also varied using a pitch of 10 μm, and the results are shown in Fig. 4.1b. Generally, higher temperature equates to higher diffusivity of molecules and thus greater flux of material to irradiated areas, resulting in higher relief structures. However, at temperatures above the optimum, there could be unwanted migration of radicals to non-exposed regions, diminishing the driving force for diffusion [2].

(a)

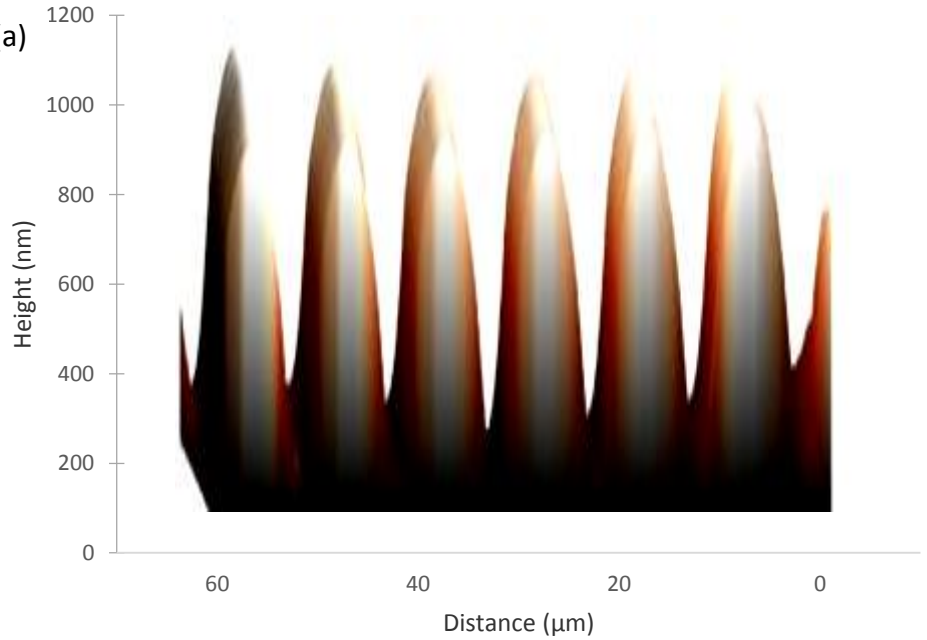
1200
1000
800
600
400
200
0
Height (nm)
60
40
20
0
Distance (µm)

(b)

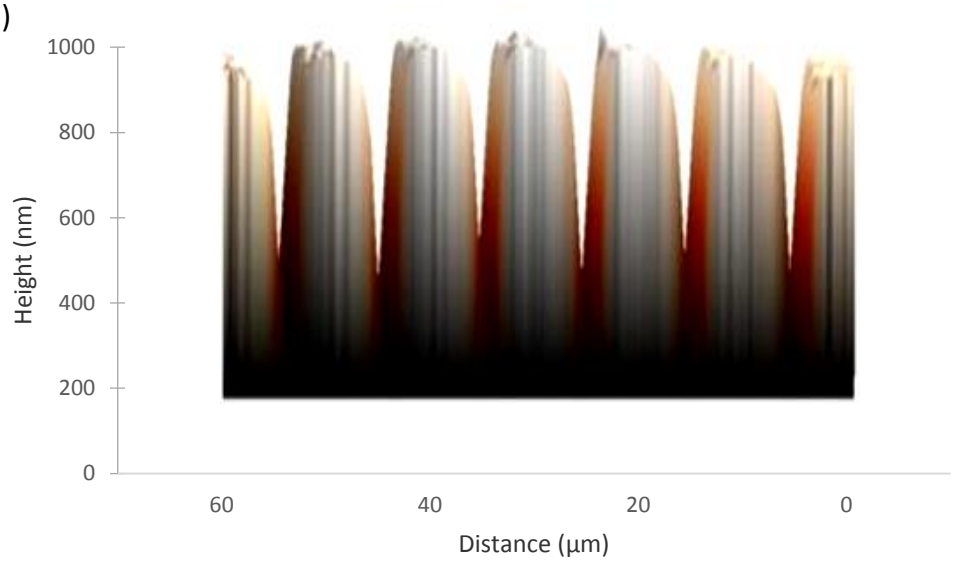
1000
800
600
400
200
0
Height (nm)
60
40
20
0
Distance (µm)

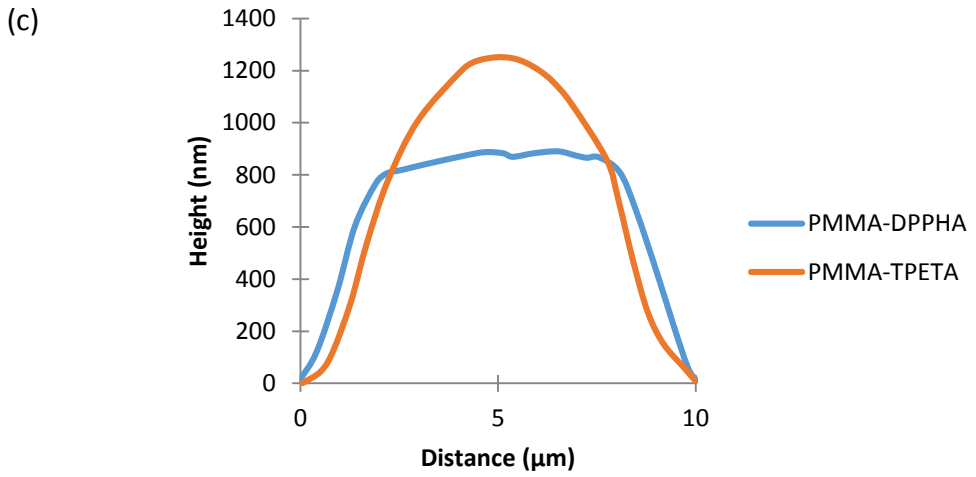


*Figure 4.2: AFM image of photoembossed DPPHA (a) and PMMA-TPETA (b). (c) is a plot showing the geometry of the relief structures obtained by AFM for a 10 µm pitch film.*

Fig. 4.2 shows the profile of the relief features measured by AFM. In both dosage and temperature experiments, PMMA-TPETA systems showed higher relief structures, compared with PMMA-DPPHA. Furthermore, the shape profiles are different at the optimum processing parameters, with PMMA-TPETA showing a sinusoidal profile and PMMA-DPPHA having a more 'table top' profile. The differences between these two photopolymer blends can be attributed to conversion rate and crosslinking of the monomer.

Anseth et al. [3] showed that an increase in functionality results in a decrease in maximum conversion and average number of reacted double bonds per monomer. TPETA and DPPHA are triacrylate and hexaacrylate, respectively. Conversion of the monomers was then calculated by the area under cured and non-cured peaks at 1407

(=$CH_2$) and 1630 (C=C) $cm^{-1}$ using the equation: % Conversion = $(A_{nc}-A_c)/A_{nc}$, where $A_{nc}$ and $A_c$ are the area under the curve for non-cured and cured photopolymer blends, respectively.

Fig. 4.3 shows absorption of the =$CH_2$ and C=C peaks before and after UV curing in nitrogen for 20 min. The reduction of the =$CH_2$ peak of PMMA-DPPHA and PMMA-TPETA was calculated to be 70% and 90%, respectively.

(a)

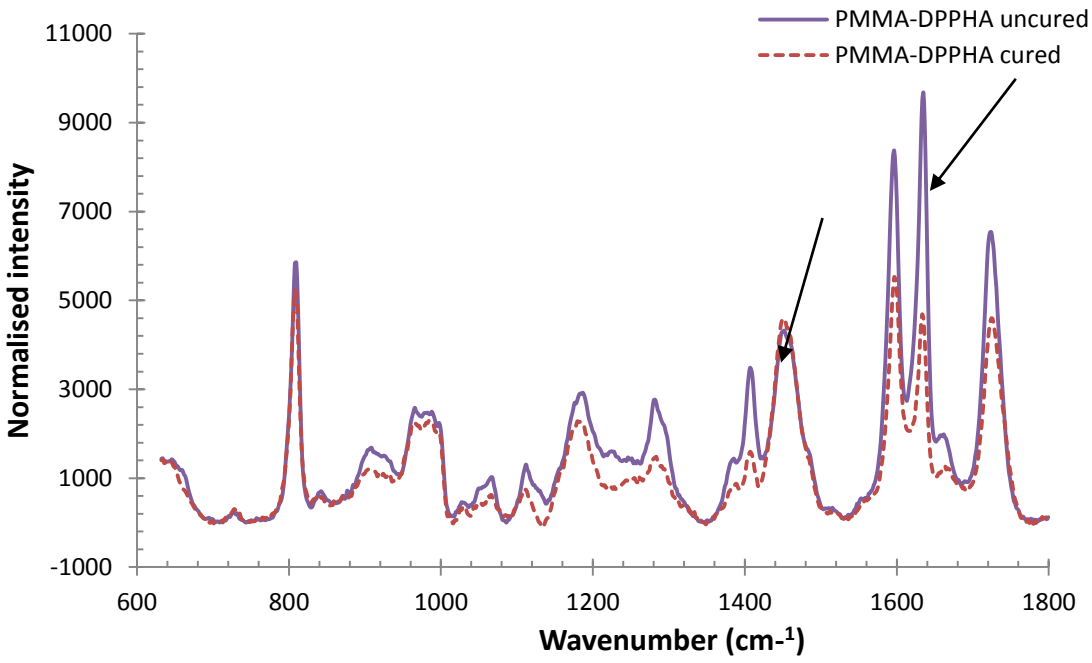

(b)

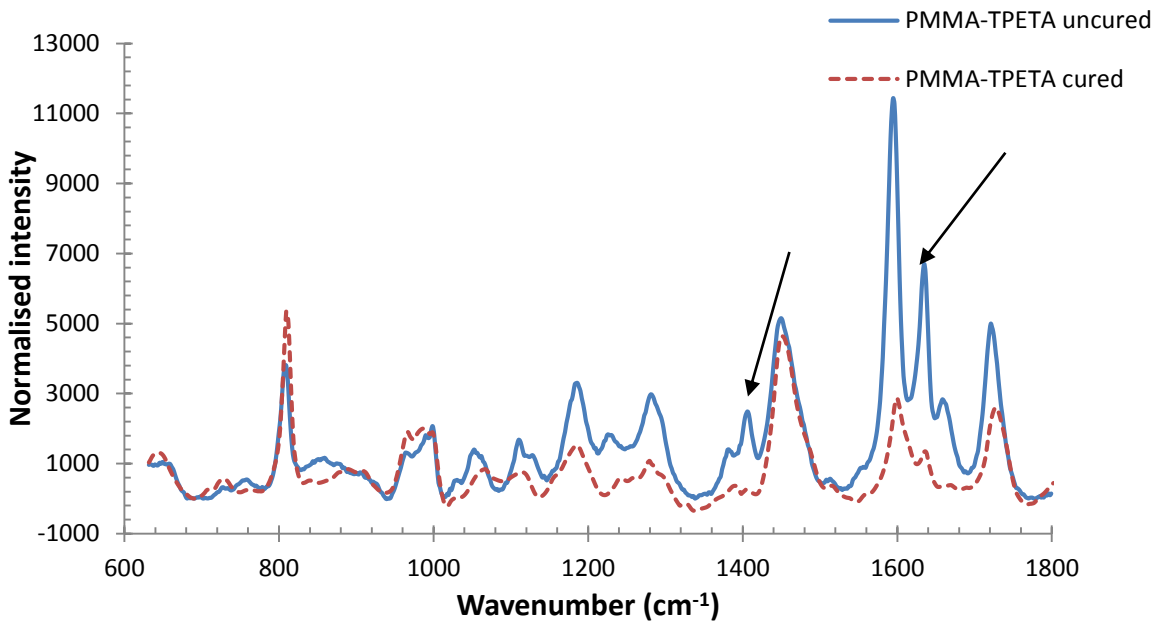


*Figure 4.3: FT-IR graphs of PMMA-DPPHA (a) and PMMA-TPETA (b) before and after curing. The bonds studied here are absorption of the acrylate bonds 1407 $cm^{-1}$ (=CH2) and 1630 $cm^{-1}$ (C=C).*

Additionally, the characteristic stretching of the acrylic double bond at frequencies of 1630 $cm^{-1}$ disappeared completely for PMMA-TPETA, and this confirmed that the monomer had been polymerized. Part of this peak was still present for PMMA-DPPHA, indicating that there was still unreacted monomer. Due to higher functionality of DPPHA, much earlier conversions result in diffusion-limited propagation [3]. The high-end conversion of TPETA can be a factor that results in the higher-relief structures of PMMA-TPETA. Higher conversion in irradiated regions generates a higher chemical and concentration gradient for monomer diffusion from non-irradiated regions. Furthermore, due to the high functionality of DPPHA, a high cross-link density is formed early on, hindering monomer diffusion to the core of the irradiated region resulting in less material reaching the centre from the lateral sides. This explains why the profile of

PMMA-DPPHA has a broader peak compared with PMMA-TPETA. Other factors that can affect the height of the relief structures (not shown here) include interaction between monomer and monomer/polymer, and the shape and size of the monomer [4-6]. Nevertheless, it is shown that the height of photoembossed structures can be controlled with both UV and temperature for both PMMA-DPPHA and PMMA-TPETA.

***Cell culture***

Very often, functionalisation of polymer surfaces with biological molecules like collagen or fibronectin is often important to promote cell adhesion. However, in this study, the substrates were not coated or functionalised in order to fully investigate material properties. Fig. 4.4a is the fluoresence staining of PS, PMMA, PMMA-TPETA and PMMA-DPPHA from left to right, respectively. The live cells are stained green (top) and dead cells are red (bottom). All materials showed similar viability of 90%. This result was in agreement with the typan blue result after trypisinization. After 7 days of culture, all surfaces apart from PMMA-DPPHA were nearly confluent. Cell number on PMMA-DPPHA was significantly lower ($p<0.05$) than substrates with the same surface area (glass slide, PMMA and PMMA-TPETA). Generally, monomers are harmful to cells, and thus conversion of monomer during photopolymerisation is important for cell compatibility. Adhesion of fewer cells on the surface of PMMA-DPPHA could be attributed to the presence of non-converted monomer. Nevertheless, the PMMA-TPETA

showed promising results as a biocompatible material for cell culture and thus was analysed further for cell orientation under SEM.

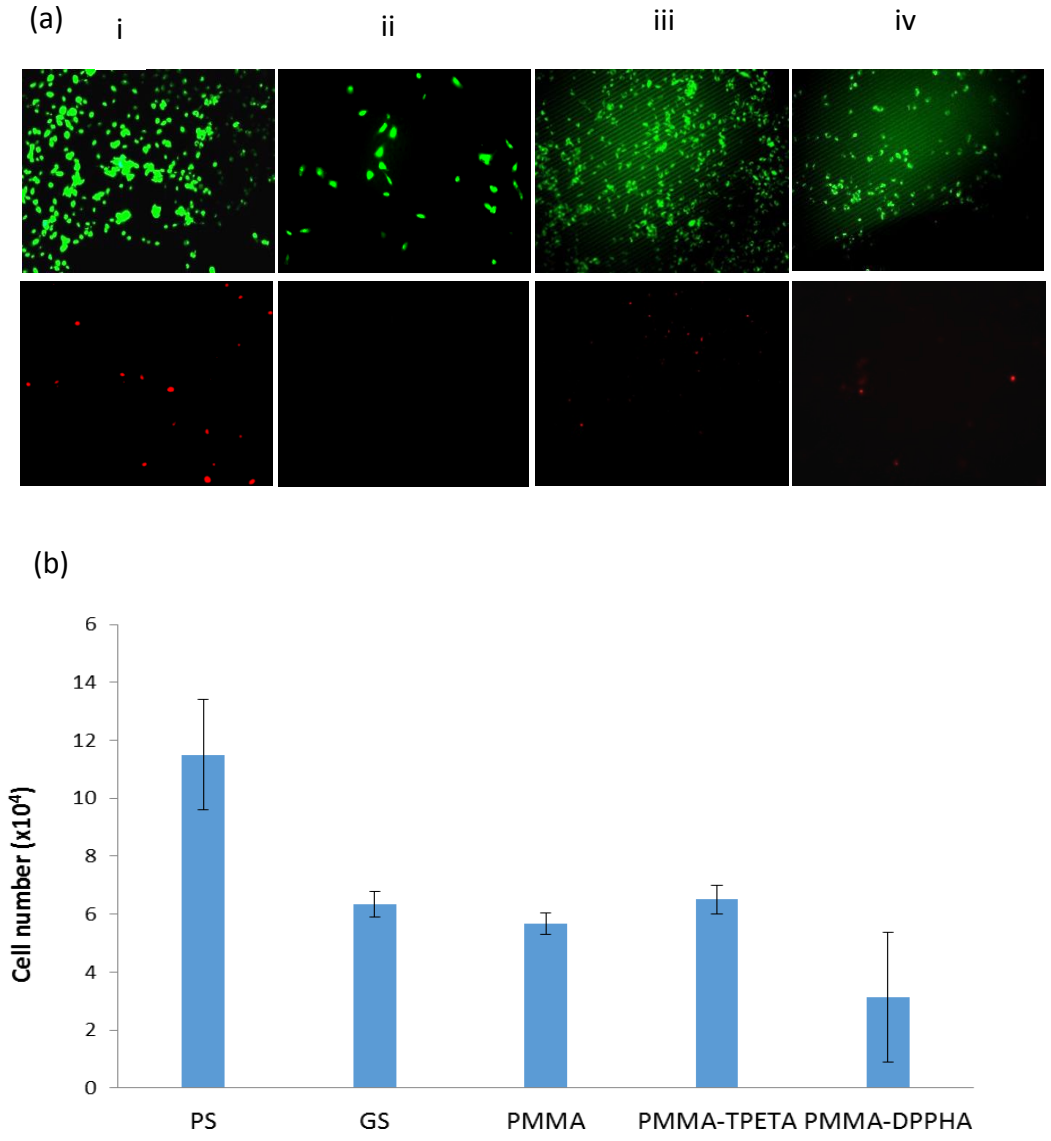


*Figure 4.4: Live (top) and dead (bottom) cells staining for (a) PS (i), PMMA (ii), PMMA-DPPHA (iii) and PMMA-TPETA (iv) (left to right) after 7 days of culture. (b) Graph showing cell number of live cells after trypsin and trypan blue staining. The cell number of the glass slide (GS) was included to compare similar surface area. This figure shows that PMMA-TPETA has a significantly higher number of cells compared to PMMA-DPPHA ($p<0.05$).*

PMMA-TEPTA films were photoembossed with pitches from 4-100 µm on each film to determine the appropriate pitch for HUVECs using the optimum conditions for the 10 µm pitch. It was observed that more cells adhered in the regions with 20 µm pitches. Fig. 4.5 shows cell orientation on 20 µm pitch films, which had a relief height of 2 µm. The long axis of the cells appeared to be aligned with the direction of grooves (Fig. 4.5a). The results of cell orientation on the surface-textured PMMA-TPETA evaluated after 72 hrs is shown in Fig. 4.5b. Cells are aligned if their major axes were within 20° with respect to the direction of the groove [1, 7]. The groove orientation is taken as $90^{o}$, and thus 60% HUVECs were oriented on the photoembossed substrate with 20 µm pitch and 2 µm depth. This shows that the cells respond to the surface topography and that contact guidance is achieved on these substrates.

(a)

.

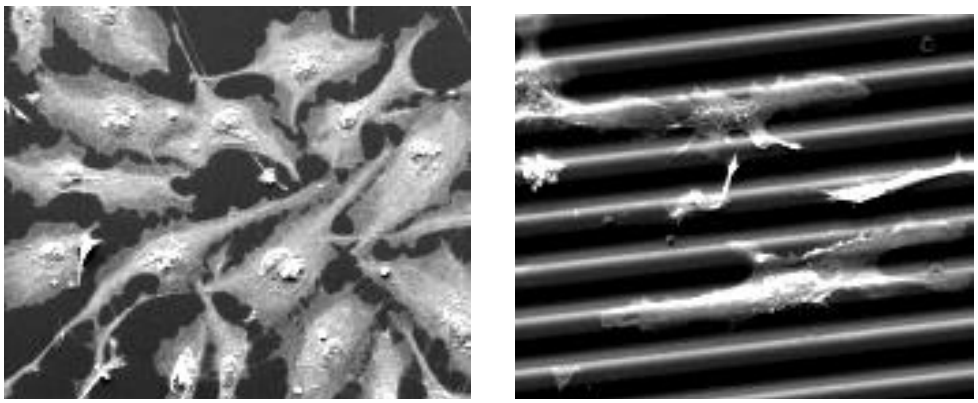

(b)

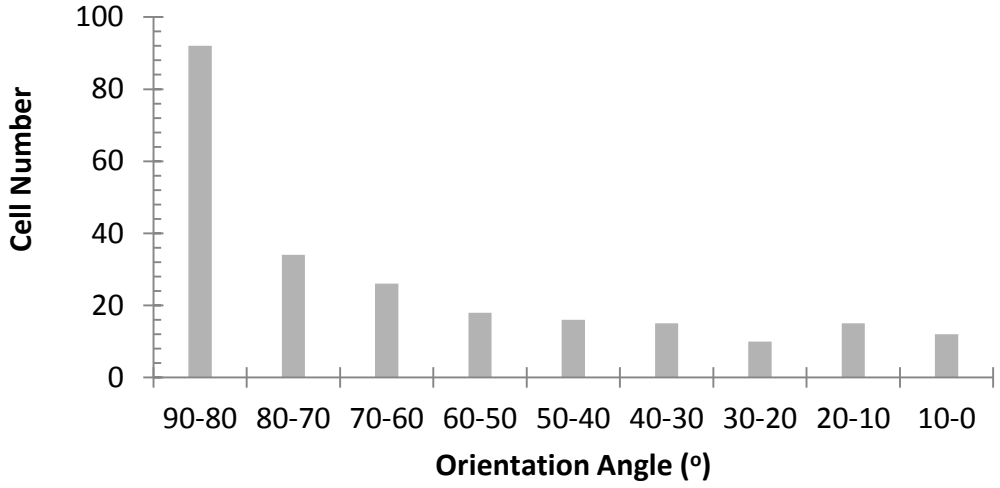


*Figure 4.5: (a) shows SEM images of HUVEC on flat film (i) and on textured 20 µm pitch and 2 µm height grooves (ii). (b) is the cell orientation distribution with groove direction taken as 90°.*

## 4.3. Conclusions

Biocompatible PMMA photopolymers have been successfully textured by photoembossing. The height of the relief structures was controlled by altering UV dosage or processing temperature to obtain different relief height. The main advantage of this type of surface texturing over traditional lithographic and embossing techniques

is its potential to create complex relief features without the need of an etching step. It can also be utilised in automated in-line manufacturing processes. Biocompatibility of the photopolymer blends was evaluated by culturing HUVECs in vitro. It was shown that PMMA-TPETA had similar adhesion to PMMA in the absence of protein coating. PMMA-TPETA showed highest cell adhesion compared with PMMA-DPPHA, and this was attributed to the higher conversion of monomer of TPETA compared with DPPHA. Contact guidance of HUVEC cells was also observed on the photoembossed substrate with a pitch of 20 μm and depth 2 μm, with 60% of the cells aligning in the direction of grooves.

In the next chapter, the biocompatible PMMA-TPETA is processed into fibres using the electrospinning technique. The spun photopolymer fibres are then photoembossed to create texture on fibre surfaces, and the effect of this fibrous textured morphology on cell adhesion will be evaluated.

## References

[1] P. Uttayarat, G. K. Toworfe, F. Dietrich, P. I. Lelkes, and R. J. Composto, "Topographic guidance of endothelial cells on silicone surfaces with micro- to nanogrooves: Orientation of actin filaments and focal adhesions," *Journal of Biomedical Materials Research Part A,* vol. 75A, pp. 668-680, 2005.

[2] C. Sánchez, B. J. de Gans, D. Kozodaev, A. Alexeev, M. J. Escuti, C. van Heesch, T. Bel, U. S. Schubert, C. W. M. Bastiaansen, and D. J. Broer, "Photoembossing of

Periodic relief structures using polymerization- induced diffusion: a combinatorial study," *Advanced Materials,* vol. 17, pp. 2567-2571, 2005.

[3] K. S. Anseth and C. N. Bowman, "Reaction behavior and kinetics of multifunctional (meth)acrylate photopolymerizations," *Abstracts of Papers of the American Chemical Society,* vol. 207, pp. 427, 1994.

[4] C. M. Leewis, A. M. de Jong, L. J. van IJzendoorn, and D. J. Broer, "Reaction–diffusion model for the preparation of polymer gratings by patterned ultraviolet illumination," *Journal of Applied Physics,* vol. 95, pp. 4125-4139, 2004.

[5] C. M. Leewis, A. M. de Jong, L. J. van IJzendoorn, and D. J. Broer, "Simulations with a dynamic reaction-diffusion model of the polymer grating preparation by patterned ultraviolet illumination," *Journal of Applied Physics,* vol. 95, p. 8352, 2004.

[6] C. Leewis, P. Mutsaers, A. De Jong, L. Van Ijzendoorn, D. Broer, and M. De Voigt, "Monomer diffusion assisted preparation of polymer gratings: A nuclear microprobe study," *Nuclear Instruments and Methods in Physics Research Section B: Beam Interactions with Materials and Atoms,* vol. 181, pp. 367-371, 2001.

[7] S. Britland, H. Morgan, B. WojiakStodart, M. Riehle, A. Curtis, and C. Wilkinson, "Synergistic and hierarchical adhesive and topographic guidance of BHK cells," *Experimental Cell Research,* vol. 228, pp. 313-325, 1996.

# Chapter 5

## Photoembossing of electrospun PMMA-TPETA fibres using holographic exposure

Non-woven biomaterials based on electrospun nano- or micro-fibres are presently being extensively investigated for biomedical applications such as tissue engineering and drug delivery. Here, fibres for such applications are electrospun from blends using a volatile solvent, and solid fibres containing a polymer and monomer mixture are collected on a substrate. To study the effect of UV dosage and temperature on photoembossing of these fibres, non-woven mats with fibre diameter of 2 μm are electrospun and

patterned using interference of two coherent UV laser beams followed by a thermal development step. In this study, a patterned exposure with a pitch of 8 µm is used to texture these fibres. AFM measurements revealed that the patterned exposure using interference holography resulted in a surface texture on the fibres. The effect of temperature and UV dosage on fibres was similar to results seen in photoembossed films.

Fibronectin and cell adhesion was evaluated on 1 µm fibres with a pitch of 2µm. Results showed that cells and fibronectin adhered better onto the PMMA-acrylate fibres (smooth and textured) compared to pure PMMA fibres after culturing for 24 hrs. Vinculin staining revealed focal adhesions along the fibre axis. However, texturing did not improve cell adhesion to photoembossed fibres compared with their non-embossed counterparts.

## 5.1. Materials and methods

Poly(methyl methacrylates) with molecular weights of 120 kg/mol and 350 kg/mol were used as received from Sigma Aldrich. The monomer (trimethylolpropane ethoxylate triacrylate; TPETA), photo-initiator Irgacure 369, and dimethyl formamide (DMF) were all used as received from Sigma Aldrich. Dapi, phalloidin-TRITC, mouse anti vinculin, rabbit vinculin antibody, anti-rabbit antibody (594-conjugate), fibronectin and Polyl-lysine polyethylene gylycol (PLL-PEG) were obtained from SuSoS. Phosphate buffer

saline (PBS), 4-(2-hydroxyethyl)-1-piperazineethanesulfonic acid (HEPES), paraformaldehyde, TritonC, and gelatine were obtained from Sigma Aldrich.

***Electrospinning***

A 60:40 wt% ratio of PMMA (120 kg/mol) and TPETA were dissolved in 70 wt% of DMF. Irgacure 369 was dissolved at 10 wt% of the monomer. This solution was electrospun using a single nozzle with 1 mm diameter at a collector distance of 20 cm. The applied voltage was 20 kV with a flow rate of 0.8 ml/hr. The fibres obtained had a diameter of 2 ± 0.5 µm. Films were also prepared by wire-bar coating with this solution as a control to compare texturing of films and fibres.

To obtain fibres with a diameter of 1 µm, PMMA with a molecular weight of 350 kg/mol was blended with TPETA at a ratio of 60:40 wt% of PMMA and TPETA, respectively. The monomer and polymer were dissolved in 82 wt% DMF. An initiator was added at 10 wt% of the monomer. Fibres of 1 µm diameter were achieved by using a solution flow rate of 1 ml/hr. PMMA on its own was dissolved in 82 wt% DMF and was electrospun as a control.

***Photoembossing***

The first set of experiments was carried out to study the effect of UV dosage and processing temperature on 2 µm diameter fibres. Wire-bar coated films on glass cover slips with a thickness of 20 ± 5 µm were used as positive controls for the photoembossing process. The pitch used for these experiments was 8 µm. The 2 µm

spun fibres were exposed to a UV-light pattern generated by interference of two coherent beams from a pulsed Nd:Yag laser coupled to second and third harmonic modules, emitting 4 ns pulses of 355 nm linearly polarized light with vertical polarization (repetition rate 10 Hz) UV source. The exposure was done in ambient air at room temperature. Fig. 5.1 shows a schematic of the photoembossing procedure. Different UV intensities were studied to obtain the optimum intensity. The intensity of the source was varied between 0 - 150 mJ/cm$^2$. For this study, the temperature used for the thermal processing step was 120 $^o$C in ambient air. At the optimum UV dosage, the thermal development temperature was also varied in order to study the effect of processing temperature on the relief height. After the thermal development stage, the fibres underwent flood exposure with UV-light using an Omnicure S2000® from Lumen Dynamics at 120 $^o$C in ambient air to cure the residual monomer. The height of the relief structures was analysed on the films and fibres using atomic force microscopy (AFM) and scanning electron microscopy (SEM). The second part of the photoembossing study involved patterning 1 µm fibres with a 2 µm pitch for cell adhesion studies. The pitch sizes were varied using the equation $p = \lambda/n.2\sin\theta$, where $p$ is pitch, $\lambda$ is the wavelength, $n$ is the refractive index of air, and θ is the angle of interference.

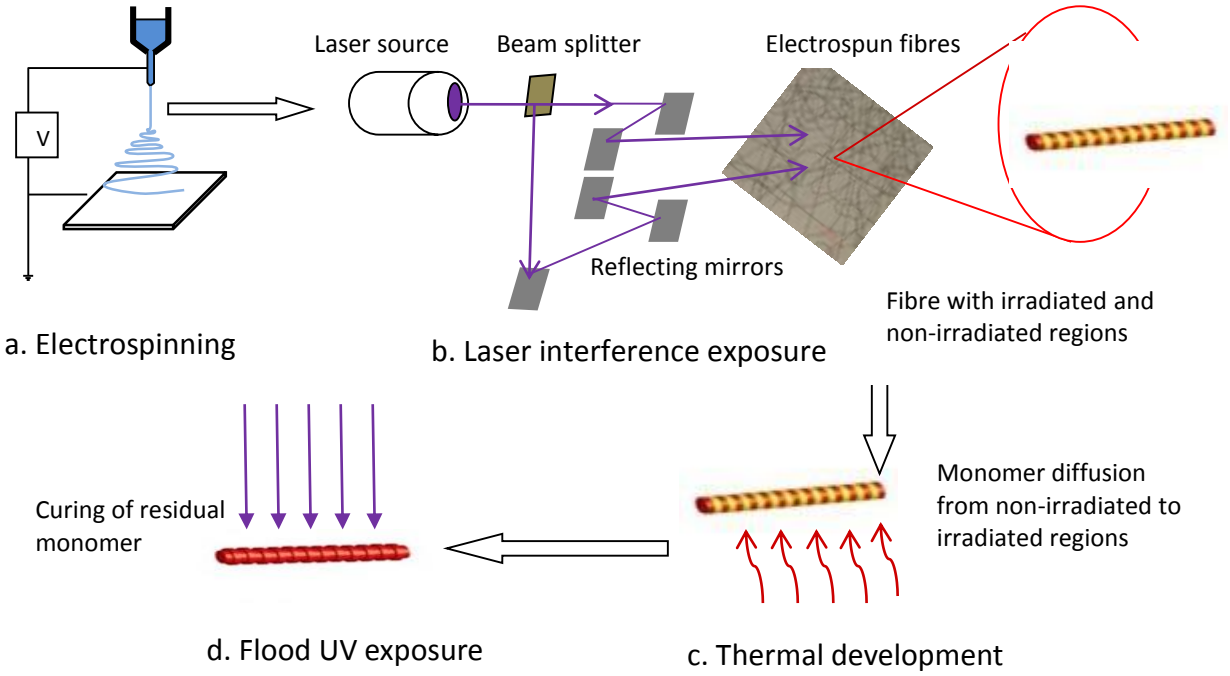


*Figure 5.1: Photoembossing procedure on fibres by holographic exposure.*

***Fibronectin coating***

PMMA and PMMA-TPETA fibres with an average diameter of 1 µm were electrospun on a 12 mm diameter glass substrate. Non-textured and photoembossed PMMA-TPETA electrospun fibres were analysed for fibronectin adhesion. PMMA fibres were used as control. The samples were placed in a 24-well plate and were first coated with PLL-PEG, which was dissolved in 0.25 µg/ml in HEPES to prevent protein adhesion onto the glass for 45 min. The samples were then washed with PBS and coated with 10 µl/ml of fibronectin in PBS. The samples were left to incubate for 45 min and washed with PBS. The samples were blocked with serum, gelatin and PBS in a ratio 1:0.025:10,

respectively, and incubated with a rabbit vinculin antibody at 400x dilution in the blocking buffer for 45 min. The samples were then washed and incubated for 45 min with anti-rabbit antibody (594-conjugate) at 1000x dilution in the blocking buffer to stain red. The samples were washed with PBS 3 times and once with deionised water. The slides were mounted with movial and analysed using a LEICA fluorescence microscopy.

***Cell culture***

To study keratinocyte behaviour on smooth and photoembossed electrospun fibre, a layer of 1 µm fibres was electrospun onto 13 mm glass slides. This was followed by a PLL-PEG coating to prevent non-specific cell adhesion onto the glass. The substrates were then coated with fibronectin and seeded with human primary keratinocytes at a density of 20,000 cells/ml in a 24 well plate for 24 hrs. The cells were washed in PBS and fixed in 4% paraformaldehyde for 5 min. The samples were then washed with PBS followed by incubating with triton for 5 min. After washing with PBS, they were incubated in blocking buffer for 30 min. Each sample type was stained for actin and vinculin using phalloidin-TRITC (500x) and mouse anti-vinculin (500x), respectively, in blocking buffer. All samples were also stained with Dapi (1000x) to observe cell nuclei. Cells cultured on photoembossed 1 µm fibres were also stained with actin and vinculin to study the effect of surface-textured fibres on cell adhesion and spreading.

## 5.2. Results and discussions

***Photoembossing***

Electrospinning of 2 µm fibres of PMMA-TPETA fibres resulted in homogenous fibres, shown in Fig. 5.2. Few beads were observed in the fibre mat, which may be due to fluctuation in ambient conditions, particularly humidity and temperature, which influence fibre morphology [1].

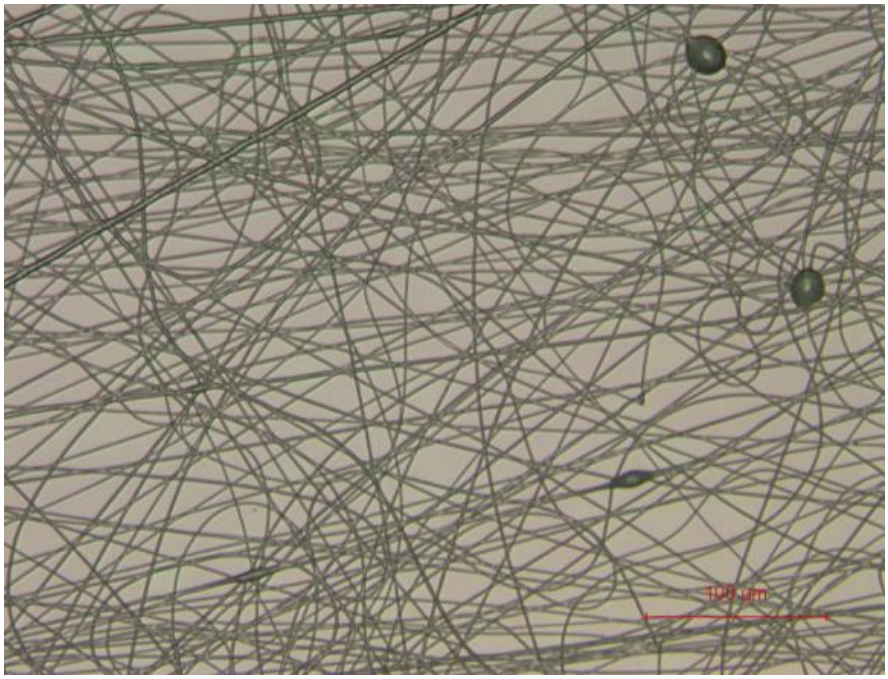

*Figure 5.2: Electrospun fibres using PMMA (MW = 120 kg/mol) 60:40 TPETA blend before photoembossing.*

The fibres and films were photoembossed with a pitch of 8 µm. The results in Fig. 5.3 show that the optimum UV dosage is similar for both films and fibres. The fibres and films had an optimum relief height of 510 nm and 600 nm, respectively, at a UV intensity

of 0.08 J/cm$^2$. Films showed higher relief structures, and this could be attributed to the thicker film sample (20 µm) compared to fibres (2 µm), as more monomer participates in the diffusion process in thicker samples. We have previously shown (see Chapter 4) that the optimum processing temperature for PMMA-TPETA was 120 $^{o}$C, and thus all thermal development steps were performed at this temperature.

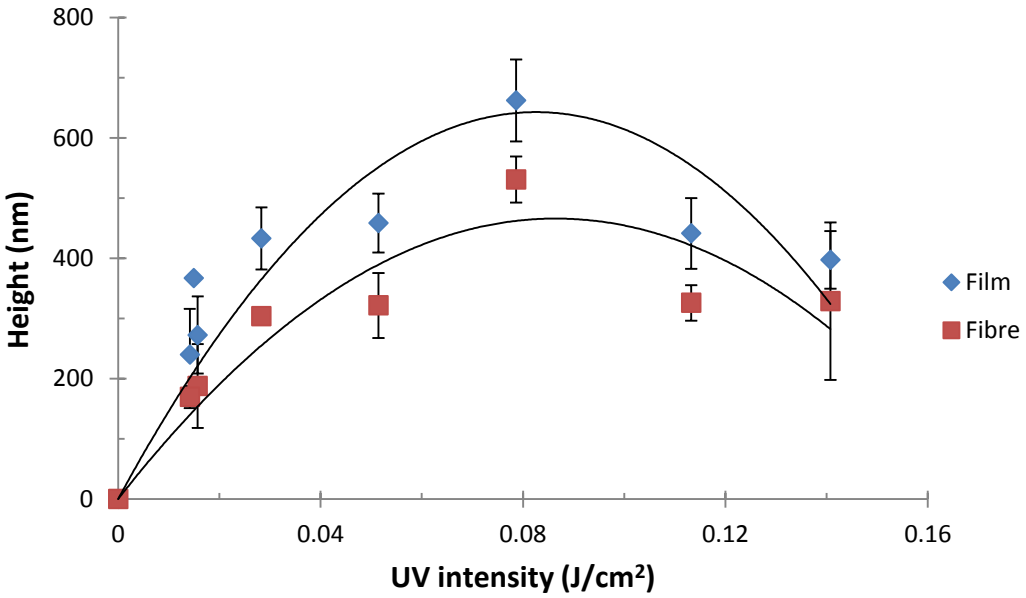


*Figure 5.3: Relief height of photoembossed substrates with an 8 µm pitch at different UV dosages.*

The effect of UV intensity has previously been studied by Sanchez et al. [2] and De Gans et al. [3] for photopolymer films. Their results also showed that above an optimum UV dosage, the height of relief structures decreases, and this was attributed to high crosslink density, which inhibits monomer diffusion [16, 20].

(a)

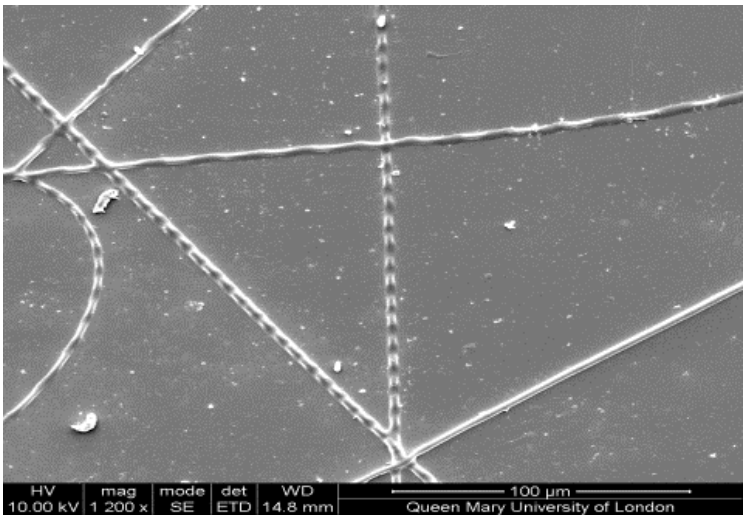


(b)

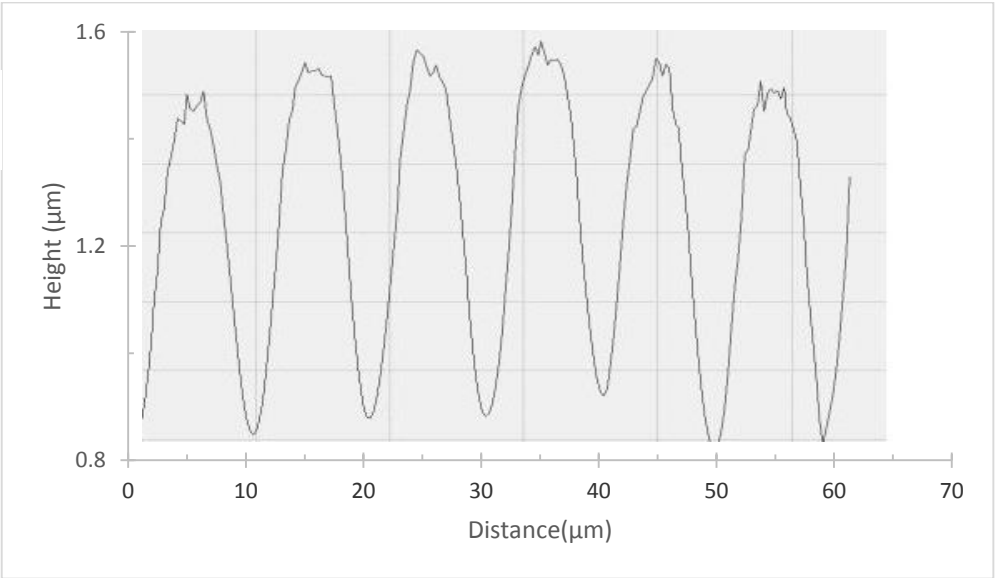


*Figure 5.4: SEM of photoembossed PMMA-TPETA. (a) Fibres oriented in the appropriate axis were textured, whereas those completely parallel to the interference pattern showed no texture. The pitch size on the fibre surface also changed depending on orientation. (b) AFM profile of the textured fibres.*

The fibres maintained their fibrous structure after photoembossing as shown in Fig. 5.4. SEM images also revealed that not all the fibres are textured during photoembossing. Fibres that were parallel to the interference pattern were not embossed, while those perpendicular had a pitch equal to the interference pattern. Therefore, the relief height shown in Fig. 5.3 was obtained by using only samples with a pitch of 8 µm (i.e. fibres perpendicular to the interference axis). To obtain surface textures on fibres with uniformly distributed pitches, all fibres should be aligned in one direction and exposed perpendicular to the interference pattern. This can be beneficial in tendon and ligament regeneration, when anisotropic fibre mats are preferred [4]. Nevertheless, we have shown that surfaces of electrospun fibres can be textured by photoembossing while maintaining their morphology with the height of the relief structures to be controlled by the UV dosage. Furthermore, we have shown that processing parameters used for the photoembossing of films can be adapted for fibres.

For endothelial cell culture, fibres of 1 µm diameter were selected for electrospinning because the fibre mat was less affected by ambient spinning conditions, unlike the 2 µm fibres. 1 µm fibres were obtained by increasing the molecular weight of the polymer binder from 120 kg/mol to 350 kg/mol. Hence, the concentration of the polymer and monomer could be reduced to achieve a spinnable solution. Fig. 5.5 shows a fluorescent microscopy image of electrospun fibres before and after photoembossing. The photoembossed fibres shown in Fig. 5.5 are fibres processed at the optimum UV intensity at this pitch. Fig. 5.6 presents the height of the surface structures as a function of UV intensity.

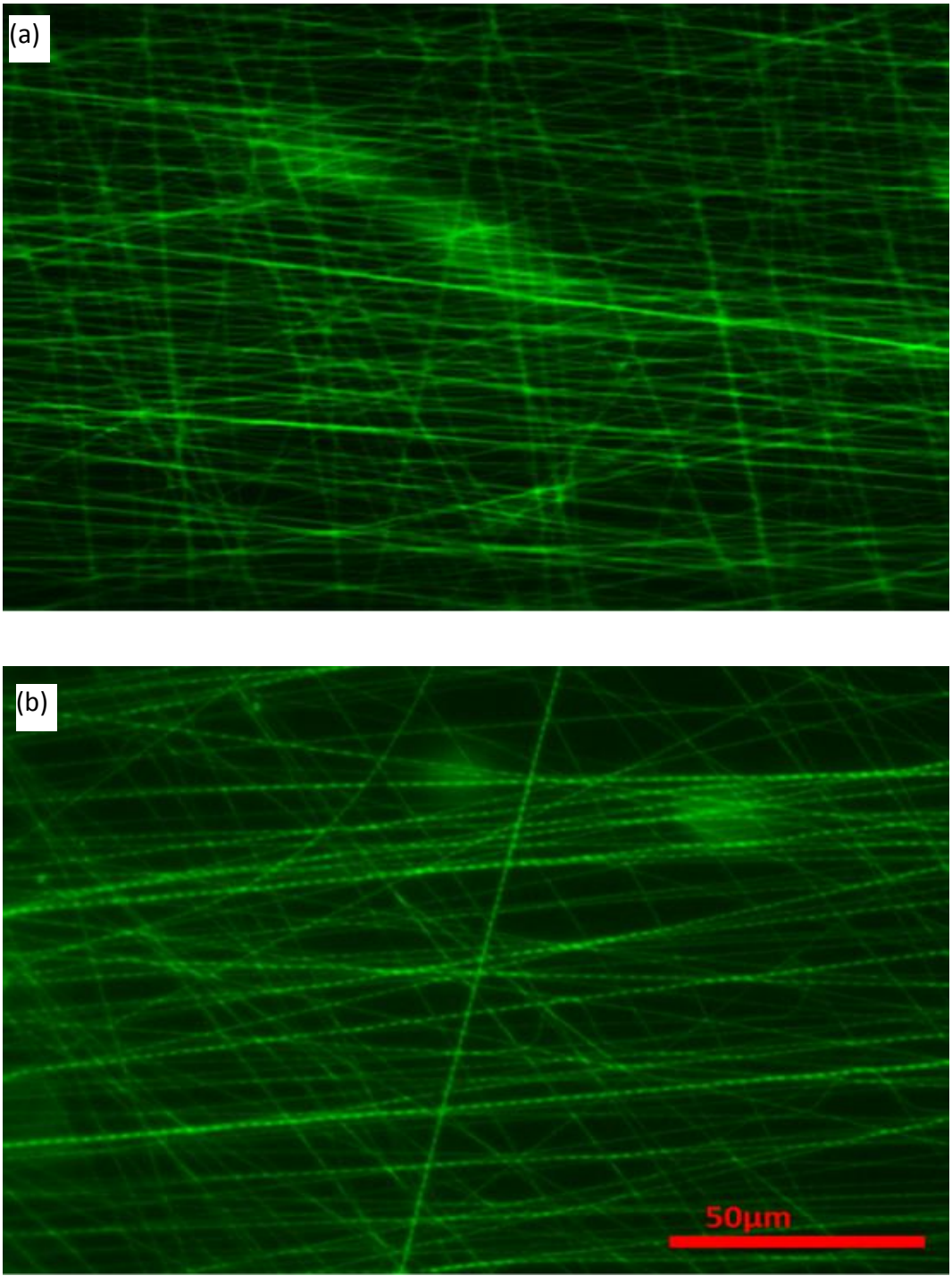


*Figure 5.5: Fluorescence microscopy image of electrospun 1 µm PMMA-TPETA fibres before (a) and after photoembossing with 2 µm pitch (b).Fibres are fluorescent due to the photoinitiator.*

The optimum UV intensity for a 2 µm pitch shown in Fig. 5.6 is 0.2 J/cm$^2$; about 2.5 times that of the 8µm ptich. Sanchez et al. [2] and De Gans et al. [3] showed that in the case of films, a higher optimum UV intensity is required for lower pitches. Higher UV intensity results in a higher crosslink density of the network. For smaller pitches, the diffusion path is shorter and thus less affected by these high crosslink densities. Similar effects are operative in the current study on fibres.

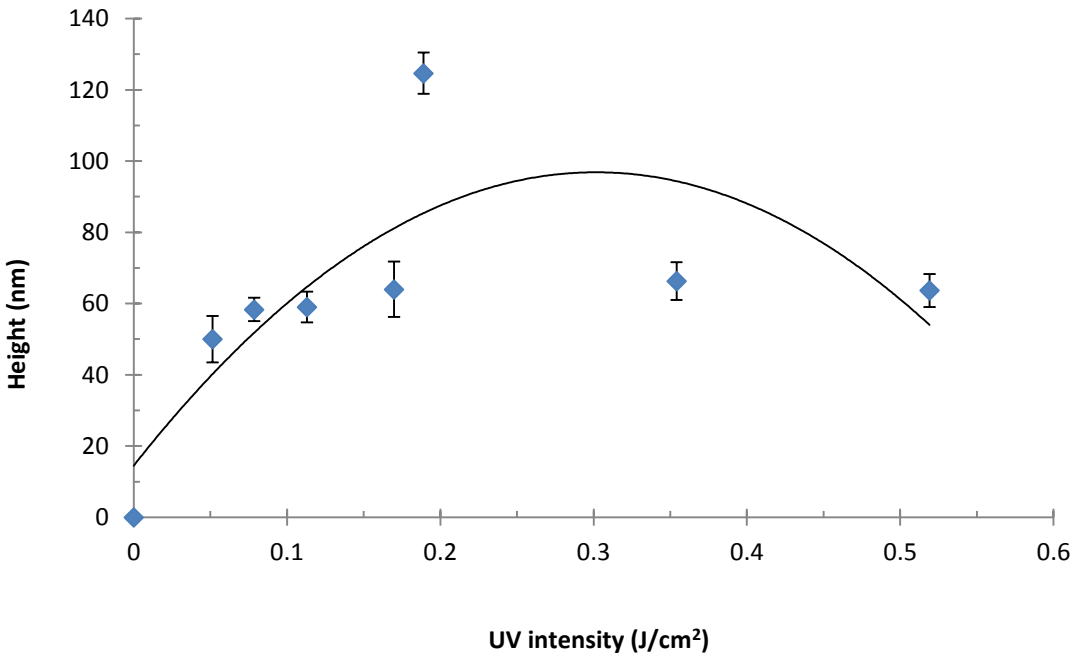


*Figure 5.6: Influence of UV intensity on the height of surface structures for a photoembossed 1 µm diameter fibre with a pitch of 2 µm. The thermal development step was performed at 120 $^o$C in ambient air.*

To demonstrate that the photoembossing technique can also generate sub-micron texturing, we embossed the surface of electrospun fibres at a pitch of 0.5 µm and a UV dosage of 0.2 J/cm$^2$ at 120 $^o$C. The height of the structures formed was 30 nm. AFM images of the relief structures with 2 µm and 0.5 µm pitches are shown in Fig. 5.7.

(a)

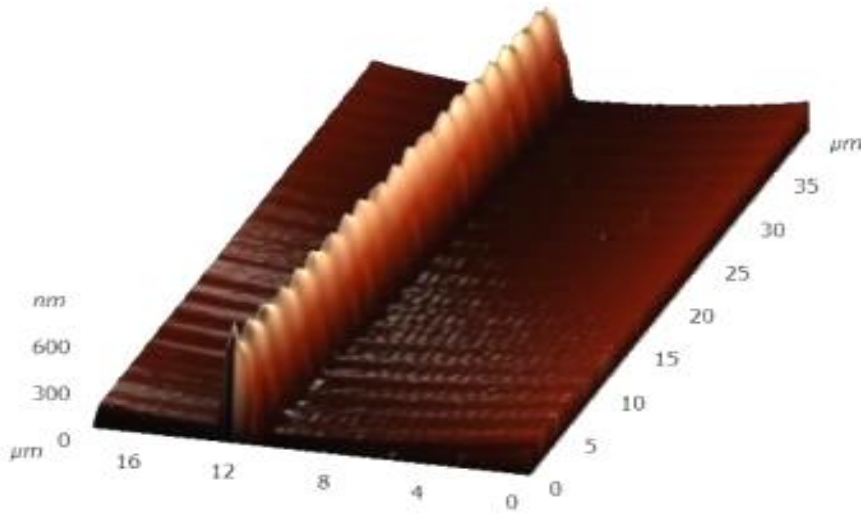


(b)

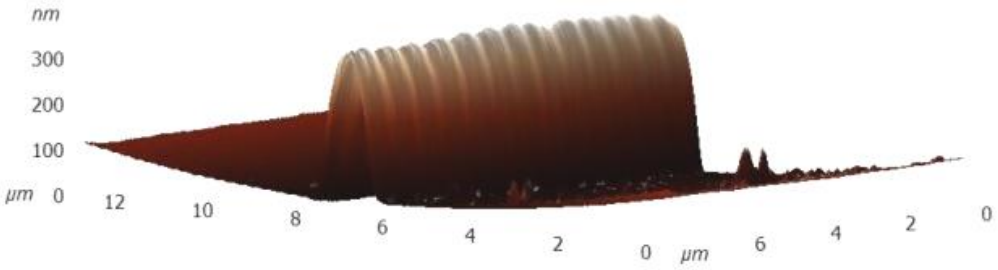


*Figure 5.7: Surface textured PMMA-TPETA fibres with 2 µm (a) and 0.5 µm (b) pitches on 1 µm diameter fibres as analysed by AFM.*

In this chapter, we have shown that electrospun fibres can be textured by photoembossing using a holographic patterned laser exposure followed by a thermal development step. The fibres maintained their morphology after photoembossing. The effect of UV intensity on relief height showed a similar trend as in films, i.e. an increase in relief height was observed with increasing UV intensity until an optimum value above which the height again decreases. Furthermore, a reduced pitch size requires a higher optimum UV intensity, which is also in agreement with results obtained by Sanchez et al. [2] for films. In summary, it has been shown that the photoembossing technique can be used to create submicron textures on electrospun fibres by patterned holographic exposures that mimic the surface of natural collagen. In the next section, we will evaluate the effect of such surface texturing on cell culture.

***Fibronectin adhesion***

Cell adhesion is mediated by extracellular matrix (ECM) molecules such as fibronectin, vitronectin, collagen or laminin [5-7]. During *in vivo* cell culture, the surface of synthetic biomaterials is generally coated with these molecules to promote cell adhesion, which is essential to promote keratinocyte viability. Fibronectin protein has been used previously to promote keratinocyte adhesion on the surface of polymeric biomaterials [8]. The adhesion of fibronectin to the surface of 1 µm fibres was qualitatively analysed by checking the fluorescence of stained adhered fibronectin on the surface of the fibres. After electrospinning, photoembossing and curing, the substrates were coated with PLL-

PEG to prevent protein adhesion onto the glass slide. The assumption here was that the PLL-PEG will attach to the glass slide and not the polymer fibres. This was then followed by the fibronectin coating on the fibres. Fibronectin coating on glass slide with (Fig. 5.8a) and without (Fig. 5.8b) PLL-PEG were used as reference. The reference samples showed that PLL-PEG diminished fluorescence intensity (Fig. 5.8b) of fibronectin. After 24 hr of incubation, PMMA fibres did not show a substantial presence of fibronectin (Fig. 5.8c), as no obvious fluorescent fibres were observed. PMMA-TPETA fibres were fluorescent even in the absence of fibronectin (Fig. 5.8d). However, the intensity of the red fluorescence increased significantly after fibronectin coating on the non-textured PMMA-TPETA surface (Fig. 5.8e). After surface texturing by photoembossing, the intensity of the red fluorescence decreased (Fig. 5.8f), compared with the non-textured surface (Fig. 5.5e). Unfortunately, this indicated that fibronectin adhered better on smooth PMMA-TPETA fibres rather than their textured counterparts. This result seems surprising, as micro-texturing has been shown previously to promote fibronectin deposition, which has been attributed to the increase in surface area and increase in surface energy [9-11]. However, this seems not to be the case for the photoembossed PMMA-TPETA. Two possible causes for this could be: (i) the formation of PMMA-rich zones during photoembossing, and/or (ii) some degree of adhesion of PLL-PEG on the fibre surface. From the fluorescent image, it seems more likely that PLL-PEG adhered to the surface of the textured fibres, thus reducing the adhesion of fibronectin. Cell adhesion on these substrates is also evaluated in terms of cell number and cell area. In Chapter 4, photoembossing of PMMA-TPETA films did not make any difference in the

cell number adhered to a textured film. Therefore, the minimum expectation here would be to observe no difference between embossed and non-embossed surface structures. However, if there is a reduction of fibronectin adhesion caused by the presence of PLL-PEG on the surface of the fibres, then a reduction in cell adhesion should also be observed.

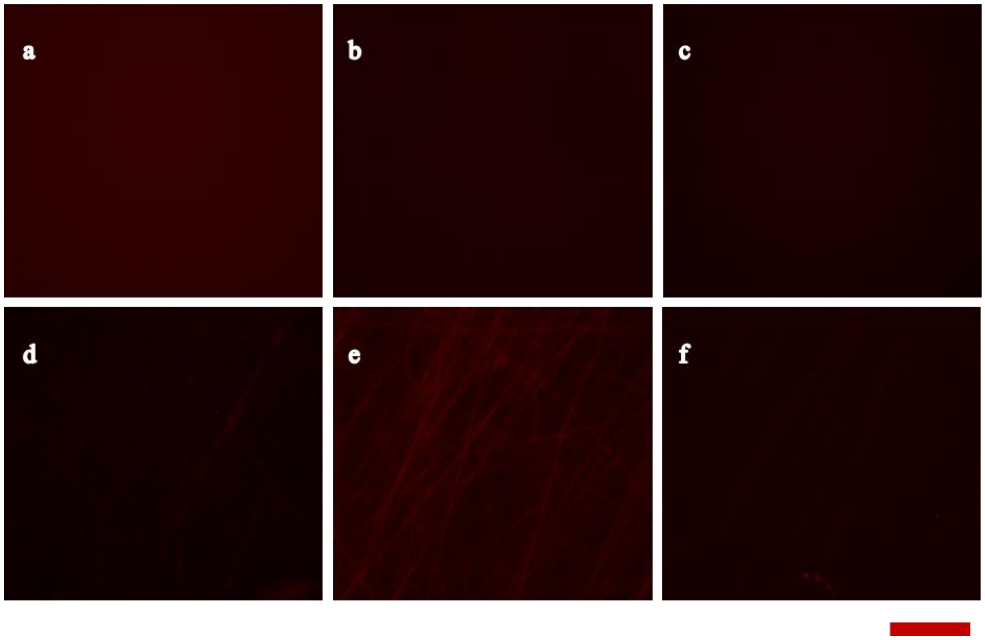


*Figure 5.8: (a) Fibronectin staining on glass, (b) Glass coated with PlL-PEG, and (c) PMMA fibres coated with PLL-PEG and fibronectin. (d) shows PMMA-TPETA without fibronectin and (e) and (f) are fibronectin-coated fibres without and with surface texture, respectively. Scale bar represents 60 µm.*

***Cell interaction***

To observe the effect of fibre surface texturing on cell behaviour, the 1 µm diameter fibres were photoembossed. The substrates were coated with PlL-PEG to prevent protein adhesion on the glass substrates, followed by a fibronectin functionalization of

the fibres. The effect on cell adhesion was evaluated after 24 hrs of culture. Vinculin staining revealed focal adhesion points on smooth and textured PMMA-TPETA as shown in Fig. 5.9a and 5.9b respectively. This demonstrates that cells formed real adhesion sites on both smooth and textured PMMA-TPETA fibres in Fig. 5.9a and Fig. 5.9b, respectively. However, there was a slight decrease in cell number and cell area on the textured fibres, compared with the smooth ones. Previously, the effect of surface topography in fibres has been studied using porous and rough fibres [12]. Moroni et al. [12] demonstrated that cell adhesion and proliferation increased when nanopores were formed on the surface of the fibres. However, in this study, micro-texture on the fibre surface seems to decrease cell adhesion and spreading to the fibre surface. This is similar to results obtained for protein fibronectin adhesion in the previous section. Thus, it is also not surprising that cell quantity is observed to be smaller on the textured surfaces, because fibronectin increases cell adhesion. This suggests that the PLL-PEG coating post fibre deposition is not the optimal method of preventing cell adhesion onto the glass slide. To fully quantify the effect of surface texturing of fibres by photoembossing, fibres should be spun on cell-repulsive surfaces (e.g. mica), which can withstand patterned exposure by a UV laser source. Furthermore, different pitch sizes have to be evaluated to fully characterise the effect of surface texturing by photoembossing.

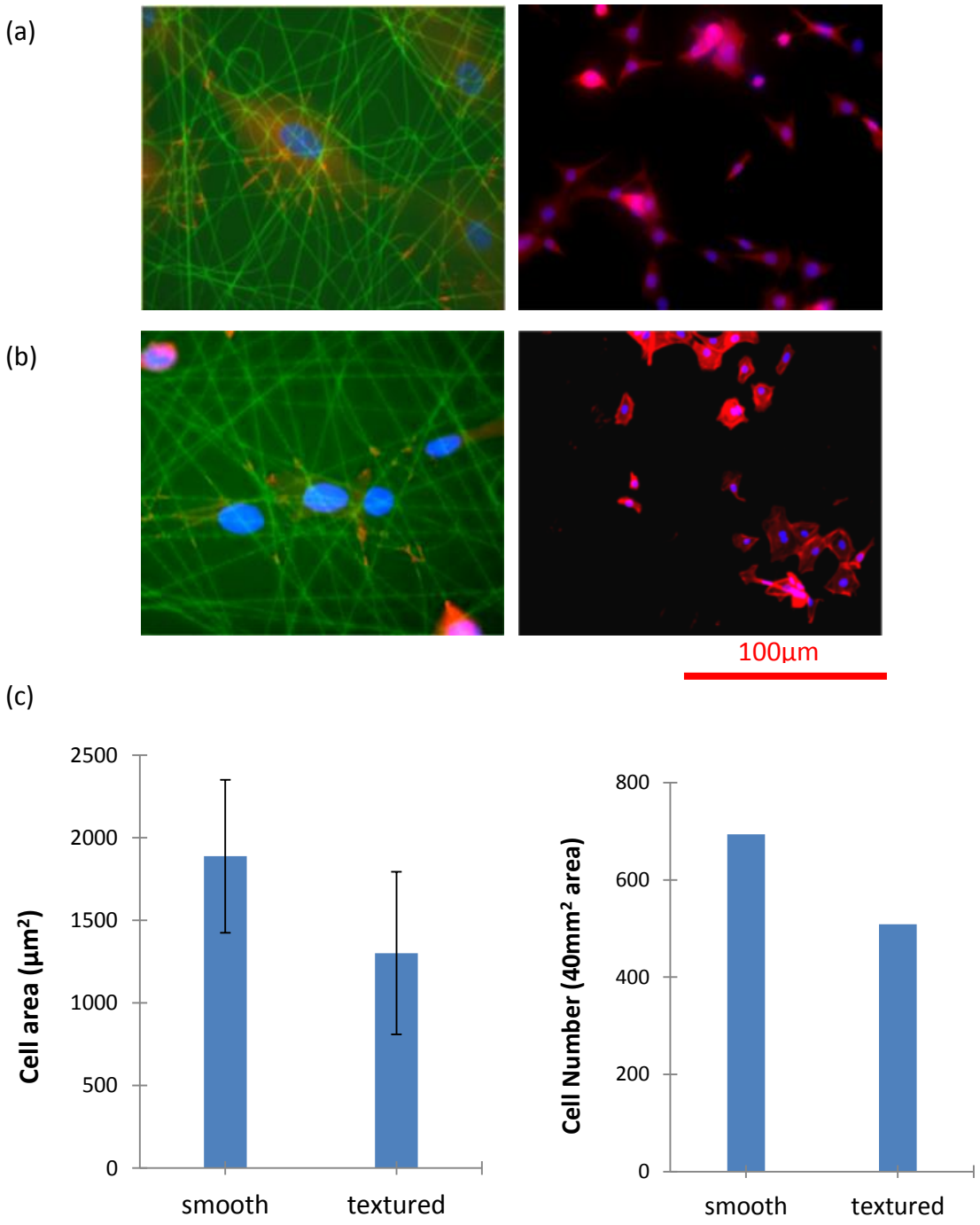


*Figure 5.9: Cell adhesion on (a) smooth and (b) textured PMMA-TPETA surfaces. The left images reveals vinculin staining along the fibre axis and the right image shows actin staining by phalloidin to reveal cell area. (c) Plot of cell area (left) and a cell number (right) on smooth and textured PMMA-TPETA. Total cell number was obtained from three 13mm coverslips.*

## 5.3. Conclusions

We have shown that reactive PMMA-TPETA blends can be electrospun and textured using photoembossing whilst maintaining a fibrous structure. Fibre diameter of the photopolymer blend was varied by changing the molecular weight of the PMMA binder in line with classical electrospinning of fibres. The pitch of the relief structures that could be achieved on the electrospun fibres was controlled by changing the distance or angle where the two beams interfere, which is given by the equation $p = \lambda / n\, 2\sin\theta$, and the height of these structures can be controlled by changing the UV dosage. Fibronectin deposition was higher on both smooth and textured PMMA-TPETA photopolymer, compared with smooth PMMA. Cells adhered readily to smooth and textured photopolymers after 24 hrs of culture, but not on the smooth PMMA. However, cell adhesion was unfortunately not improved on textured PMMA-TPETA fibres, compared with their smooth counterpart. In fact, the cell adhesion seemed slightly worse on textured fibres, and this was attributed to adhesion of PLL-PEG on the textured fibre surface, thus reducing fibronectin coating and cell adhesion.

The next chapter will evaluate the use of biocompatible and biodegradable poly L lactide-co-glycolide as a polymer binder. This polymer has been used widely in the field of tissue engineering due to good cell adhesion on material surfaces. This chapter will also evaluate if photopolymers made from PLGA-TPETA blends are as biocompatible as PLGA films, and whether surface texturing further improves cell adhesion.

## References

[1] S. Tripatanasuwan, Z. Zhong, and D. H. Reneker, "Effect of evaporation and solidification of the charged jet in electrospinning of poly(ethylene oxide) aqueous solution," *Polymer,* vol. 48, pp. 5742-5746, 2007.

[2] C. Sánchez, B. J. de Gans, D. Kozodaev, A. Alexeev, M. J. Escuti, C. van Heesch, T. Bel, U. S. Schubert, C. W. M. Bastiaansen, and D. J. Broer, "Photoembossing of periodic relief structures using polymerization- induced diffusion: a combinatorial study," *Advanced Materials,* vol. 17, pp. 2567-2571, 2005.

[3] B. J. de Gans, C. Sanchez, D. Kozodaev, D. Wouters, A. Alexeev, M. J. Escuti, C. W. Bastiaansen, D. J. Broer, and U. S. Schubert, "Optimizing photo-embossed gratings: a gradient library approach," *J Comb Chem. (2). pp. 228-36,* 2006

[4] S. Shang, F. Yang, X. Cheng, X. F. Walboomers, and J. A. Jansen, "The effect of electrospun fibre alignment on the behaviour of rat periodontal ligament cells," *Eur Cell Mater* vol. 19 pp. 180-92, 2010.

[5] G. Altankov and T. Groth, "Reorganization of substratum-bound fibronectin on hydrophilic and hydrophobic materials is related to biocompatibility," *Journal of Materials Science: Materials in Medicine,* vol. 5, pp. 732-737, 1994.

[6] L. Lu, C. A. Garcia, and A. G. Mikos, "In vitro degradation of thin poly(DL-lactic-co-glycolic acid) films," *Journal of Biomedical Materials Research,* vol. 46, pp. 236-244, 1999.

[7] C. J. Wilson, R. E. Clegg, D. I. Leavesley, and M. J. Pearcy, "Mediation of biomaterial-cell interactions by adsorbed proteins: a review," *Tissue Eng,* vol. 11, pp. 1-18, 2005.

[8] A. Takashima and F. Grinnell, "Fibronectin-mediated keratinocyte migration and initiation of fibronectin receptor function in vitro," *J Invest Dermatol,* vol. 85, pp. 304-8, 1985.

[9] F. Rupp, L. Scheideler, D. Rehbein, D. Axmann, and J. Geis-Gerstorfer, "Roughness induced dynamic changes of wettability of acid etched titanium implant modifications," *Biomaterials,* vol. 25, pp. 1429-38, 2004.

[10] P. Uttayarat, G. K. Toworfe, F. Dietrich, P. I. Lelkes, and R. J. Composto, "Topographic guidance of endothelial cells on silicone surfaces with micro- to nanogrooves: Orientation of actin filaments and focal adhesions," *Journal of Biomedical Materials Research Part A,* vol. 75A, pp. 668-680, 2005.

[11] P. Elter, R. Lange, and U. Beck, "Atomic force microscopy studies of the influence of convex and concave nanostructures on the adsorption of fibronectin," *Colloids and Surfaces B: Biointerfaces,* vol. 89, pp. 139-146, 2012.

[12] L. Moroni, R. Licht, J. de Boer, J. R. de Wijn, and C. A. van Blitterswijk, "Fiber diameter and texture of electrospun PEOT/PBT scaffolds influence human mesenchymal stem cell proliferation and morphology, and the release of incorporated compounds," *Biomaterials,* vol. 27, pp. 4911-4922, 2006.

# Chapter 6

## Photoembossing of semi-degradable biocompatible PLGA-TPETA films

We have shown previously that PMMA-acrylate photopolymers are biocompatible, showing improved cell similar compared to PMMA. However, the photoembossed surfaces with groove texture showed no improvement in cell adhesion. This was attributed to the low cell adhesion to PMMA polymer binder. PLGA has been used widely in the study of soft tissue regeneration due to its high biocompatibility and cell adhesion. This polymer is also biodegradable and thus can be utilised in the field of vascular regeneration. In this study, PLGA is blended with a triacrylate monomer (TPETA). The

surface relief structure is formed on the PLGA-TPETA by photoembossing. An optimum height of 950 nm was achieved for 10 µm pitch and the height of these relief structures can be controlled by changing UV intensity, processing temperature and time. Degradation study of this blend revealed a bulk degradation mechanism and PLGA-TPETA degraded slower compared to PLGA. We also evaluated the adhesion of human umbilical vein endothelial cells (HUVEC) on both smooth and textured PLGA-TPETA. The embossed PLGA-TPETA had a higher cell adhesion compared to the smooth substrates. Furthermore HUVECs proliferated faster on the embossed surface compared to their smooth counterparts.

## 6.1. Materials and methods

PLGA (75/25) and Trimethyllolpropane ethoxylate triacrylate (TPETA) was obtained from Sigma Aldrich. The photo-initiator 2-benzyl-2-(dimethylamino)-4'-morpholinobutyrophenone (Irgacure 369) and Propylene glycol monomethyl ether acetate (PGMEA) solvent was used as received from Sigma Aldrich.

PLGA , TPETA and Irgacure 369 were dissolved in 60 wt.% PGMEA at a ratio of 1:1:0.1. This solution was coated on acrylate-functionalised glass slides using a wire-bar coater to obtain a film thickness of about 40 µm. The films were irradiated with UV via a contact photomask using different dosages ranging from 0-1000 mJ/cm$^2$. The films were heated at 80 $^o$C for 20 min followed by flood UV exposure at intensity of 15 J/cm$^2$ to cure residual monomer. Another set of films was made to study the effect of temperature

ranging from 25 $^{o}$C to 110 $^{o}$C at 178.5 mJ/cm$^2$ dosages and a developing time of 20 min. Finally the effect of processing time was evaluated from 1 min to 24 hrs using UV intensity of 178.5 mJ/cm$^2$ processed at both room temperature (RT) and at 80 $^{o}$C.

The height of the relief structures were measured using NT-MDT® AFM in semi-contact mode to obtain relief profile and height.

***Cell culture***

HUVECs (Lonza Cologne AG, Germany) were grown in M199 medium (Gibco) at 37 ℃ and 5% $CO_2$. The culture medium contains 10% foetal bovine serum (FBS), EC growth factor-β (1 ng/ml), EC growth supplement from bovine neural extract (3 µg/ml), thymidine (1.25 µg/ml), heparin (10 µg/ml), 100 U/ml penicillin, 100 mg/ml streptomycin (all supplements are from Sigma Aldrich). Cells with less than 7 passages were used in all reported experiments *in vitro*. The medium was changed every 2 days. Cells were seeded onto the substrates after confluence. The substrates were washed 2 times with ethanol and rinsed 2 times with PBS before cell seeding. Cells were seeded on all the substrates with density of $1.5 \times 10^4$ cells/cm$^2$ and cultured up to 7 days.

***Degradation***

PLGA and PLGA-TPETA (non-embossed) and PLGA-TPETA-E (embossed) films with thickness of 60 µm were degraded in PBS at 37 $^{o}$C. Every week, the pH of each sample type was measured. Every 2 weeks each sample type was removed from PBS medium and dried overnight in a vacuum chamber at room temperature (R.T.). The weight of

each dried sample was measured and FT-IR in transmission and DSC was also performed on each sample.

## 6.2. Results and discussion

***Photoembossing***

So far photoembossing has solely been used to produce surface texture on acrylate based polymers and monomers. Here, for the first time, we have evaluated photoembossing on a polyester-acrylate system. PLGA is blended with an acrylate monomer TPETA. First a DSC scan is performed on film made from PLGA and TPETA blend to check its miscibility. The $T_g$ of pure PLGA is 45 $^oC$ and after blending it at a 1:1 ratio of TPETA, the DSC traces (Fig. 6.1a) show a single $T_g$ at 28 $^oC$ indicating miscibility of the photopolymer blend. Previously, it has been shown that the optimum processing temperature for photoembossing poly benzyl methacrylate (PBMA) and poly methyl methacrylate (PMMA) was at least $T_g$ + 60 $^oC$. Therefore for our first set of experiments to study the effect of UV intensity on height of relief structures, the films were thermally developed at 80 $^oC$ for 20 min. Fig. 6.1b shows the effect of UV dosage on relief height. The optimum UV dosage for PLGA-TPETA was 88.4 mJ/cm$^2$. This value was lower than the 145 mJ/cm$^2$ obtained for PMMA-TPETA in Chapter 4. Kaczmarek and Kwiatkowska [1] demonstrated the effect of matrix $T_g$ on acrylate conversion. They showed that acrylate conversion occurred at lower intensities in more plasticised matrices. The reason for this being that, macromolecules (monomer and photo-initiator) can move

more freely in the plasticised network. Thus lower dose is required for an optimum balance between diffusion and crosslinking/ polymerisation rate. Thus it is not surprising that PLGA photopolymer with a lower glass transition requires lower dose than PMMA photopolymer. Fig. 6.1c shows the effect of processing temperature on height of relief structures. Previously, the effect of processing temperature on photoembossing has been studied[2-5]. Similar to studies for other photopolymer systems, the height of the relief structures increases as the temperature increases till an optimum condition after which it begins to decrease. However, unlike previous studies [2,5], relief structures could also be formed at room temperature below the $T_g$ of the blend (Fig. 6.1a).

(a)

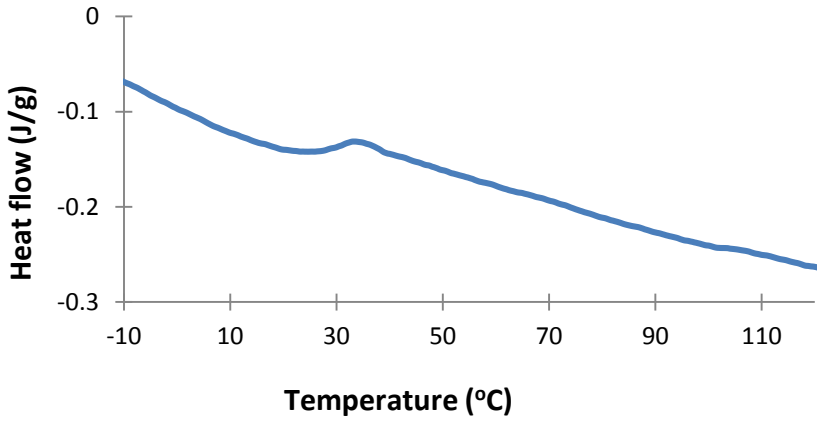


(b)

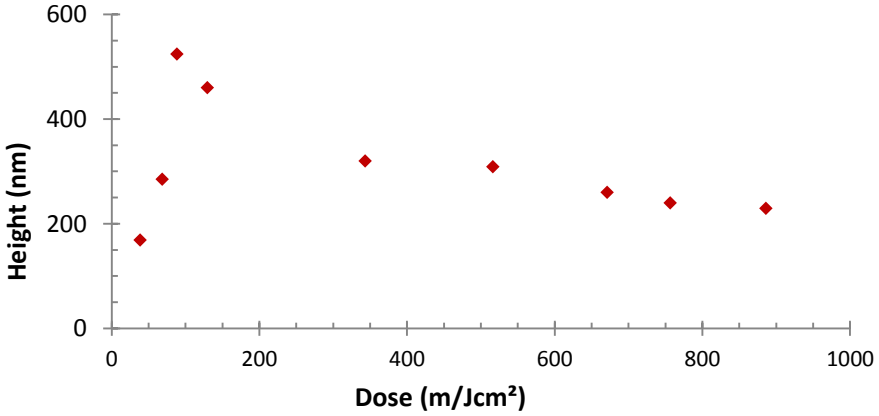

(c)

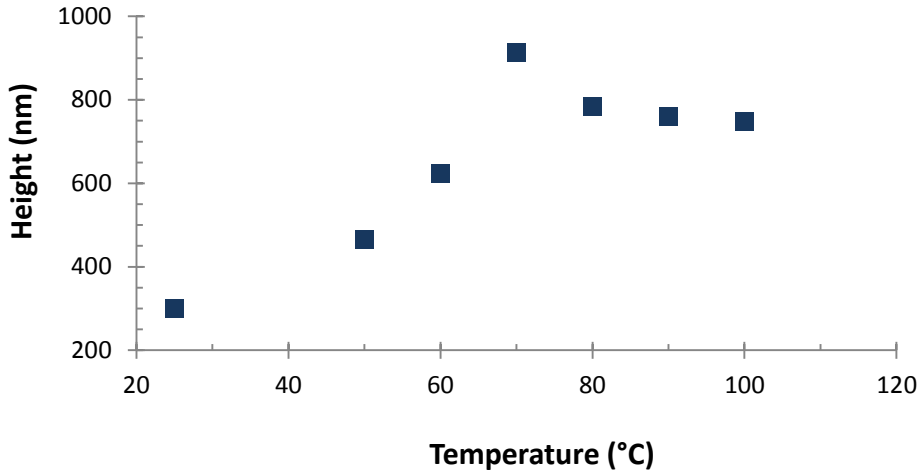


*Figure 6.1: DSC traces showing the glass transition of PLGA-TPETA blend (a), effect of UV intensity (b) and developing temperature (c) on photoembossed PLGA-TPETA (PLGA-TPETA-E) photopolymer.*

Previously it has been suggested that diffusion of monomers during photoembossing does not occur at temperatures below $T_g$ of the blend[2, 5]. However, in the current system there is a substantial increase in relief height of 300 nm at R.T. 1 min after patterned exposure. Various factors can cause the formation of the relief height at these low temperatures: 1) onset of glass transition at room temperature 2) heating of the blend above $T_g$ during UV exposure and 3) diffusion at temperatures below $T_g$. Glass transition of polymers occur at a range of temperature due to polydispersity of polymer matrices. Short chains are able to move at lower temperatures below the defined glass transition obtained from a DSC curve. Therefore it is possible that although the film appears to be glassy at room temperature, shorter chains (monomers and oligomers) chain can become flexible and mobile and thus making diffusion of monomers possible.

Furthermore it has been shown that diffusion of molecules through glassy polymers is known to be possible if there is enough free volume at its equilibrium state [6]. Diffusion is time dependent as well as temperature dependent and the diffusion rate of monomers is lower in the glassy state than at elevated temperatures as is shown in Fig. 6.2. The optimum height is reached at 10 min at 80 $^{o}$C and in 24hrs for those developed at R.T. For the films developed at 80 $^{o}$C (Fig. 6.2b), the height of the relief structures increased till 10 min of heating and then decrease after. Nevertheless, a similar optimum relief height of 950 nm is obtained for both samples developed at R.T. and 80 $^{o}$C at 24 hrs and 10 min, respectively. This shows that as expected diffusion of monomer through a polymer matrix occurs at faster rate with increasing temperatures. Furthermore, this optimum heating time is less for substrates developed at higher temperatures.

(a)

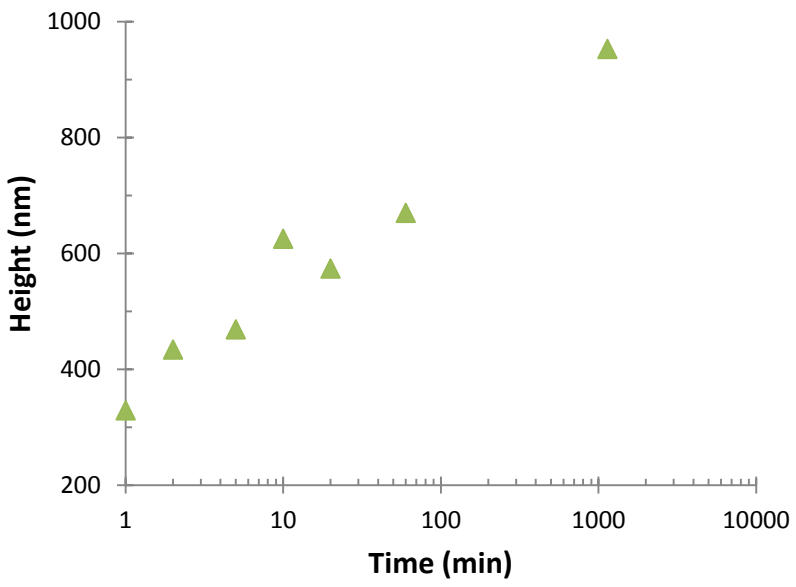

(b)

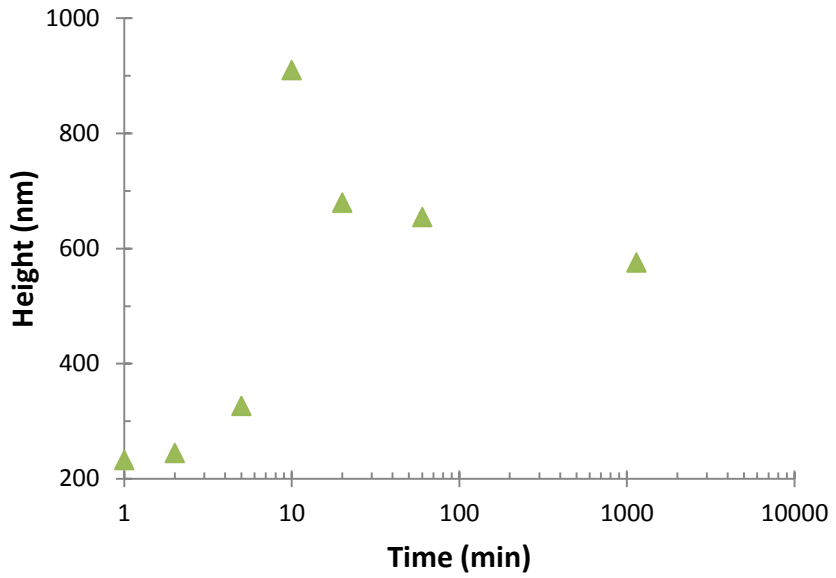


*Figure 6.2: Effect of thermal processing time on relief height at room temperature (a) and at 80 $^{o}$C (b).*

***Degradation***

PLGA degrades by hydrolysis where ester bonds are cleaved to form lactic and glycolic acid [7]. *In vitro* degradation is generally studied in phosphate buffer saline, and characterised by pH, mass, and molecular weight loss. In this section we study the degradation of pure PLGA, smooth photopolymer blend (PLGA-TPETA) and embossed photopolymer blend (PLGA-TPETA-E). Due to the presence of a crosslinked network in this system, molecular weight could not be evaluated.

After one week of degradation, there is a clear drop in pH for all samples to about 6.8 after which the pH remains constant till week 4. A sudden drop in pH is observed after week 4 and the drop is different for the different sample types. A similar trend is also observed in weight loss where only 10 wt.% is lost after the first 4 weeks for all sample

and therefore corresponding to similar pH. After 4 weeks, the mass loss profile became different for the different sample types.

In the first weeks of degradation, short chains already present in samples leaches out in solution medium causing slight drop in pH and mass. After this phase longer oligomer chains formed after degradation are insoluble in the aqueous media and therefore become trapped in the bulk of the polymer film [7]. Thus no significant change either in pH or mass is observed. As degradation progresses, shorter chains are formed and become soluble in the media. The acidic moieties formed increases the pH of the media and autocatalysis degradation increasing the rate of degradation[7, 8]. From the mass loss profile, the degradation is similar for PLGA and PLGA-TPETA and lower in the textured substrate PLGA-TPETA-E between 4-8 weeks. After 10 weeks of degradation, PLGA, PLGA-TPETA and PLGA-TPETA-E had lost 80 wt.%, 37 wt.% and 22 wt.% respectively of their original mass as shown in Fig. 6.3.

PLGA-TPETA and PLGA-TPETA-E contain 50 wt.% of PLGA and thus assuming that only PLGA degrades, the maximum mass loss will be 50 wt.%. Therefore, at week 10 wt.%, an 80 wt.% mass loss for PLGA will correspond to a 40 % loss for the photopolymer blends.

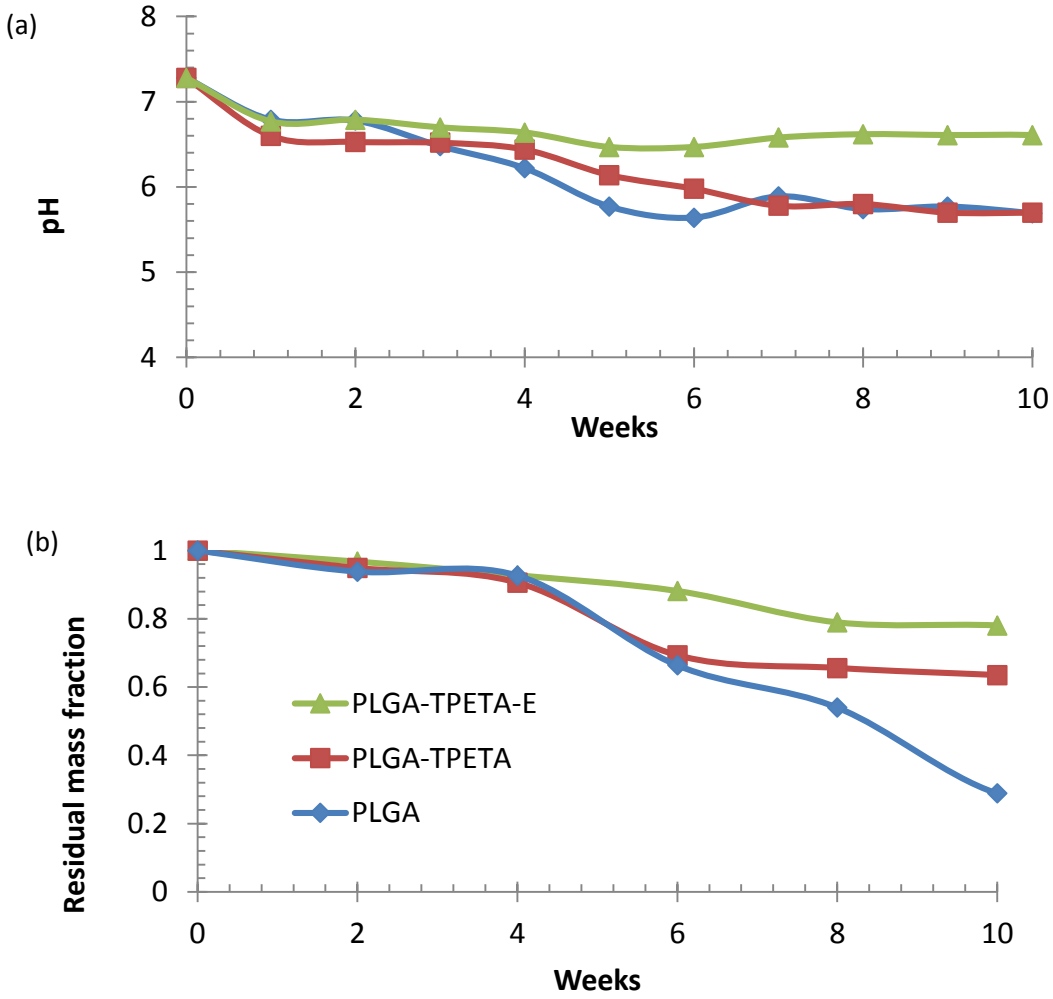


*Figure 6.3: Change in pH (a) and residual mass (b) with degradation time in PBS.*

Previously, it has been shown that the addition of acrylate monomers to polyesters decreases the rate of degradation due to the presence of a highly cross-linked network[9]. This highly cross-linked network reduces mobility and prevents degraded chains from escaping. Therefore only very short chains can escape from the network to cause bulk degradation. Phong et al. showed that after cross-linking PLGA with 10 wt.% penta-acrylate the degradation rate and the uptake of water decreased significantly [9].

From pH and mass loss results, indeed textured PLGA-TPETA-E films degraded at a slower rate compared to PLGA. However, the smooth PLGA-TPETA films appear to degrade at the same rate compared to PLGA. DSC thermograms after crosslinking showed an increase in *Tg* of PLGA-TPET-E from 45 $^{o}$C to 50 $^{o}$C whereas a decrease from 45 $^{o}$C to 35 $^{o}$C was observed for the PLGA-TPETA system. This suggested incomplete conversion of TPETA monomer in smooth substrates compared to textured, acting as a plasticiser. The unconverted monomers may have leached out of the film during degradation causing a higher loss in mass. The C=O found in PLGA decreases with time. However, the same bonds are present in acrylate monomers and this bond decreases during cross-linking. At 100% conversion, this bond disappears completely. To evaluate the amount of C=O bonds at t = 0 in PLGA-TPETA blends, FT-IR was performed on samples at t = 0 and t = 8 weeks. All peaks were normalised using the 2937 $cm^{-1}$ peak (C-H stretching). PLGA and PLGA-TPETA-E had a similar amount of C=O whereas PLGA-TPETA showed a significant higher concentration of this bond at t = 0 (Fig. 6.4). This further illustrates the presence of residual acrylate monomer after curing PLGA-TPETA samples.

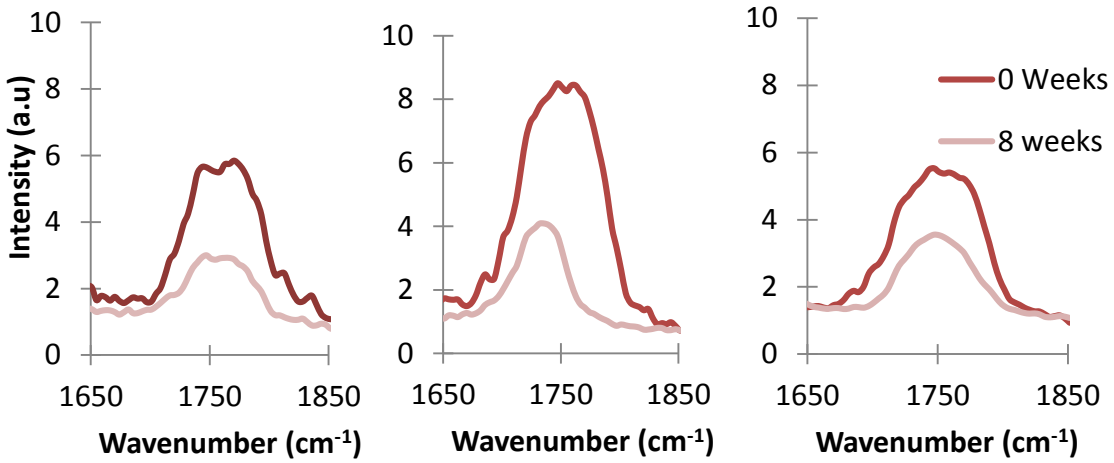


*Figure 6.4: FT-IR peak of C=O at 0 weeks and 8 weeks after degradation for PLGA, PLGA-TPETA and PLGA-TPETA-E (from left to right).*

PLGA-TPETA-E is exposed to UV and heated for a longer time due to pattern mask exposure and the thermal development step. This could have led to a better end conversion of PLGA-TPETA-E. To avoid the presence of residual monomer in cell culture which can be toxic, non-textured PLGA-TPETA was exposed to the same total UV intensity and heating time as PLGA-TPETA-E.

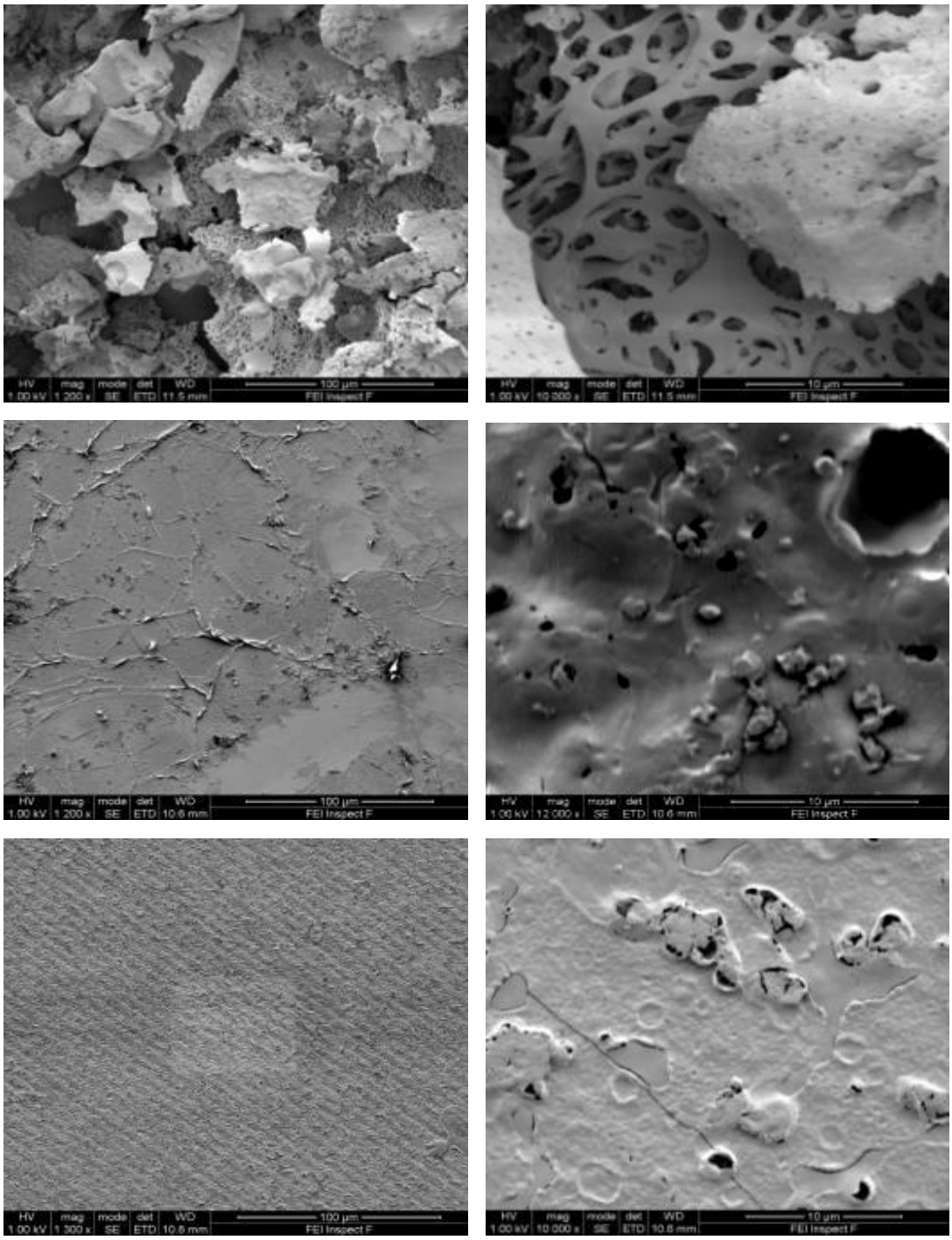

*Figure 6.5: SEM images showing surface topography 10 weeks after degradation for PLGA, PLGA-TPETA and PLGA-TPETA-E (top to bottom) with low (left) and high (right) magnifications.*

Samples were analysed under SEM after 10 weeks to characterise the morphology of the degraded samples. These images show that all samples degraded by bulk erosion and holes were formed throughout the bulk of the film. The surface texture of PLGA-TPETA-E was still evident as seen in Fig. 6.5.

***Cell culture***

Adhesion and complete endothelial cover on the surface is essential to prevent thrombosis on surfaces of cardio-vascular scaffolds or implants. To evaluate cell adhesion and proliferation on our substrates cell density on the surface was evaluated using a glass slide as a positive control. All experiments were performed in triplicate twice. After 24 hrs of culture, cells adhered on all substrates as shown in Fig. 6.6. Dapi staining and SEM images revealed that cells were homogenously spread on the substrate surface. Furthermore, long lamellopodia extension of the cell membrane meant that the cells also migrated on the surface of the film [10]. The lamellopodia of PLGA-TPETA-E was extended along the texture direction and thus cell migration was also mainly along this axis shown in Fig. 6.6c.

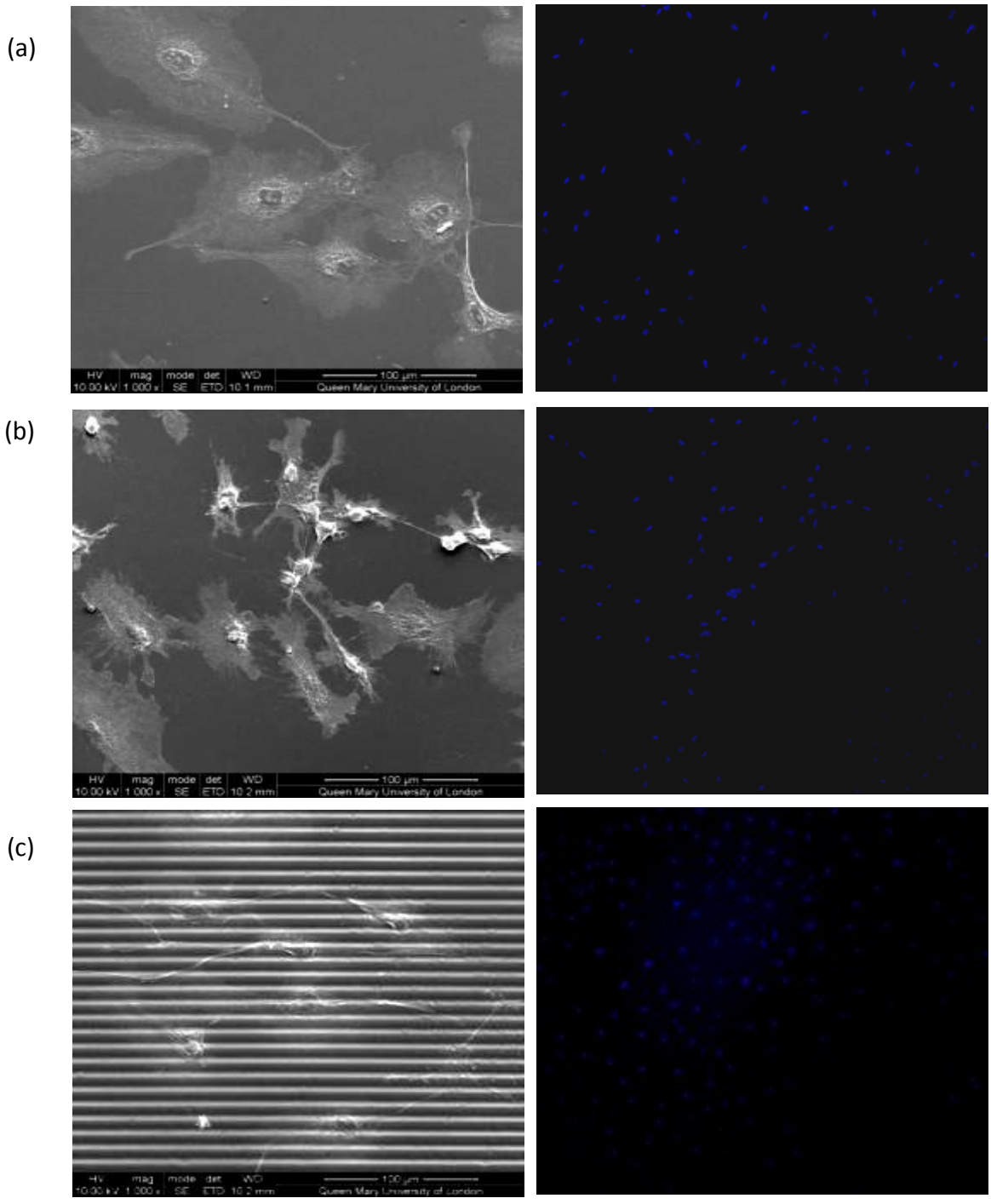


*Figure 6.6: SEM image (left) and Dapi staining (right) of cell adhesion on PLGA (a), PLGA-TPETA (b) and PLGA-TPETA-E (c) after 24 hrs of culture.*

The number of adhered cells over 7 days culturing period are shown in Fig. 6.7. After 24 hrs cell adhered to all substrates at similar densities. After 48 hrs the effect of texturing was evident as PLGA-TPETA-E showed a significantly higher ($p<0.05$) cell number compared to PLGA-TPETA. Faster proliferation was even more evident on photoembossed surface by 5 days where the PMMA-TPETA-E had already reached confluence faster than for PLGA and PLGA-TPETA. Our findings showed that cell adhesion and proliferation were improved on the textured surface compared to its non-embossed counterpart. This seems to be in agreement with previous research which showed that microgrooves on surfaces affects endothelial cell alignment, migration and proliferation rate[11-15]. Although, the science behind this effect is not fully understood, most researchers agree that an increase in focal adhesion sites promotes cell adhesion.

Jing et al. observed that HUVEC adhesion and proliferation was increased on microgroove textured surfaces with a pitch of 25 µm, 50 µm and 100 µm compared to its smooth counterparts. Lu et al. [16] evaluated the effect of texturing titanium stents on rat endothelial cell adhesion. Their study was to promote restoration of the endothelium over the stent which will enable its isolation from circulating blood, and therefore reduce the potential for restenosis and thrombosis. They studied endothelial cell number on different pitches of microgrooves ranging from 750 nm to 100 µm. Their results showed that depending on pitch size, texturing can increase or decrease cell number on stent surface. Cells adhered faster on the 750 nm and 20 µm after 4 hrs and cell proliferation was best on the sub-micron features after 24 hrs. Photoembossing can

be adapted in stent texturing where surfaces of stents can be coated with these photopolymer to promote endothelialisation. Furthermore, partial degradation of films will promote cell and tissue infiltration, which in turn could promote better adhesion between endothelium and stent.

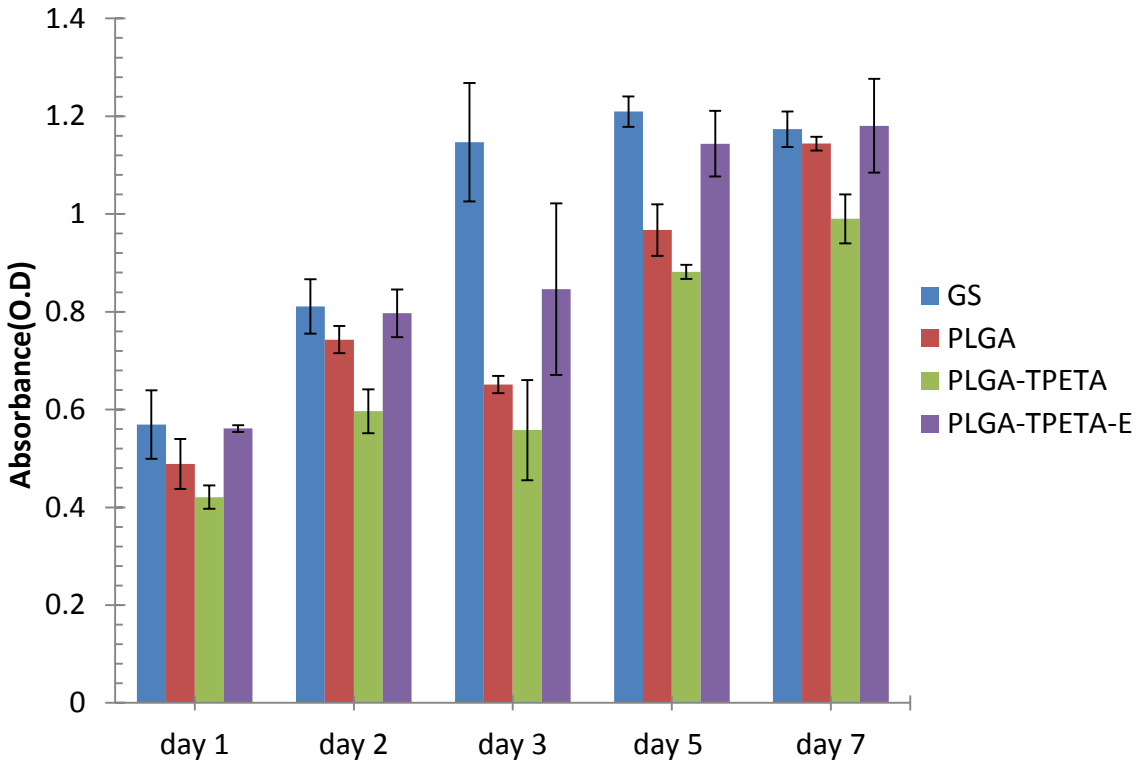


*Figure 6.7: Adhesion on the different substrates after 1, 2, 3, 5 and 7 days analysed by MTS assay.*

Furthermore, it is important that cell form strong adhesion on the surface of the scaffold/ stent to prevent delamination during blood flow in the body. Fig. 6.8 reveals focal adhesion sites formed by HUVEC on textured PLGA-TPETA-E.

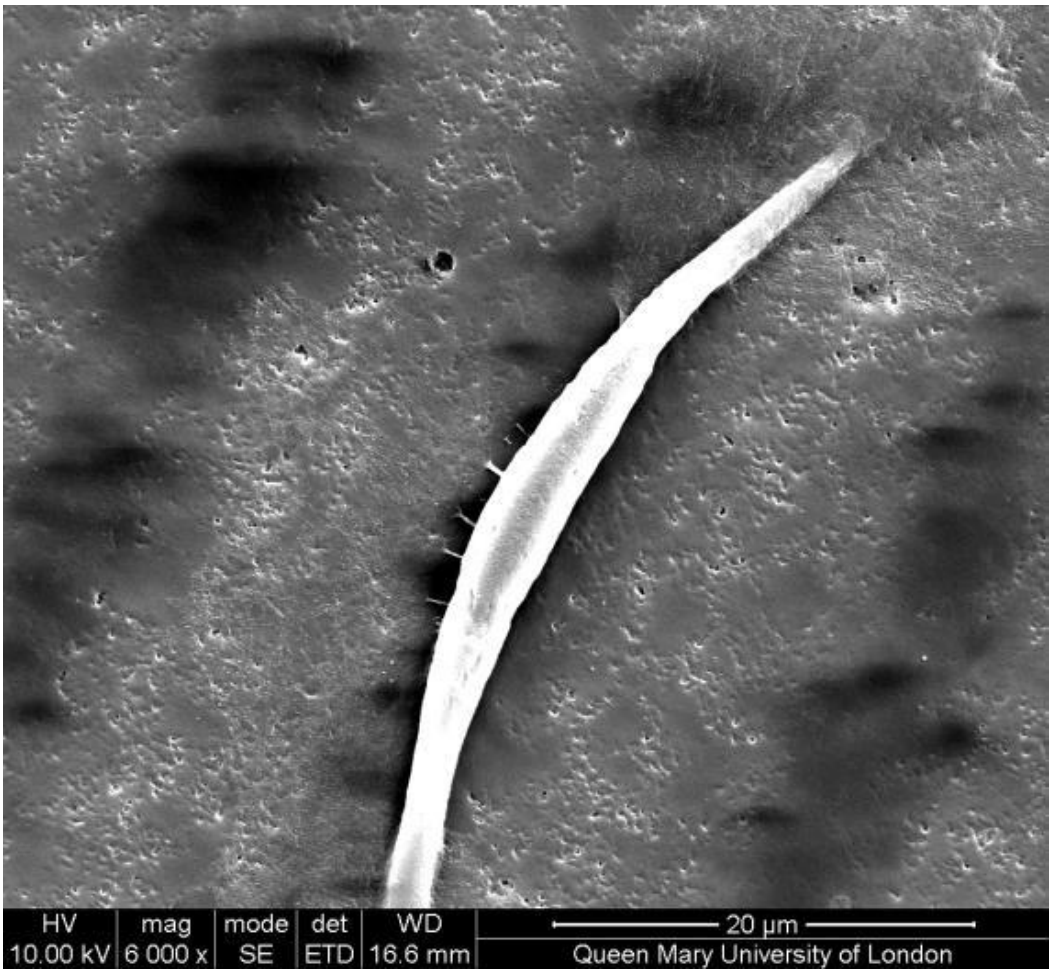


*Figure 6.8: SEM image of PLGA-TPETA-E revealing focal adhesion on film surface.*

## 6.3. Conclusions

A PLGA and TPETA blend was processed into films without phase separation. These films can be photoembossed to generate relief structures with height of the relief structure controlled by UV dosage, processing temperature and time. The maximum relief height is reached at shorter times at higher processing temperature. Degradation of this photopolymer progresses via bulk degradation with holes/pits forming in the films as

time progressed. Results also revealed a decrease in degradation rate of the photopolymer blend compared to the pure PLGA polymer. Furthermore the drop in pH was lower for the photopolymer and this could be beneficial for tissue engineering applications where sudden changes in pH around scaffold regions can lead to cell apoptosis.

*In vitro* cell culture showed good biocompatibility for both smooth PLGA-TPETA and textured PLGA-TPETA-E. Furthermore, surface texturing by photoembossing improved cell adhesion and proliferation rate compared to their smooth counterparts. Focal adhesion sites were observed on PLGA-TPETA-E films, indicating good adhesion on the film substrate. Furthermore, it was observed that cells migrated mainly along the grooves on film surface through the formation of lamellopodia along the direction of the grooves.

Although the PLGA-TPETA appear to be biocompatible, complete degradable polymers are sometimes required for tissue engineering application to allow complete takeover by natural regenerated tissue. In the next chapter, fully degradable photopolymer blends are created and photoembossed to produce surface texture.

## References

[1] H. Kaczmarek and I. Vukovic-Kwiatkowska, "Preparation and characterization of interpenetrating networks based on polyacrylates and poly(lactic acid)," *Express Polymer Letters,* vol. 6, pp. 78-94, 2012.

[2] B. J. de Gans, C. Sanchez, D. Kozodaev, D. Wouters, A. Alexeev, M. J. Escuti, C. W. M. Bastiaansen, D. J. Broer, and U. S. Schubert, "Optimizing photo-embossed gratings: A gradient library approach," *Journal of Combinatorial Chemistry,* vol. 8, pp. 228-236, 2006.

[3] K. Hermans, F. K. Wolf, J. Perelaer, R. A. J. Janssen, U. S. Schubert, C. W. M. Bastiaansen, and D. J. Broer, High aspect ratio surface relief structures by photoembossing, *Applied Physics Letters,* vol. 91, 2007.

[4] N. F. Hughes-Brittain, O. T. Picot, M. Dai, T. Peijs, and C. W. M. Bastiaansen, "Effect of polymer binder on surface texturing by photoembossing," *Applied Surface Science,* vol. 258, pp. 8609-8612, 2012.

[5] C. Sanchez, B. J. de Gans, D. Kozodaev, A. Alexeev, M. J. Escuti, C. van Heesch, T. Bel, U. S. Schubert, C. W. M. Bastiaansen, and D. J. Broer, "Photoembossing of periodic relief structures using polymerization-induced diffusion: A combinatorial study," *Advanced Materials,* vol. 17, pp. 2567, Nov 2005.

[6] J. L. Duda, Molecular-diffusion in polymeric systems, *Pure and Applied Chemistry,* vol. 57, pp. 1681-1690, 1985.

[7] A. Göpferich, "Mechanisms of polymer degradation and erosion," *Biomaterials,* vol. 17, pp. 103-114, 1996.

[8] L. Lu, C. A. Garcia, and A. G. Mikos, "In vitro degradation of thin poly(DL-lactic-co-glycolic acid) films," *Journal of Biomedical Materials Research,* vol. 46, pp. 236-244, 1999.

[9] L. Phong, E. S. C. Han, S. J. Xiong, J. Pan, and S. C. J. Loo, "Properties and hydrolysis of PLGA and PLLA cross-linked with electron beam radiation," *Polymer Degradation and Stability,* vol. 95, pp. 771-777,2010.

[10] D. Lauffenburger and A. Horwitz, "Cell Migration: A Physically Integrated Molecular Process," *Cell,* vol. 84, pp. 359-369, 1996.

[11] P. Uttayarat, M. Chen, M. Li, F. D. Allen, R. J. Composto, and P. I. Lelkes, "Microtopography and flow modulate the direction of endothelial cell migration," *American Journal of Physiology - Heart and Circulatory Physiology,* vol. 294, pp. H1027-H1035, 2008.

[12] E. A. Sprague, F. Tio, S. H. Ahmed, J. F. Granada, and S. R. Bailey, "Impact of parallel micro-engineered stent grooves on endothelial cell migration, proliferation, and function: an in vivo correlation study of the healing response in the coronary swine model," *Circ Cardiovasc Interv,* vol. 5, pp. 499-507,2012.

[13] L.-Y. Jiang and Y. Luo, "Guided assembly of endothelial cells on hydrogel matrices patterned with microgrooves: a basic model for microvessel engineering," *Soft Matter,* vol. 9, pp. 1113-1121, 2013.

[14] J. Lu, M. P. Rao, N. C. MacDonald, D. Khang, and T. J. Webster, "Improved endothelial cell adhesion and proliferation on patterned titanium surfaces with rationally designed, micrometer to nanometer features," *Acta Biomaterialia,* vol. 4, pp. 192-201, 2008.

[15] F. J. Jing, N. Huang, L. Wang, R. K. Y. Fu, Y. F. Mei, Y. X. Leng, J. Y. Chen, X. Y. Liu, and P. K. Chu, "Behavior of human umbilical vein endothelial cells on micro-patterned amorphous hydrogenated carbon films produced by plasma immersion ion implantation & deposition and plasma etching," *Diamond and Related Materials,* vol. 16, pp. 550-557, 2007.

[16] J. Lu, M. P. Rao, N. C. MacDonald, D. Khang, and T. J. Webster, "Improved endothelial cell adhesion and proliferation on patterned titanium surfaces with rationally designed, micrometer to nanometer features," *Acta Biomaterial, v*ol. 1, pp. 192-201, 2008

# Chapter 7

## Photoembossing of degradable thiol-acrylate networks

Non-degradable and semi-degradable photopolymer blends have been developed and photoembossed in previous chapters. These blends have been shown to be biocompatible by adhesion and proliferation of endothelial cells on their surfaces. However, in some application of tissue engineering and drug delivery complete degradation of the biomaterial is needed for total tissue take over or drug release respectively. In this chapter, a photopolymer blend is made by blending PLGA with a PEG-diacrylate and a thiol to create a fully degradable photopolymer blend that can be photoembossed. Photoembossing shows that different UV intensities and processing

temperatures can be used to tune relief heights. Surface texturing was achieved on both flat films and electrospun photopolymer blends. Accelerated degradation results showed complete degradation of the photopolymer blends, with its degradation being much faster than for pure PLGA polymer. This was attributed to the high hydrophilicity of the degradable cross-linked network which further enhanced hydrolysis of ester bonds in PLGA. Cell culture after 72 hrs showed cell adhesion on the photopolymer surface indicating biocompatibility.

## 7.1. Materials and methods

PEG diacrylate (PEG-Da) with a molecular weight of 258 g/mol, and dithiothreitol(DTT) were used as received from Sigma Aldrich. PLGA (72:25), phosphate buffer saline (PBS), photo-initiator 2-benzyl-2-(dimethylamino)-4'-morpholinobutyrophenone (Irgacure 369) and ethyl acetate were used as received from Sigma Aldrich.

### *Photoembossing*

20 wt.% PEG-Da was dissolved in ethyl acetate. DTT was added to the solution at a mole ratio of 0.8:1 of PEG-diacrylate. The solution was allowed to stir for 20 min. PLGA and Irgacure 369 were added to this solution in a ratio of 1:0.1 of PEG-diacrylate. The solution was again allowed to stir till complete dissolution. This solution was coated on a 12 mm acrylate functionalise cover slips by wire bar coating. 70 µl of solution was pipetted on each cover slip and a wire-bar was used to coat the solution onto the glass

surface. The films were placed in a convection oven at 80 $^{o}$C and allowed to dry for 20 min. A photomask with a pitch of 20 µm was placed in contact with the films. These films were photoembossed using UV intensity ranging from 0-300 mJ/cm$^2$ at R.T. and in ambient air. This was followed by a thermal development step at 80 $^{o}$C in ambient air. Flood UV exposure of 15 J/cm$^2$ was used to cure the residual monomer. Another set of experiments to obtain an optimum developing temperature was performed by patterned exposure at 106 J/cm$^2$. Here the thermal development step was performed at different temperatures from 40 $^{o}$C to 120 $^{o}$C.

The solution was electrospun using a voltage of 18 kV and a spinning distance of 18 cm at a flow rate of 0.8 ml/hr. The fibres obtained were photoembossed by inference of two coherent UV beams to create patterned exposure (set-up used in Chapter 5). The intensity used for the patterned exposure was 80 mJ/cm$^2$ followed by a heating step at 120 $^{o}$C for 20 min. The fibres were then exposed to a flood UV exposure at elevated temperature to cure the residual monomers.

The relief structures on the films were measured by semi-contact mode atomic force microscopy (AFM, NT-MDT). Optical microscopy is used to reveal surface texture on films and fluorescent microscopy was used to reveal surface texture on fibres.

***Degradation***

0.5 ml of solution was pipetted in stainless steel moulds coated with Teflon spray to produce discs with 10 mm diameter. The mould was dried in a convection oven at 80 $^{o}$C

for 24 hrs. Each disc was irradiated to UV on both sides and heated at 80 $^{o}$C for 30 min. Discs with thickness of around 5 mm were obtained after drying and crosslinking. Accelerated hydrolysis was performed in 1 M of NaOH in deionised water at R.T. A disc was removed every 4-8 hrs and washed with deionised water. The sample was then dried in vacuum at R.T. and weighed to obtain the mass loss.

***Cell culture***

HUVECs (Lonza Cologne AG, Germany) were grown in M199 medium (Gibco) at 37 °C and 5% $CO_2$. The culture medium contains 10% foetal bovine serum (FBS), EC growth factor-β (1 ng/ml), EC growth supplement from bovine neural extract (3 µg/ml), thymidine (1.25 µg/ml), heparin (10 µg/ml), 100 U/ml penicillin, 100 mg/ml streptomycin (all supplements are from Sigma Aldrich). Cells with less than 7 passages were used in all reported experiments *in vitro*. The medium was changed every 2 days. The substrates were washed 2 times with ethanol and rinsed 2 times with PBS before cell seeding. Cells were seeded on all the substrate with the density at $1.5\times10^4$ cells/cm$^2$ and cultured up to 7 days. Cell density was analysed by MTS assay. The cells were washed 2x with serum-free media. 250 µl of serum free media was added to each well and 50 µl of CellTiter 96® Aqueous One Solution Reagent from Promega was used and incubated for 3 hrs. After 3 hrs, 100 µl of the solution is pipetted into 96 well plates and the absorbance at 490 nm is recorded using Fluo Star Galaxy reader.

## 7.2. Results and discussion

Photoembossing of PLGA blended with 1:0.8 mole ratio of PEG diacrylate and DTT was photoembossed at different UV intensity and temperature shown in Fig. 7.1. Similar to classical photoembossing where only acrylate monomers are used, a change in UV dosage and developing temperature resulted in different relief height. Generally, an optimum UV intensity and temperature is reached for a particular photopolymer blend. Fig. 7.1a shows an optimum UV dosage at 106 J/cm$^2$. In Fig. 7.1b an increase in processing temperature correlated to an increase in relief height. No optimum temperature was seen as the relief height increased till 120 $^{o}$C.

(a)

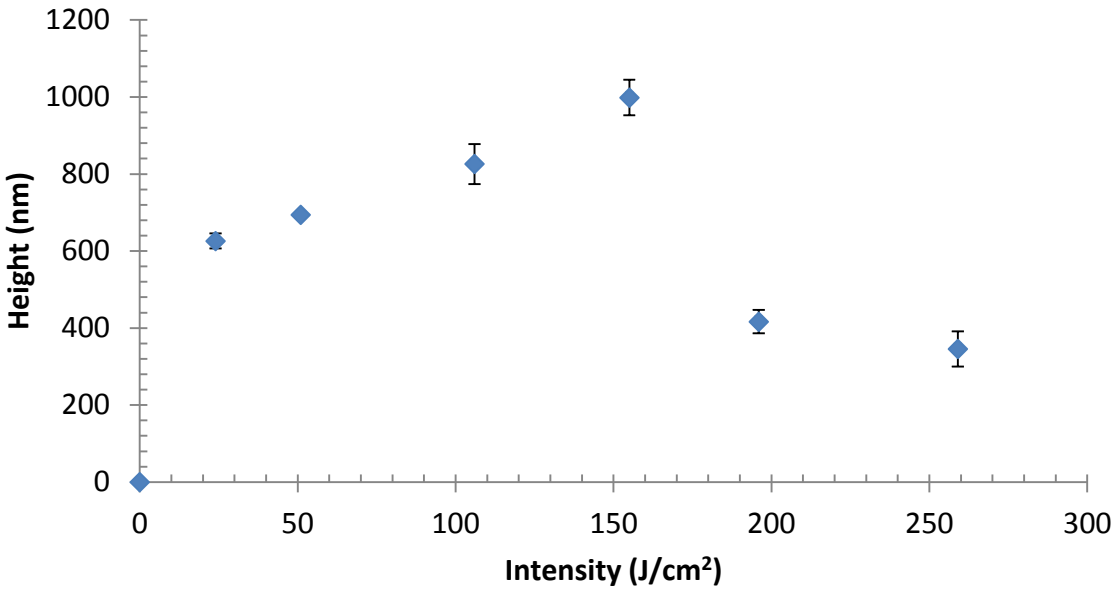


(b)

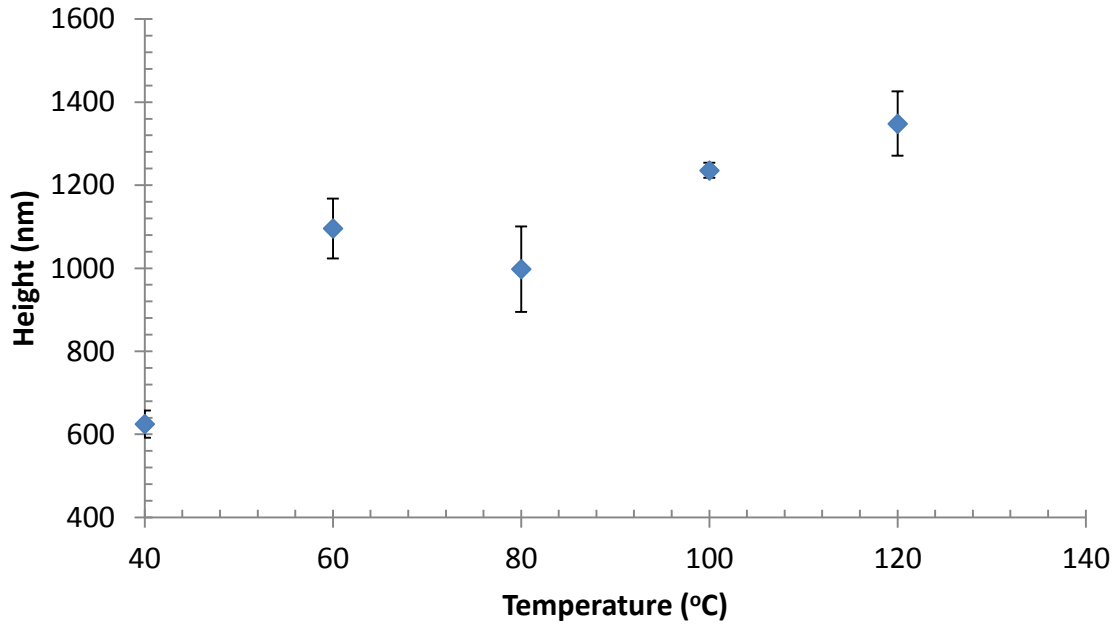


*Figure 7.1: Photoembossing of PLGA-PEGDa-DTT using different UV intensity (a) and processing temperature (b).*

AFM topography and phase contrast shown in Fig. 7.2 revealed two different contrast in the ridge and groove. The groove shows a dark topographic contrast whiles the phase contrast appears bright and vice versa was observed at the peaks. A bright phase contrast infers a stiffer matrix compared to the surrounding. The groove, which is where the monomers diffuse from contains a higher amount of PLGA, whereas the peaks contained more of the cross-linked network. This sugests that the cross-linked acrylate-thiol network had a more plasticising effect on the crosslinked photopolymer system.

(a)

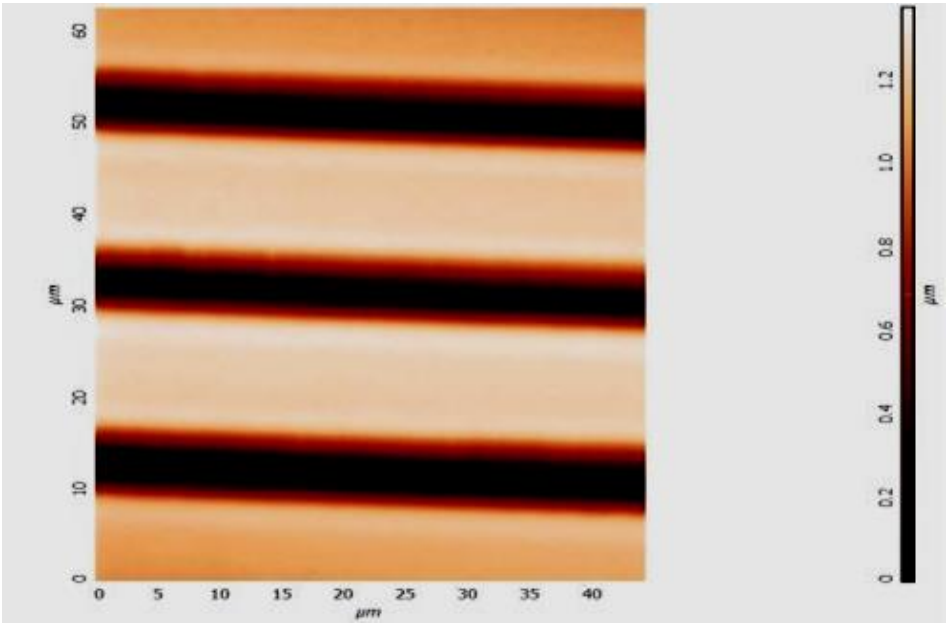


(b)

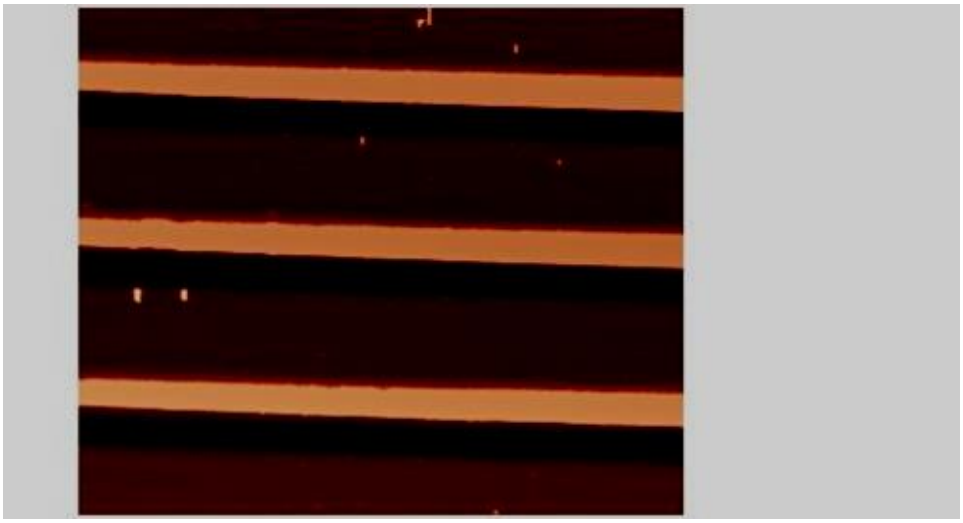

*Figure 7.2: AFM image of photoembossed PLGA-PEGDa-DTT substrates, showing topography (a) and phase contrast (b).*

Furthermore, phase seperation is observed for both non-textured and photoembossed films as shown in Fig. 7.3a and Fig. 7.3b respectiveky after crosslinking. This means that the crosslinked thiol-acrylate network is not miscible in the PLGA polymer binder.

However, the phases were homogenously dispersed and no regions of large aggregates were observed. Furthermore, an accurate reproduction of pitch size of the mask is achieved on the photoembossed substrate as shown in Fig, 7.3b.

(a)

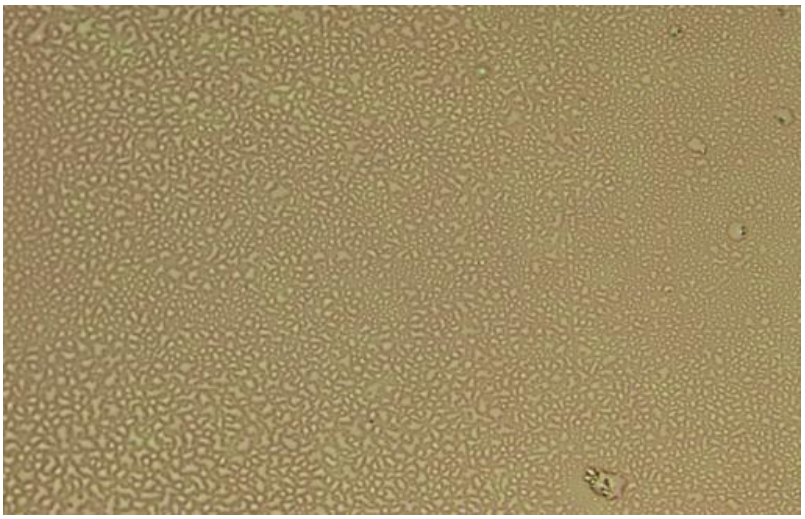

(b)

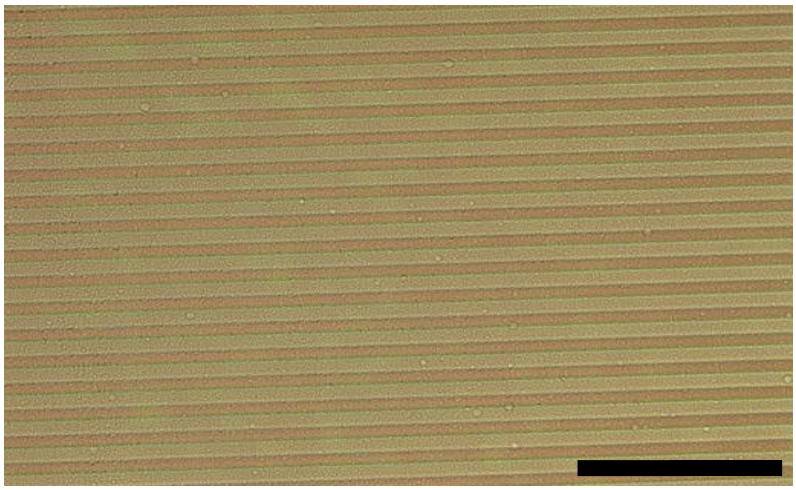

*Figure 7.3: Optical microscope image of PLGA-PEGDa-DTT non-textured film (a) and embossed film(b) after cross-linking scale bar is 100 µm.*

To demonstrate that this phase separated system can be electrospun and photoembossed, the solution was electrospun on a glass slide and photoembossed using

the pulse laser holographic set-up shown in Chapter 5. Although the solution was not fully optimised for spinning fibres with homogenous diameter and distribution, the surface of the fibres after photoembossing revealed texture with a pitch of 2 µm as shown in Fig. 7.4.

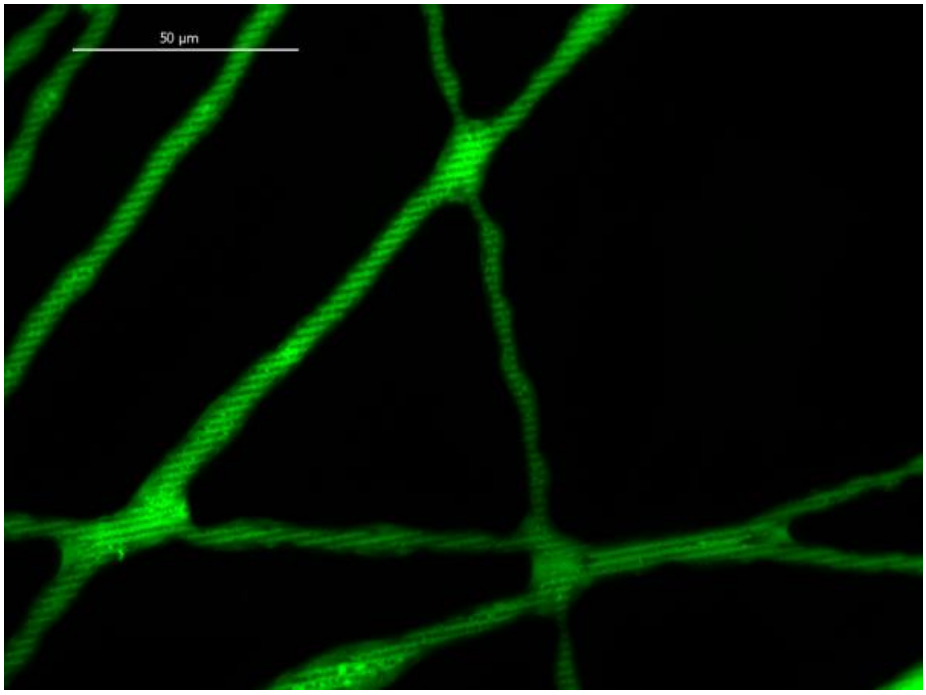


*Figure 7.4: Photoembossed electrospun PLGA-PEGDα-DTT electrospun fibres.*

Thus photoembossing can create surface texture using acrylate and thiol monomers on both films and fibres. Furthermore, texturing can be achieved on phase separated systems whose domain sizes are smaller than the pitch of the relief structures. Also, diffusion of monomers from non-irradiated region to exposed areas causes a difference

in mechanical properties between groove and ridges of the texture. This is evident in the phase contrast AFM in Fig. 7.2.

Results for accelerated hydrolysis degradation performed in 1 M NaOH at room temperature is shown in Fig. 7.5. The results indicate that photopolymer degrades faster compared to pure PLGA samples. After 48 hrs of degradation, the PLGA-PEGDa-DTT had lost 95 wt.% whereas PLGA had only lost 45 wt.%. Degradation results show that both PLGA and PLGA-PEGDa-DTT reduce in weight by hydrolysis. Faster degradation of the photopolymer blend can be attributed to high hydrophilicity of the cross-linked PEGDa-DTT network [1-3]. Even the PLGA binder in the network (50 wt.%) seems to degrade very fast compared to the pure PLGA discs. Previously, it has been shown that the degradation rate of acrylate-thiol networks can be controlled by changing the ratio between the acrylate and thiol mole ratio and the molecular weight of the acrylate [4]. Increasing the mole ratio of acrylate in the photopolymer blend decreases the rate of degradation whereas an increase in molecular weight of the acrylate increases degradation rate. This is because longer chains of acrylate networks are formed by homo-polymerisation resulting in less ester regions formed [4, 5]. The use of hydrophobic acrylates can also decrease the degradation rate significantly, for example the triacrylate TPETA used in Chapter 6. Using this photo-crosslinkable acrylate network helps tune degradation time to suit the application intended for the scaffolds. Furthermore, complex surface texture can be achieved using the photoembossing technique.

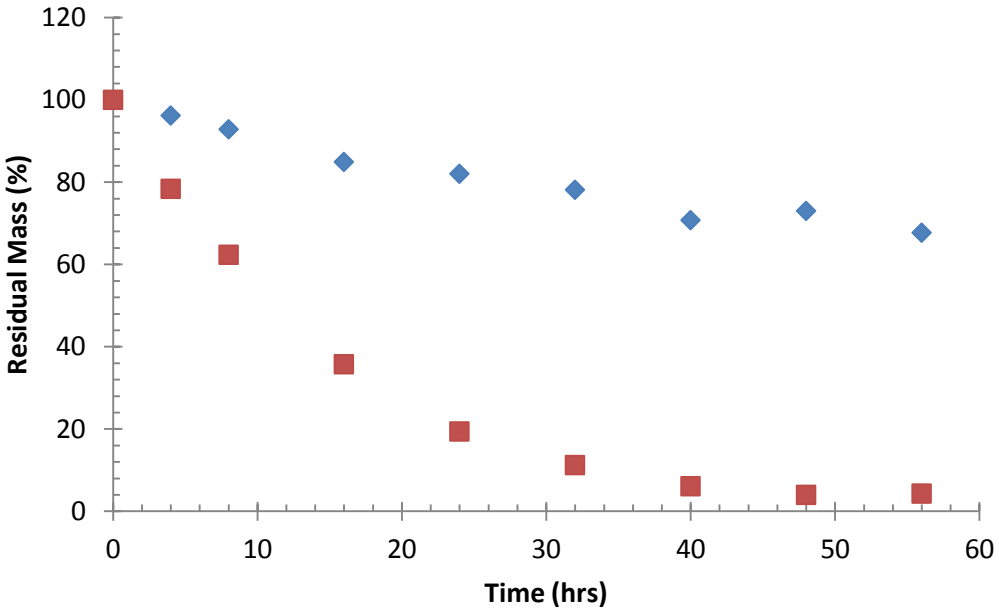


*Figure 7. 5: Mass loss profile of pure PLGA (blue) and PLGA-PEGDa-DTT (red) discs in 1 M NaOH with time.*

Cell adhesion on substrates was evaluated without pre-adsorbed proteins after 24, 48 and 72 hrs cell of culture. The photopolymer blends did not show significant differences between embossed and smooth substrates for endothelial cells. These results also show a reduced number of cells compared to the cover slips and PLGA polymer.

(a)

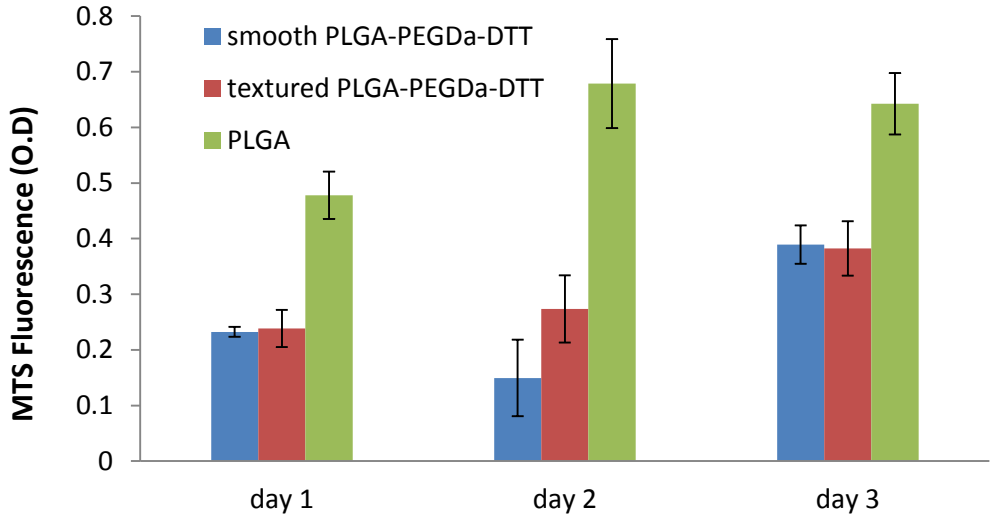


(b)

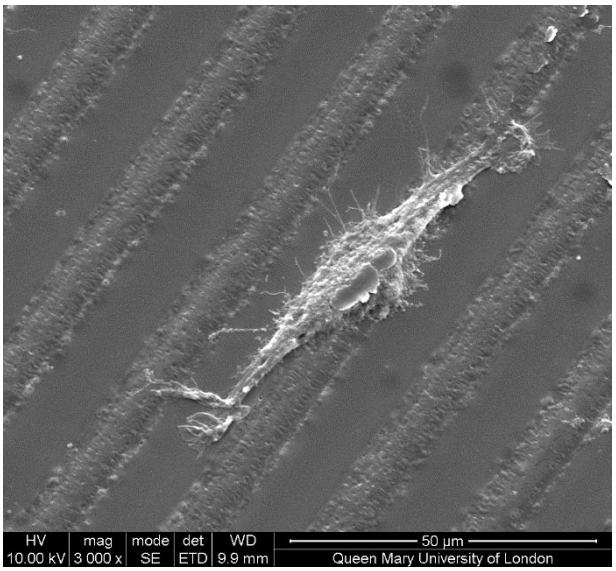


*Figure 7.6: MTS results for endothelial cell adhesion on smooth and textured photopolymer blend (a) with PLGA as a control and SEM image (b) of endothelial cell adhesion on surface 24 hrs after culture.*

HUVECs adhered on these substrates after 24 hrs showing biocompatibility of the photopolymer blend. However, no significant difference was observed between smooth

and textured photopolymer blend after 3 days of culture. Further quantification on cell proliferation with time and matrix synthesis is needed to fully characterise the photopolymer blend (This is beyond the scope of this thesis). Nevertheless, photoembossing provides a tool for surface texturing on films and fibres for applications in biomedical engineering. In Chapter 6, photoembossed PLGA-TPETA films served as a substrate for endothelial cell culture and cell adhesion and proliferation was increased on photoembossed substrates compared to smooth surfaces. However, degradation only occurred in the PLGA regions leaving behind a cross-linked acrylate network. In this study, a degradable photoembossed substrate is produced by forming liable ester bonds generated by reaction of an acrylate and a thiol. Excess mole ratio of acrylate is used to allow crosslinking using a UV radiation and hence the photoembossing procedure.

## 7.2. Conclusions

In previous studies photoembossing has only been perform on blends containing acrylate monomers and a miscible polymer binder. Depending on the polymer binder used, these blends, after crosslinking can be non-degradable (PMMA) or partially degradable (PLGA). Here, for the first time we have shown that fully degradable PLGA-acrylate-thiol blends can be photoembossed to create surface relief structures. Similar to classical photoembossing the height of the relief structures formed can be controlled by UV intensity and temperature. Surface texture could be achieved on both films and electrospun fibres even with the phase separated substrates. Both polymer binder and

cured acrylate-thiol network undergo degradation by hydrolysis to allow complete degradation of the photopolymer. Cell cultured on non-textured and embossed photopolymer blend show endothelial cell adhesion after 24 hrs with a doubling in cell number after 72 hrs.

## References

[1] G. A. Hudalla, T. S. Eng, and W. L. Murphy, "An approach to modulate degradation and mesenchymal stem cell behavior in poly(ethylene glycol) networks," *Biomacromolecules,* vol. 9, pp. 842-849, 2008.

[2] Y. Qiu, J. J. Lim, L. Scott Jr, R. C. Adams, H. T. Bui, and J. S. Temenoff, "PEG-based hydrogels with tunable degradation characteristics to control delivery of marrow stromal cells for tendon overuse injuries," *Acta Biomaterialia,* vol. 7, pp. 959-966, 2011.

[3] A. E. Rydholm, K. S. Anseth, and C. N. Bowman, Effects of neighboring sulfides and pH on ester hydrolysis in thiol-acrylate photopolymers, *Acta Biomaterialia,* vol. 3, pp. 449-455, 2007.

[4] G. A. Hudalla, T. S. Eng, and W. L. Murphy, "An approach to modulate degradation and mesenchymal stem cell behavior in poly(ethylene glycol) networks," *Biomacromolecules.* vol. 9 (3), pp 842-9, 2008.

[5] A. E. Rydholm, C. N. Bowman, and K. S. Anseth, "Degradable thiol-acrylate photopolymers: polymerization and degradation behavior of an in situ forming biomaterial," *Biomaterials,* vol. 26, pp. 4495-4506, 2005.

# Chapter 8

## Conclusions & Future work

In this thesis, photoembossing technique has been used to create surface relief structures on both films and fibres for biomedical applications. For the first time, this technique has been used to texture surfaces of electrospun fibres with reproducible patterns. To adapt photoembossing for the biomedical field, the polymer binder as well as the cross-linked monomer network have to be biocompatible, and thus should not cause cell apoptosis or elicit an immune response. In this study, two polymer binders are investigated for the creation of such systems: poly(methyl methacrylate) (PMMA) and poly(lactic-co-glycolic acid) (PLGA).

PMMA has been used widely as bone cement in orthopaedic surgery and has been shown to be biocompatible. PMMA blended with acrylate monomer was processed into films and fibres and was photoembossed to obtain surface texture on the electrospun fibres. Endothelial cell adhesion was investigated here, and it was shown that cells adhere faster onto the photopolymer blend, compared with pure PMMA without pre-coating the surface with proteins. However, there was no significant difference between the smooth photopolymer and the embossed surface. This was attributed to the PMMA binder not being suitable for endothelial cell adhesion. Thus, in a subsequent study, this polymer binder was changed to PLGA, which has been widely utilised in studies for vascular regeneration. Photoembossed PLGA-photopolymers with a pitch of 20 µm and height of 2 µm showed superior cell adhesion and proliferation compared with smooth photopolymer and pure PLGA films. Degradation studies of these PLGA-TPETA photopolymers showed erosion of the PLGA binder, leaving behind a cross-linked acrylate network. Furthermore, the presence of the acrylate network slowed down the rate of degradation of the PLGA polymer binder. Degradation of polyesters results in formation of acidic products. It is important that the change in pH in the tissue vicinity as a result of polymer degradation should not cause cell death and thus, a minimal decrease in pH during degradation is preferred. Here, the degradation study showed that PLGA-TPETA showed less pH drop compared with pure PLGA. The superior cell adhesion and proliferation, as well as better degradation rate, means that this photopolymer system can be utilised for implant coatings to promote adhesion between implant and surrounding tissue. It can also be used in stent fabrication, especially for

older patients in which full degradation of implant is not needed. The cross-linked network can serve as a mechanical support, while at the same time allowing tissue in-growth during degradation of the PLGA binder. However, for some applications it is essential to have a fully bioresorbable system that can be photoembossed to allow complete tissue takeover. Thiol-ene chemistry is adopted here, and two monomers are utilised by reacting a thiol in excess of acrylate. Here, the crosslinks themselves are not degradable, but dithiol “bridges” are, which are hydrolytically labile. The hydrolytic lability of DTT bridges is due to the presence of a thioether bond proximal to the acrylate ester bond. Specifically, the presence of this proximal thioether group establishes a more positive atomic charge on the carbonyl carbon of the ester, thereby enhancing ester hydrolysis. Mixed-mode polymerisation of the acrylate network allows radical mediated UV polymerisation, thus making it possible to photoemboss these blends. Photoembossing of such systems revealed classical photoembossing trends, where height could be controlled by UV intensity and developing temperature. Furthermore, these mixtures could be electrospun and photoembossed to generate fibres with surface texture. Further tuning of spinning conditions with good fibre morphology is needed. Also, the choice of acrylate monomer was based on a hydrophilic species that will promote faster degradation. However, for slower degradation rates, more hydrophobic and biocompatible acrylate such as TPETA can be used. Further studies to fully characterise this type of blend in terms of long term biocompatibility and processing is currently being investigated in a follow-up thesis.

Furthermore, the photoembossing technique has been shown to be suitable for texturing surfaces of electrospun fibres. The technique can be used to mimic surface topography of collagen fibres to study cell response to these textures. The pitch of the structure should be on the order of 100 nm, and different fibre diameters in the same order will have to be investigated to mimic this collagen topography.